Division of Solid Mechanics

ISRN LUTFD2/TFHF--01/5102--SE (1-120)

ANALYTICAL DIMENSIONING OF CASTING STRUCTURES IN DRAW DIES

Master's Dissertation by

Jörgen Larsson

Supervisors
Ingrid Svensson, Div. of Solid Mechanics
Bengt Persson, Volvo Cars Body Components
Nader Asnafi, Volvo Cars Body Components

Copyright © 2003 by Div. of Solid Mechanics, Jörgen Larsson
Printed by KFS i Lund AB, Lund, Sweden, 2003.

For information, address:
Division of Solid Mechanics, Lund University, Box 118, SE-221 00 Lund, Sweden.
Homepage: www.solid.lth.se

1. Summary

Today the casting structure in draw dies is dimensioned according to standard guidelines. No attention is paid to the size of the stamped part and the properties of the blank. The aim of this study was to derive analytical expressions that can be used during the design of the draw dies. From required input, geometrical data of the casting structure, punch and blank holder force, allowable stress or deflection, thickness of the casting structure can be calculated. Different types of draw dies as well as different stages in a press (stamping) stroke have been considered.

In an arbitrary point the stress vary with time during a press stroke. Therefore the stroke was divided into three significant sequences: when the blank holder hits the lower die, when the punch hits the blank and when the die is closed. The results from the analytical expressions were compared to the results from finite element calculations.

Both the shape of the part stamped in the draw die and the shape of the draw die itself vary in a wide range. In the study the extremes, flat dies and V-shaped dies were studied. In the analytical expressions, regardless of die type, it seems to be a too coarse approximation assuming the punch load to be equally distributed over the whole forming area. Instead it is suggested to introduce the load as equally distributed over the areas with forming radii.

The load on the vertically walls in lower die, punch and blank holder in flat dies, seems to be possible to describe adopting a uni-axial stress state. The same applies for the vertically walls in blank holder in V-shaped dies, but in V-shaped punches and lower dies probably a bi-axial stress state has to be considered. Many of the expressions can be refined taking a position dependence of the area over which the stress is distributed into account.

In the section at the bottom of a V-shape, a tri-axial stress state seems to be applicable. A major part of the load is distributed over the upper half of the cross section. The expression can be refined by adopting a varying stress distribution.

The deflection of the area between the walls in the forming area, were calculated using Kirchoff plate theory. I was concluded that the analytical model only is valid if the length of the shortest side exceeds one tenth of the thickness. The analytical expression was applicable even if this condition not was fulfilled. This is explained in how the loads were applied. In the derivation of the analytical expression the load was assumed to be equally distributed, whilst it was applied only at the areas with forming radii in the FE-calculations.

An approach to dimension the blank holder surfaces with respect to bending was suggested. However, more dies have to be studied before reliable expressions can be derived.

Finally it should be pointed out that in order to be able to make a definite statement regarding the validity of the derived expressions, more comprehensive finite element calculations, including the use of software with possibility to solve advanced contact problems, or measurements in real dies, have to be performed.

It is also worth mentioning that, since the applied blank holder and punch loads are representative for deep drawing operations and the stresses and deflections in common are

low, there seems to be a potential to reduce weight and cost by reducing the die casting dimensions.

Keywords: analytical expressions, casting structure, dimensioning, draw dies, finite element calculations

2. Preface

This report is a master thesis, obligatory within the program of Master of Science in Engineering Physics at University of Lund, which has been performed at Volvo Cars Body Components in Olofström. The report deals with dimensioning of casting structures in draw dies used for stamping of automotive steel sheet parts. The increased use of high strength steels and ultra high strength steels, which requires higher press forces compared to the steel grades used up to now, has accentuated the need for being able to design the casting structure with respect to the conditions valid for each die, instead of using standard guide lines.

Many thanks to Ingrid Svensson, department of Solid Mechanics at University of Lund, Bengt Persson and Nader Asnafi, department of R&D Materials and Forming, for support and comments, Björn Axelsson, department of Virtual Verification at Volvo Cars Body Components, for introduction to the software *Ansolid* and finally Tommy Johansson and Veronica Gullberg, department of Die Design at Volvo Cars Body Components, for preparation of the solid models.

Olofström, 030917
Jörgen Larsson

3. Index

1. Summary 1
2. Preface 4
3. Index 6
4. Introduction 8
   4.1. Nomenclature 8
   4.2. Background 11
   4.3. Formulation of the problem 11
   4.4. Aim 11
   4.5. Terminology 11
   4.6. Restrictions 12
   4.7. Methodology 12
   4.8. Presentation of the principal 12
5. Description of the analyzed dies 14
6. Considered sequences during a press stroke 19
7. Derivation of analytical expressions valid for different phases during a press stroke ... 22
   7.1. Load cases when the blank holder hits the lower die - analytical expressions 22
      7.1.1. Lower die - analytical expressions (Load case I and II) 22
      7.1.2. Blank holder - analytical expressions (Load case III, IV and V) 25
   7.2. Load cases when the punch hits the blank - analytical expressions (Load case VI and VII) 31
   7.3. Load cases when the die is closed - analytical expressions 34
      7.3.1. Lower die - analytical expressions (Load case VIII, IX, X, XI, XII, XIII and XIV) 34
      7.3.2. Punch - analytical expressions (Load case XV, XVI, XVII and XVIII) 46
      7.3.3. Blank holder – analytical expressions (Load case XIX and XX) 47
8. Derivation of analytical expressions for some other situations of interest 49
   8.1. Two blanks accidentally at the same time 49
   8.2. Die on trestles (Load case XXI and XXII) 49
9. Evaluation of the analytical expressions using finite element calculations 57
   9.1. Load cases when the blank holder hits the lower die- evaluation 57
      9.1.1. Lower die – evaluation (Load case I and II) 57
      9.1.2. Blank holder – evaluation (Load case III, IV and V) 61
   9.2. Load cases when the punch hits the blank – evaluation (Load case VI and VII) 67
   9.3. Load cases when the die is closed - evaluation 69
      9.3.1. Lower die – evaluation (Load case VIII, IX, X, XI, XII, XII and XIV) 69
      9.3.2. Punch – evaluation (Load case XV, XVI, XVII and XVIII) 79
      9.3.3. Blank holder – evaluation (Load case XIX and XX) 97
   9.4. Die on trestles – evaluation (Load case XXI and XXII) 101
10. Results 105
11. Discussion 107
12. References 113
13. Mathematical appendix 115
   13.1. Part A-Plate with equally distributed load 115
   13.2. Part B-Determination of shear centre of U-shaped profiles with different lengths of the flanges 129

4. Introduction

4.1. Nomenclature

$A, B, C, D, F, G, H, I, J$	
K, L, M, R, a, b, h, l	Geometrical quantities
A_C, A_{PA}, A_{PB}	Areas projected on the horisontal plane
B_A, B_B, B_C	Wall thickness
E	Young's modulus of elasticity
F_{BH}	Applied blank holder force
F_{BH}^{A}	Blank holder force acting in region A
F_{BH}^{B}	Blank holder force acting in region B
F_{BH}^{C}	Blank holder force acting in region C
F_{BH}^{VA}	Vertical component of blank holder force acting in region A
F_{BH}^{VB}	Vertical component of blank holder force acting in region B
F_{BH}^{VC}	Vertical component of blank holder force acting in region C
F_P	Applied punch force
F_A	Punch force acting in region A
F_B	Punch force acting in region B
F_C	Punch force acting in region C
F_I	Resulting force due to shear stress
F_{VA}	Vertical component of punch force acting in region A
F_{VB}	Vertical component of punch force acting in region B
F_{VC}	Vertical component of punch force acting in region C
F_H	Horisontal component of F_A and F_B
F_1, F_2	Friction forces
H_1, H_2, H_3, H_4, H_5	Horizontal forces
I_x, I_y, I_z	Moment of inertia
I_{xy}	Product moment of area
I_1	Stress invariant
J_2	Stress deviator invariant
K_t	Torsion constant
M_{nm}, M_t, M_{xy}	Torsion moments
$M_1, M_2, M_3, M_4, M_5,$	
$M_A, M_B, M_b,$	

M_{nn}, M_{xx}, M_{yy}	Bending moments
N_1, N_2	Normal forces
P	Tension force
R_A, R_B	Reaction forces
S	Area
S_y, S_z	First area of moment
S_{ij}	Stress deviator tensor
T	Average shear stress
T_y, T_z	Resulting transversal forces
U	Internal energy
V	Volume
V_1, V_2, V_3, V_4, V_5	Vertical forces
W	Mass
Q	Force per unit length
e_y, e_z	Coordinates defining the location of shear center
g	Acceleration of gravity
k, m	Parameters in Drucker - Prager yield criteria
n, n_A, n_B, n_C	Numbering of different items in die
t	Thickness of casting at the forming areas
t_b	Thickness of blank
q	Force per unit area
u_z	Displacement
u, w	Deflections
x, y, z	Coordinates
y_{tp}, z_{tp}	Coordinates center of mass
$\mathbf{K}$	Stiffness matrix
$\mathbf{N}$	Global shape functions
$\mathbf{a}$	Nodal value vector
$\mathbf{C}$	Element specific matrix
$\mathbf{D}$	Constitutive matrix
$\mathbf{f}_b$	Boundary vector
$\mathbf{f}_l$	Load vector
$\mathbf{n}, \mathbf{m}$	Normal vectors
$\boldsymbol{\alpha}$	Coefficient vector

α, β	Angles defining V - shape
δ	Deflection due to torsion
δ_{ij}	The Kronecker delta
$\varepsilon_x, \varepsilon_z$	Strains
φ	Angle of twist
μ	Friction coefficient
ν	Poisson's ratio
ρ	Density
σ	Stress in blank
σ_{ij}	Stress tensor
σ_t	Tensile yield stress
σ_c	Compressive yield stress
σ_W	Stress in wall
σ_{WA}	Stress in wall located in region A
σ_{WB}	Stress in wall located in region B
σ_{WC}	Stress in wall located in region C
$\sigma_1, \sigma_2, \sigma_3$	Principal stresses

4.2. Background

Parts made of steel sheet in car bodies are stamped in a press line, which consists of 5 to 6 presses in a row. In each press a die, with a weight from a few tons to up to 40 tons, is fastened. When the blank passes through the press line, it successively becomes more and more refined. Handling of the part between the presses is operated by special loading/unloading devices. Typically a part is run in the following order:

- Deep drawing- the part obtains the most of its final shapes.
- Trimming and piercing- the contours are trimmed and holes are pierced
- Flanging- the boundary of the part is bent as a pre-operation to subsequent hemming.
- Restrikeing- certain areas with narrow tolerance are calibrated.

Depending on the shape of the part, numerous combinations of the scheme above occurs.

This thesis deals with the casting structure in draw dies and how to find expressions to design the structure with respect to the actual conditions. Today the die casting guide lines are based on estimations and experience without any considerations to shape, size or material quality of the part. There are two reasons to design the die more individually. Firstly, there is a potential for a cost saving if it turns out to be possible to reduce the dimensions. However, compared to other costs in connection to die manufacturing, the potential cost saving related to casting is rather small. Secondly, the increased use of high strength steel and ultra high strength steel requires considerable higher press forces compared to those used so far, which means that it is not possible to fully rely on the present guide lines.

4.3. Formulation of the problem

During a press stroke the stress in an arbitrary point varies with time, since the forming process represents a complicated contact problem. Together with the fact that each die has its unique design, it is realised that it is fully impossible to derive expressions that are valid for all dies in all areas at every instant. The problem lies in how to divide the press cycle into representative time intervals and for each time interval derive those expressions that reflect the situation for some typical shapes of dies. Analytical modelling implies that three dimensional problems are converted into two dimensions, provided that certain conditions are fulfilled. Such conditions apply for thin walled structures and bodies where one dimension is large compared to the others. It shall be investigated whether such conditions are applicable for draw dies.

4.4. Aim

The aim is to derive analytical expressions, which will allow the die designer to dimension the casting structure during the design. Based on input such as punch force, blank holder force, allowed stresses and deflections, size of the part and geometrical quantities, dimensions of the casting structure are calculated. FE-calculations are performed in order to make **comparisons** with the analytical expression to verify their validity. If the derived expressions turn out to be useable, they are preferably incorporated in a program which handles the calculations.

4.5. Terminology

- **Flat die** - Die used to form parts, which approximately can be described as flat, for instance a roof (see Figure 5.1-5.3).

- **Forming area** - Area, located in lower die and punch, where forming of the blank take place. Corresponds to the areas indicated in Figure 5.2 and 5.5.
- **V-shaped die** - Die used to form parts, which approximately can be described with a V-shape, for instance a trunk lid (see Figure 5.4-5.6).
- **Flat bottomed V-shaped die –** Same as V-shaped die, except from the bottom, which is flat (see Figure 4.5.1)

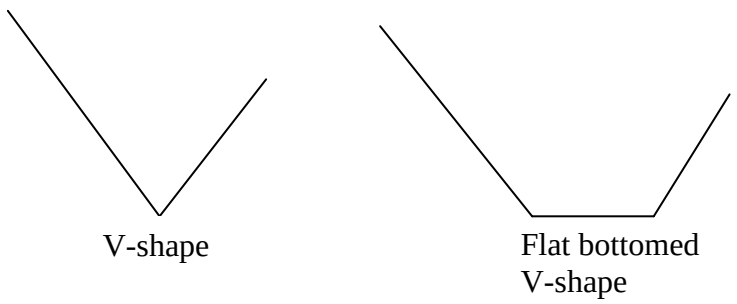

Figure 4.5.1. Schematic cross sections of V-shaped and flat bottomed V-shaped lower die.

4.6. Restrictions

In many cases holes are made in the walls in the casting structure in order to reduce the weight. In this work no notice has been taken to this, i.e. the walls are considered homogeneous.

4.7. Methodology

The analytical expressions are derived in section 7 and 8. The final expressions for each load case are framed. In section 9 the validity of the analytical expressions are evaluated. Geometrical data from dies are inserted in the analytical expressions and the result is compared to finite element calculations. This is done for different load cases and different dies. Directly after each comparison a discussion follows concerning that specific case. Throughout this work the *Catia* built-in finite element code *Ansolid* has been used, which requires models made as exact solids.

4.8. Presentation of the principal

Volvo Cars Body Components, VCBC, has long experience in tool design, sheet forming, experimental research, and finite element sheet forming simulation. The steel stamping industry in Olofström began in 1735. The many streams in the area constituted a natural power source for the stamping operations. Here the metal body components for Volvo's first car, "Jakob", were manufactured. 1969 Volvo Car Corporation purchased the plants in Olofström and today VCBC, with about 2500 employees, is *Volvo Cars Centre of Excellence for Forming of Metallic Materials*.

5. Description of the analyzed dies

There are not two draw dies that look exactly the same. The shape of the stamped part decides the shape of the draw die. Two dies with totally different shape were studied- one die with flat cross section, a roof, and one die with V-shaped cross section, a trunk lid. Common to all draw dies is that they consist of three parts- blank holder, punch and matrix. The parts of the flat die and V-shaped die are shown in figure 5.1-5.6. A press consists, roughly spoken, of one bolster on which the matrix is fastened and two different moveable slides. The punch is fastened in the inner slide and the blank holder is fastened in the outer slide. The fastening is mostly done using bolt and spacer, which are fastened in the U shaped cut-outs along the sides shown in the figure 5.1 –5.3. Some kind of guiding between the die parts is required. The two most common variants are guide pillars and wear plates. In case of draw dies wear plates, which are plates made of brass with graphite inserts, are used. The wear plates are used to guide the punch relative the blank holder as well as the blank holder relative to the matrix. The positions of the wear plates in the flat punch are indicated in figure 5.2. The blank holder clamps the blank against the matrix during forming whilst the milled contour in the punch and matrix determine the shape of the stamped part. In order to keep the gap between the blank holder and matrix under control distance plates are used. The distance plates in the V-shaped matrix are marked out in figure 5.4. At corresponding positions distance plates also are mounted in the blank holder. The flat die assembled is shown in figure 5.7.

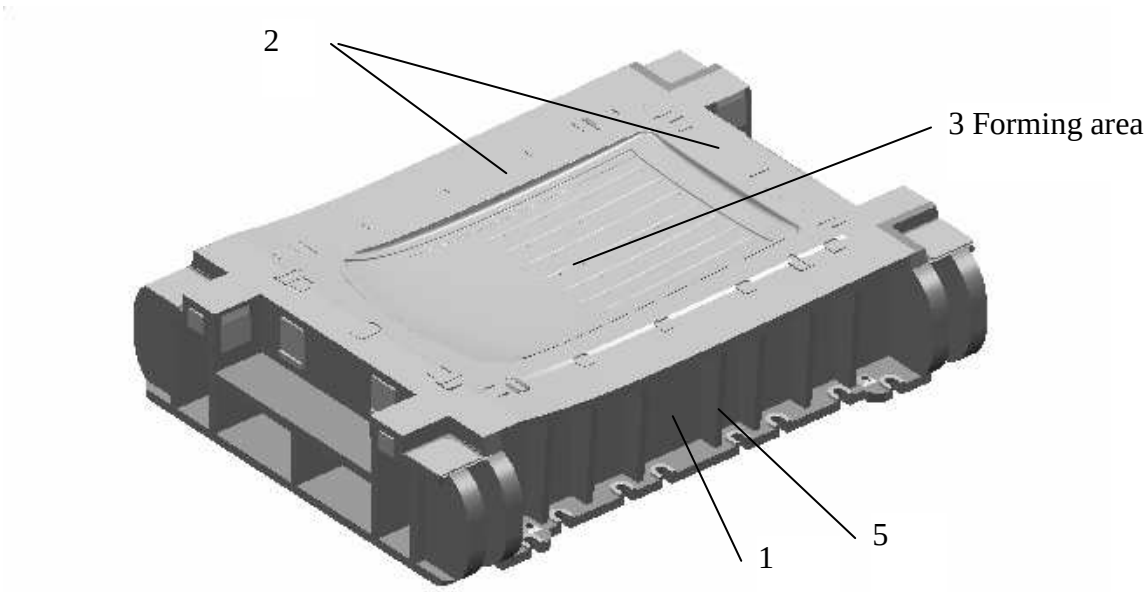

Fig. 5.1.Flat lower die

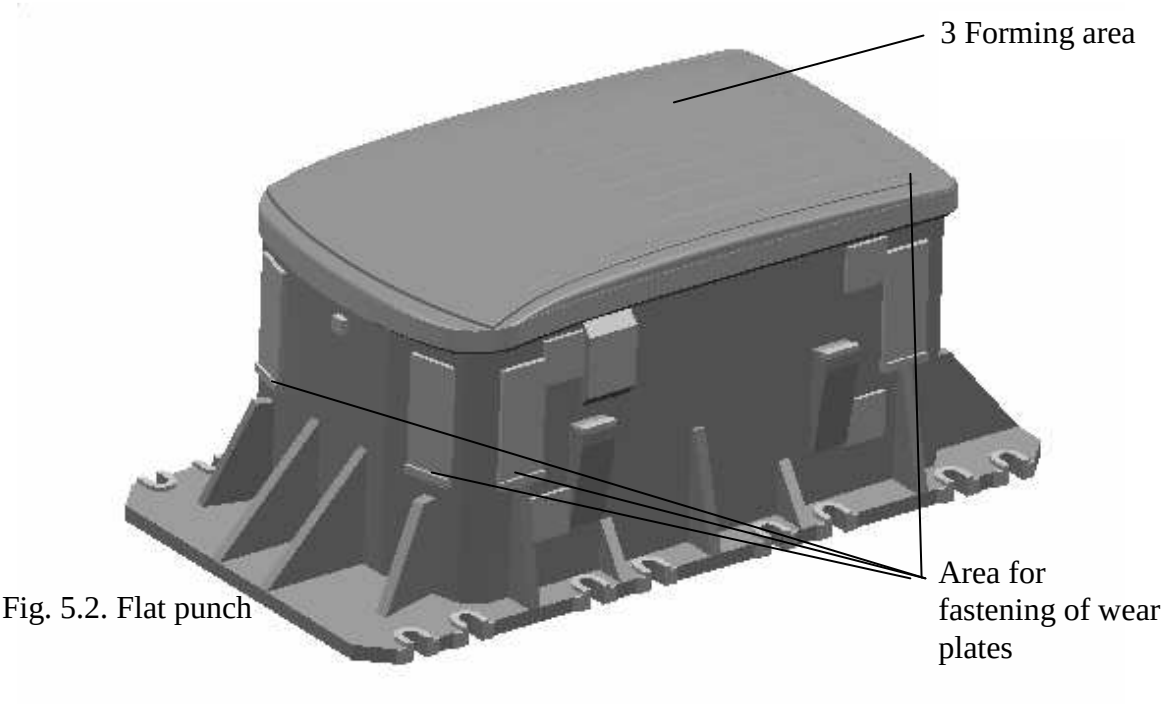

Fig. 5.2. Flat punch

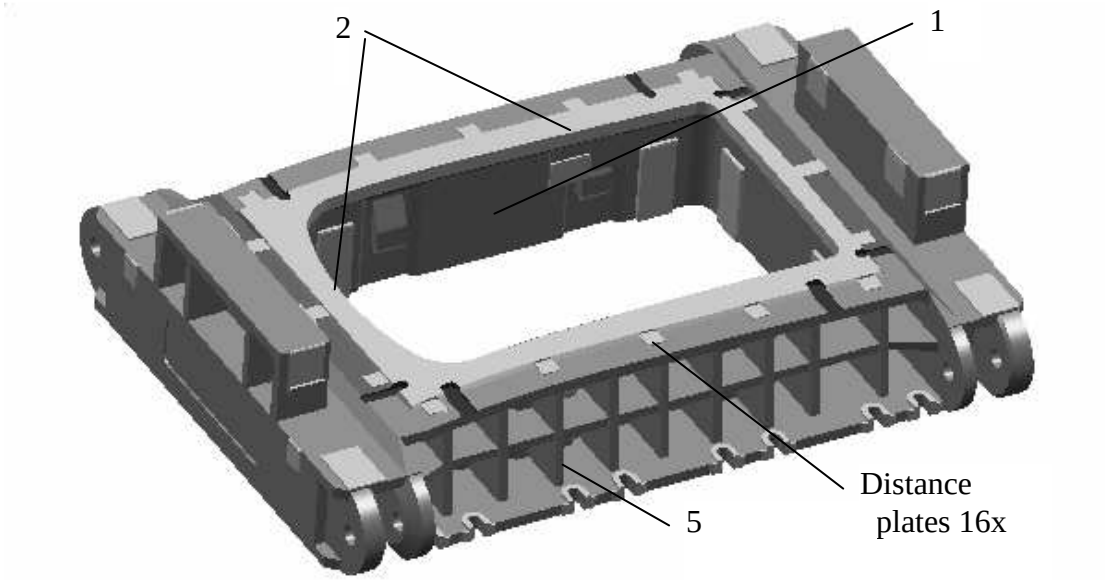

Fig. 5.3. Flat blank holder

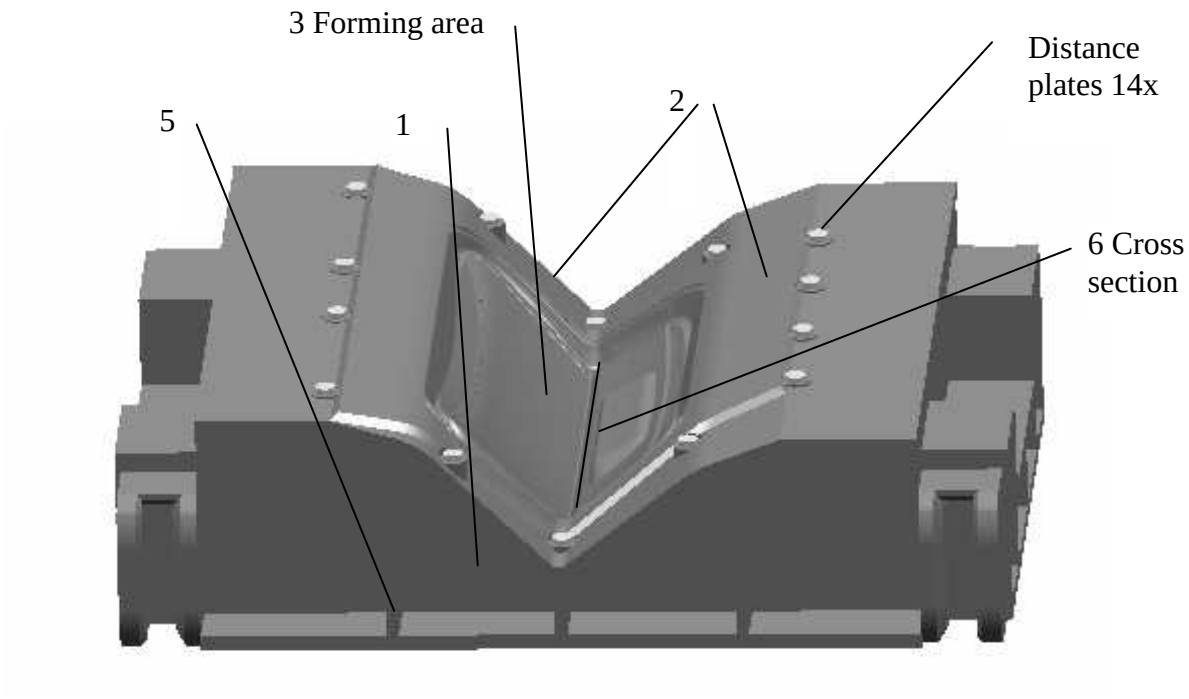

Fig. 5.4. V-shaped lower die

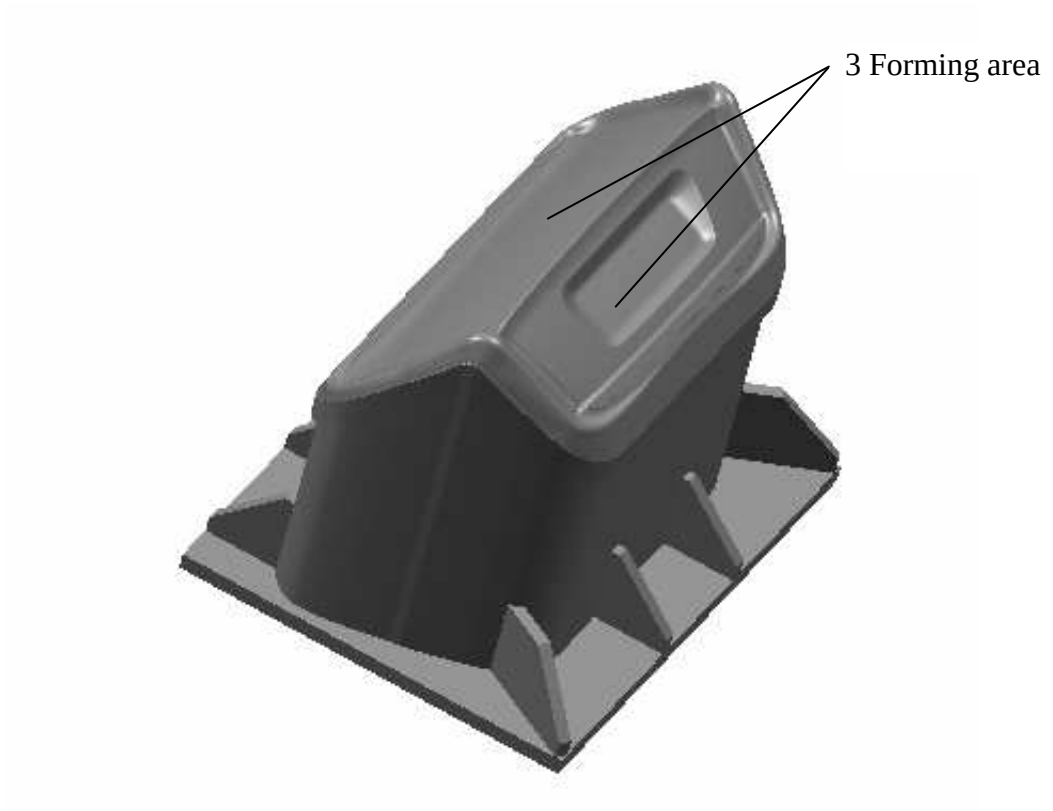

Fig. 5.5. V-shaped punch

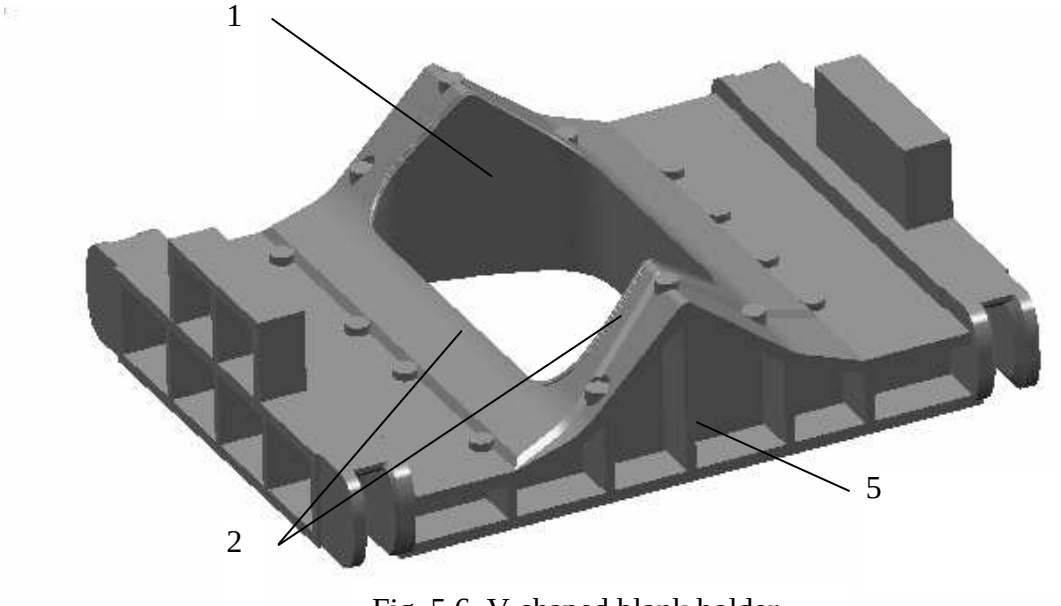

Fig. 5.6. V-shaped blank holder

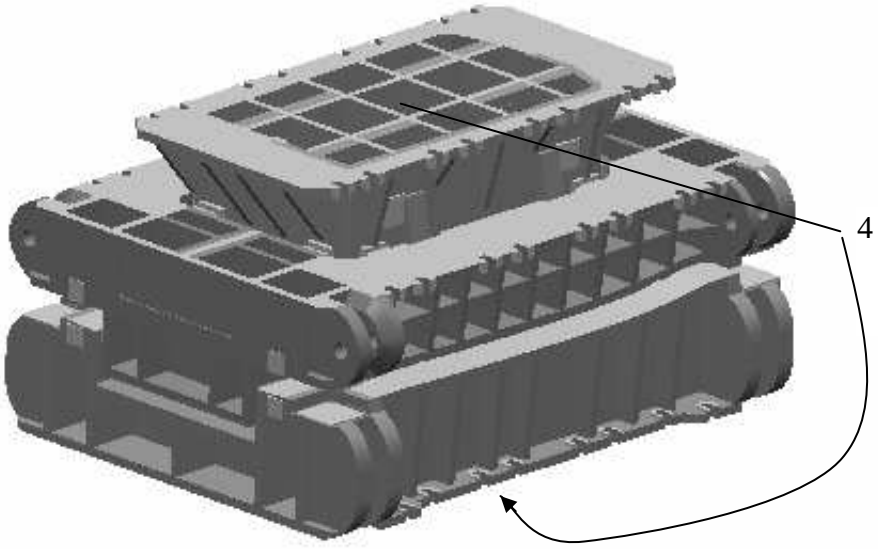

Fig. 5.7. Flat die assembled

6. Considered sequences during a press stroke

The numbering of the areas mentioned below refers to Figure 5.1-5.7 and will do so throughout this report.

During a stroke the stresses vary with time. It is not sure that all areas in the casting structure experiences their maximum load at the same instance. As far as the derivation of analytical expressions concerns, the problem lies in how to choose representative sequences and within each sequence, derive expressions covering that area exposed to the highest stress.

The blank holder and punch are mounted on two separate synchronised slides. During a stroke from the maximum open position the blank holder starts to move down. After a while also the punch starts to move down. The first contact with the blank occurs when the blank holder deforms the blank into the draw beads. A draw bead, shown in figure 7.1, is a kind of obstacle, which prevents material to flow into the forming area in order to avoid wrinkles and assure stretching. This sequence assumes mainly affect the walls denoted 1.

After the blank has been deformed into the draw beads the blank holder continues until the distance plates meet. Thereafter the punch hit the blank and the forming takes place. In the beginning of the forming, the forces acting in the blank are assumed to have a direction towards the centre of the die (see Figure 7.2.1). The areas denoted 2, are dimensioned according to this load case.

When die is near to be closed the final shape of the part is finished. At this stage a large punch force is required, since all small radii and curvatures are formed. This affects the forming areas denoted 3 and the walls denoted 4. In addition the distance plates in lower die and blank holder are in contact, which means that the walls denoted 1 and 5 are subjected to compression. Regarding V-shaped dies, the area denoted 6, is subjected to tensile stresses.

Table 6.1 shows a summing-up over the sequences mentioned above:

Sequence	Area	Load	Items considered
The blank holder hits the lower die	1	Compression	Lower die / Blank holder
The punch hits the blank	2	Bending	Lower die / Blank holder
The die is closed	3 4 1, 5 6	Bending Compression Compression Tension	Lower die / Punch Lower die / Punch Lower die / Blank holder V-shaped lower die

Table 6.1.

Based on Table 6.1, Table 6.2 shows an overview of the load cases treated in Section 7. Load cases XX and XXI, die on trestles, are derived in section 8.

Load case	Die	Die item	Area	Sequence
I	V-shaped	Lower die	1	The blank holder hits the lower die

II	Flat	Lower die	1	The blank holder hits the lower die
III	V-shaped	Blank holder	1	The blank holder hits the lower die
IV	Flat	Blank holder	1	The blank holder hits the lower die
V	Flat	Blank holder	2	The blank holder hits the lower die (Die in single acting press with blank holder on nitrogen springs)
VI	Flat	Lower die + blank holder	2	The punch hits the blank
VII	V-shaped	Lower die + blank holder	2	The punch hits the blank
VIII	V-shaped	Lower die	6	The die is closed
IX	V-shaped	Lower die	4	The die is closed
X	V-shaped	Lower die	1,5	The die is closed
XI	V-shaped	Lower die	3	The die is closed
XII	Flat	Lower die	4	The die is closed
XIII	Flat	Lower die	1,5	The die is closed
XIV	Flat	Lower die	3	The die is closed
XV	V-shaped	Punch	4	The die is closed
XVI	V-shaped	Punch	3	The die is closed
XVII	Flat	Punch	4	The die is closed
XVIII	Flat	Punch	3	The die is closed
XIX	V-shaped	Blank holder	1,5	The die is closed
XX	Flat	Blank holder	1,5	The die is closed
XXI	V-shaped	Lower die		Die on trestles
XXII	Flat	Lower die		Die on trestles

Table 6.2.

7. Derivation of analytical expressions valid for different phases during a press stroke

In the following section analytical expressions for different sequences are derived.

7.1. Load cases when the blank holder hits the lower die - analytical expressions

In this section load cases are treated, which are assumed to reflect what happens when the blank holder and the lower die initially get in contact. The force transmission is entirely covered by considering the deformation of the blank into the draw-bead. See Figure 7.1. The load of the blank holder is equally distributed over the draw beads.

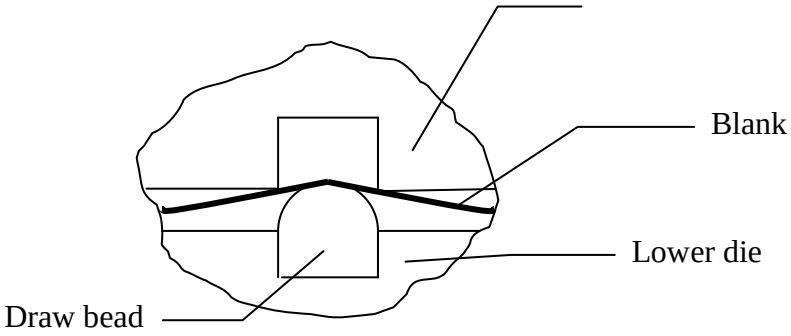

Fig. 7.1. Schematic view of draw bead area in the moment the blank holder hits the blank.

7.1.1. Lower die - analytical expressions (Load case I and II)

The parameter of interest is the stress in the walls beneath the draw beads. The area the load is distributed over is defined as the cross section of the wall beneath the draw beads. Expressions for calculating the stress in V-shaped lower dies as well as in flat lower dies are derived.

Load case I, Area 1

Figure 7.1.1.1 shows a V-shaped lower die where the walls under the draw beads are indicated by a thick line. Only the vertical stress component is considered. The horizontal stress component, giving rise to a force trying to tear the lower die apart, is neglected compared to the horizontal force due to the punch load, which is derived in section 7.3.1.

It is shown in section 7.3.1, see (7.3.1.6), (7.3.1.27) and (7.3.1.28), that the expressions for the vertical force components in a die with **flat bottomed V-shape**, with designations from Figure 7.3.1.1, read

$$F_{BH}^{VA} = F_{BH}^{A} \sin\alpha = \frac{F_{BH} \cos\beta \sin\alpha (A \sin\alpha - B \sin\beta)}{A\cos\beta + C\cos\beta\sin\alpha - B\cos\alpha - C\cos\alpha\sin\beta} \tag{7.1.1.1}$$

$$F_{BH}^{VB} = F_{BH}^{B} \sin\beta = \frac{F_{BH} \cos\alpha \sin\beta (A \sin\alpha - B \sin\beta)}{A\cos\beta + C\cos\beta\sin\alpha - B\cos\alpha - C\cos\alpha\sin\beta} \tag{7.1.1.2}$$

$$F_{BH}^{VC} = F_{BH}^{C} = F_{BH} \frac{A\cos\beta\cos^2\alpha + B\cos\beta\sin\alpha\sin\beta - A\cos\alpha\sin\alpha\sin\beta - B\cos^2\beta\cos\alpha - C(\sin\beta\cos\alpha - \sin\alpha\cos\beta)}{A\cos\beta + C\sin\alpha\cos\beta - B\cos\alpha - C\sin\beta\cos\alpha} \tag{7.1.1.3}$$

where F_{BH} denotes the blank holder force, F_{BH}^{VA}, F_{BH}^{VB} and F_{BH}^{VC} denotes the resulting vertical forces acting on the surfaces with lengths *A*, *B* and *C* in Figure 7.3.1.1, α and β denotes the angles defining the V-shape in Figure 7.3.1.1. Using Figure 7.1.1.1, where *L* denotes the wall thickness and *I*, *J*, *K*, *H* and *M* defines the regions the blank holder load is distributed over, the expressions for the compressive stress in the walls read

$$\boxed{\sigma_{WA} = \frac{F_{BH}^{VA}}{(2H+I)L} = \frac{F_{BH} \cos\beta \sin\alpha (A \sin\alpha - B \sin\beta)}{(A\cos\beta + C\cos\beta\sin\alpha - B\cos\alpha - C\cos\alpha\sin\beta)} \frac{1}{(2H+I)L}} \tag{7.1.1.4}$$

$$\boxed{\sigma_{WB} = \frac{F_{BH}^{VB}}{(2K+J)L} = \frac{F_{BH} \cos\alpha \sin\beta (A \sin\alpha - B \sin\beta)}{A\cos\beta + C\cos\beta\sin\alpha - B\cos\alpha - C\cos\alpha\sin\beta} \frac{1}{(2K+J)L}} \tag{7.1.1.5}$$

$$\boxed{\sigma_{WC} = \frac{F_{BH}^{C}}{2ML} = \left(\frac{A\cos\beta\cos^2\alpha + B\cos\beta\sin\alpha\sin\beta - A\cos\alpha\sin\alpha\sin\beta}{A\cos\beta + C\sin\alpha\cos\beta - B\cos\alpha - C\sin\beta\cos\alpha} + \frac{-B\cos^2\beta\cos\alpha - C(\sin\beta\cos\alpha - \sin\alpha\cos\beta)}{A\cos\beta + C\sin\alpha\cos\beta - B\cos\alpha - C\sin\beta\cos\alpha} \right) F_{BH} \frac{1}{2ML}} \tag{7.1.1.6}$$

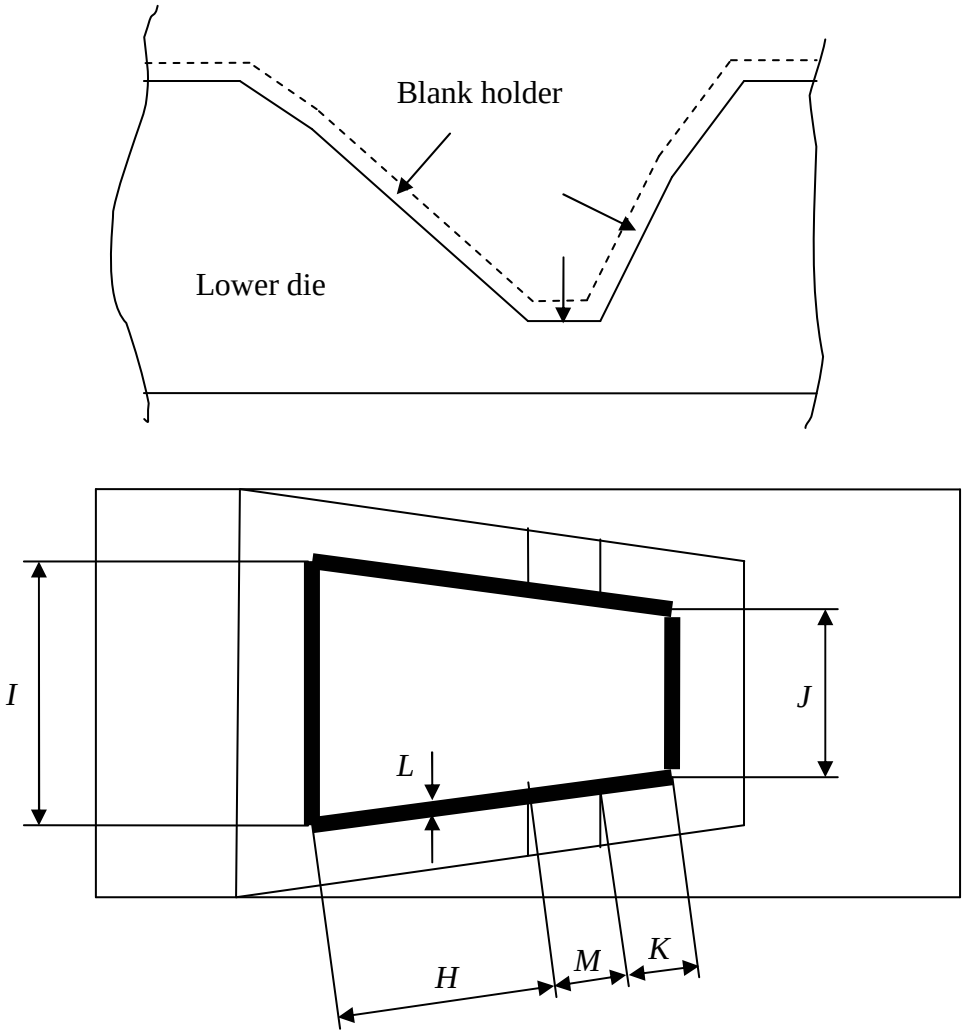

Fig. 7.1.1.1. Draw bead area in V-shaped lower die

Regarding dies with **V-shape**, i.e. the corresponding expressions from section 7.3.1, see (7.3.1.29) and (7.3.1.30), read

$$F_{BH}^{VA} = F_{BH}^{A} \sin\alpha = F_{BH} \cos\beta \sin\alpha / (\cos\alpha \sin\beta + \cos\beta \sin\alpha) \tag{7.1.1.7}$$

$$F_{BH}^{VB} = F_{BH}^{B} \sin\beta = F_{BH} \cos\alpha \sin\beta / (\cos\alpha \sin\beta + \cos\beta \sin\alpha) \tag{7.1.1.8}$$

$$\boxed{\sigma_{WA} = \frac{F_{BH}^{VA}}{(2H+I)L} = \frac{F_{BH} \cos\beta \sin\alpha}{(\cos\alpha \sin\beta + \cos\beta \sin\alpha)} \frac{1}{(2H+I)L}} \tag{7.1.1.9}$$

$$\boxed{\sigma_{WB} = \frac{F_{BH}^{VB}}{(2K+J)L} = \frac{F_{BH} \cos\alpha \sin\beta}{(\cos\alpha \sin\beta + \cos\beta \sin\alpha)} \frac{1}{(2K+J)L}} \tag{7.1.1.10}$$

In the deriving of the expressions in this section it has been assumed that only one stress component exists and that this component is acting vertically. σ_{WA}, σ_{WB} and σ_{WC} are assumed to be constant within their respective areas and it has also been assumed that the load is equally distributed over each of the areas covered by the expressions for the different stresses.

Load case II, Area 1

Regarding flat dies, the form surfaces including the draw bead areas are flat, which means that the whole load from the blank holder is transmitted in the vertical direction. Figure 7.1.1.2 shows an upper view of a lower die with the wall under the draw beads indicated by thicker lines.

Under assumption that the blank holder load is equally distributed over the draw beads the expression for the compressive wall stress reads

$$\boxed{\sigma_W = \frac{F_{BH}}{2L(I+J)}} \qquad (7.1.1.11)$$

where the thickness of the walls are constant equal to L and the lengths the blank holder load is distributed over are designated I and J. In this case the shape of the walls, over which the load is distributed, for simplicity, has been assumed to be rectangular.

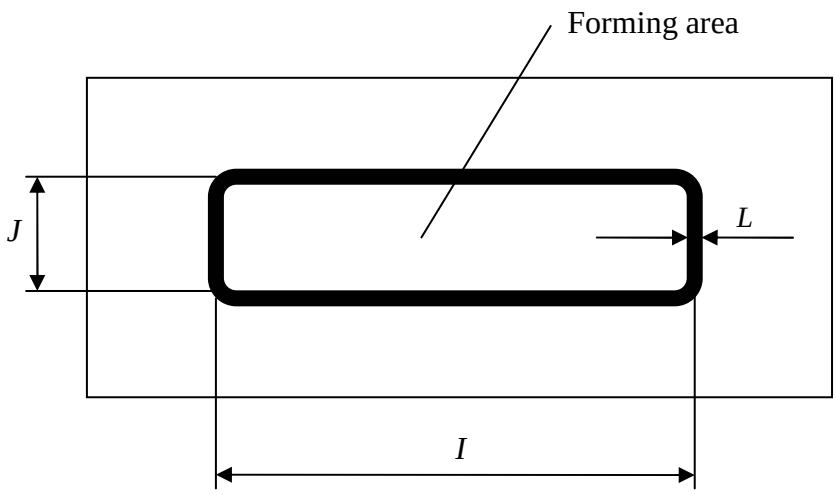

Figure 7.1.1.2. Upper view of flat lower die.

7.1.2. Blank holder - analytical expressions (Load case III, IV and V)

The situation is the same as for the lower die, i.e. the stress due to the deformation of the blank into the draw bead is of interest and the load is equally distributed over cross section of the walls beneath the draw beads. Expressions for the stresses in V-shaped blank holders as well as in flat blank holders are derived. In the case of flat blank holders another expression is derived, namely that which allows for calculating the deflection due to torsion when the die is run in a single acting press.

Load case III, Area 1

Figure 7.1.1.1 is applicable in the blank holder case as well, provided that the direction of the load is altered. Instead of horizontal forces trying to tear the lower die apart compressive forces are acting in the blank holder. However, just as in the case of the lower die, only the vertical stress components are considered.

With reference to what has been mentioned above, the expressions for the stresses in a flat bottomed V-shaped blank holder are the same as for the lower die, i.e. (7.1.1.4), (7.1.1.5) and (7.1.1.6). If the blank holder is V-shaped (7.1.1.9) and (7.1.1.10) are applicable.

Draw dies can be run in two different kinds of presses, double action and single action presses. A double action press consists of to separately moveable slides, the punch slide and the blank holder slide, whilst a single action press only has one slide. In a double acting press the lower die is fastened at the bolster, the punch in the punch slide and the blank holder in the blank holder slide. In a single acting press the die is run upside-down, meaning that the lower die is fastened at the slide and the punch is placed at the bolster together with the blank holder, which is placed on nitrogen springs or air cushion pins. Double action presses is most commonly used. In the different load cases treated in this work, it is of no importance which type of press used, except in the load case when the blank holder hits the lower die, which is covered later in this section regarding flat dies. The two ways to run a press die, applies irrespective if the dies are V-shaped or flat, but within the frame of this work, only flat dies are treated.

Load case IV, Area 1

If the die is run in a double acting press, the load is assumed to be transmitted solely in the vertical direction, just as in a flat lower die. Figure 7.1.1.2 is applicable for flat blank holders as well. The only difference is that the forming area is to be replaced with a cut out, to allow for the punch movement and consequently (7.1.1.11) will be used for this load case as well.

Load case V, Area 2

Regarding dies run in single acting presses, Figure 7.1.2.1 shows a typical blank holder.

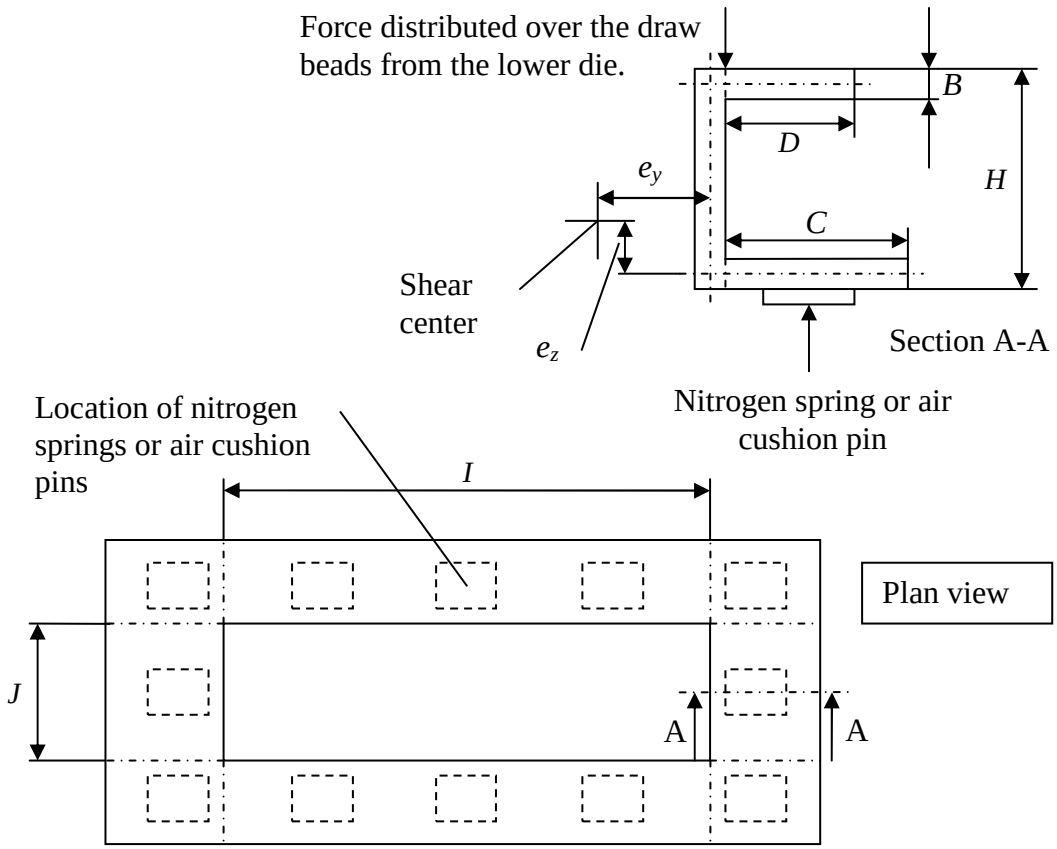

Figure 7.1.2.1. Blank holder used in single acting presses.

Before a closer investigation of this load case is done the concepts of *shear center* and *center of twist* shall be defined.

The center of twist (CT) is the position about which the cross section rotates due to application of a twisting moment.

(7.1.2.1)

The shear center (SC) is the position where application of a transverse load creates no torsion of the beam.

(7.1.2.2)

It can also be shown that for linear elastic materials the *shear center* and *center of twist* coincide [1].

For a U-shaped cross section, shown in Figure 7.1.2.1, the shear center is located to the left of the waist. This is confirmed in Figure 7.1.2.2 showing a U-shaped profile with one end clamped and the other end free. The load located close to the center line of the waist, as indicated, clearly gives rise to a clock wise twisting moment.

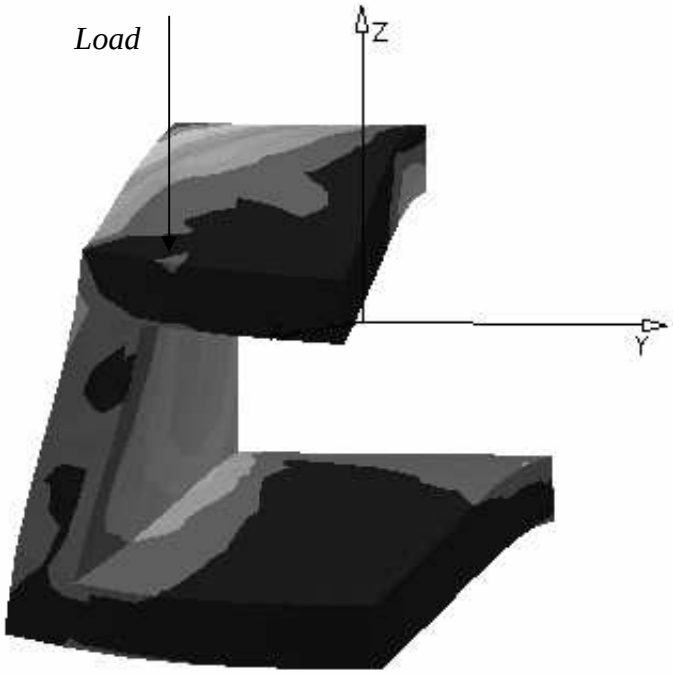

Figure 7.1.2.2. U-shaped profile loaded vertically with one end clamped and the other end free.

Also if the U-shaped profile is clamped in both ends the tendency of twisting is present, as seen in Figure 7.1.2.3. The load is applied equally distributed along the whole length at the position indicated.

To deal with U-shaped cross sections loaded transversal, it seems to be of interest to be able to determine the position of the shear center. The derivation of the location of the shear center is done in part B of the mathematical appendix and the result, with designations from Figure 7.1.2.1, reads

$e_y =$

$$
\begin{aligned}
&3\,(-H+B)\,(2\,\mathrm{D}+B)^2\,(-2\,C^4\,H+2\,C^4\,B+4\,H\,B\,C^3-4\,C^3\,H^2+6\,\mathrm{D}\,H\,C^2\,B \\
&\quad -2\,C^2\,B^2\,\mathrm{D}-2\,H\,C^2\,\mathrm{D}^2-8\,H^2\,C^2\,B-4\,\mathrm{D}\,H^2\,C^2+8\,C^2\,B^2\,H+2\,B\,C^2\,\mathrm{D}^2 \\
&\quad +4\,C\,B^2\,\mathrm{D}\,H+7\,C\,H\,B^3-2\,C\,\mathrm{D}^2\,H\,B-7\,C\,B^2\,H^2-4\,C\,H^2\,\mathrm{D}\,B+2\,C\,B^2\,\mathrm{D}^2 \\
&\quad -B^2\,H^3+B^3\,\mathrm{D}\,H+B^3\,H^2-\mathrm{D}\,B^2\,H^2)\,/\,(4\,(-72\,H^2\,C^2\,B^2\,\mathrm{D}-36\,H^2\,C^2\,\mathrm{D}^2\,B \\
&\quad +36\,H^3\,C\,\mathrm{D}^2\,B-72\,H^2\,C\,\mathrm{D}^2\,B^2+48\,H^3\,C\,\mathrm{D}\,B^2-24\,H^2\,C^3\,\mathrm{D}\,B-24\,H^2\,C\,B\,\mathrm{D}^3 \\
&\quad +36\,H^3\,\mathrm{D}\,C^2\,B-24\,B\,C\,H\,\mathrm{D}^4+42\,B^3\,C^2\,\mathrm{D}\,H+18\,B^2\,C^2\,\mathrm{D}^2\,H+42\,B^3\,C\,H\,\mathrm{D}^2 \\
&\quad -96\,B^3\,C\,\mathrm{D}\,H^2+16\,B^2\,C^3\,\mathrm{D}\,H-24\,B\,C^4\,\mathrm{D}\,H+16\,B^2\,C\,H\,\mathrm{D}^3+7\,H^4\,C\,B^2 \\
&\quad +12\,H^2\,C\,\mathrm{D}^4+12\,H^2\,C^4\,\mathrm{D}-6\,H^2\,C^4\,B+16\,H^3\,C\,\mathrm{D}^3+6\,H^4\,C^2\,B+6\,H^4\,\mathrm{D}^2\,B \\
&\quad +7\,H^4\,\mathrm{D}\,B^2+16\,H^3\,C^3\,\mathrm{D}+12\,H^3\,C^2\,\mathrm{D}^2-6\,B^3\,C\,H^3+6\,B^3\,C^3\,H+7\,B^2\,C^4\,H \\
&\quad -6\,B\,H^2\,\mathrm{D}^4-6\,B^3\,H^3\,\mathrm{D}+7\,H\,\mathrm{D}^4\,B^2-2\,C^2\,B^2\,\mathrm{D}^3+17\,C\,B^2\,\mathrm{D}^4+17\,\mathrm{D}\,B^2\,C^4 \\
&\quad -2\,\mathrm{D}^2\,B^2\,C^3+4\,H^3\,C^4+4\,B^4\,H\,\mathrm{D}^2+4\,B^4\,\mathrm{D}\,H^2+B^2\,\mathrm{D}^5+6\,H\,\mathrm{D}^3\,B^3+H^5\,B^2 \\
&\quad +4\,H^3\,\mathrm{D}^4+4\,H^4\,C^3+4\,H^4\,\mathrm{D}^3+56\,C\,B^4\,\mathrm{D}\,H+B^2\,C^5+4\,C^2\,B^4\,H+4\,C\,B^4\,H^2))
\end{aligned}
\tag{7.1.2.3}
$$

$e_z =$

$$
\begin{aligned}
&1\,(-H+B)\,(2\,\mathrm{D}+B)^2\,(B^3\,\mathrm{D}^2+C^2\,B^3+3\,C^3\,B^2+14\,C\,\mathrm{D}\,B^3-4\,H^4\,\mathrm{D}-\mathrm{D}^3\,B^2 \\
&\quad -C^2\,B^2\,\mathrm{D}-17\,C\,B^2\,\mathrm{D}^2-16\,C\,H^3\,\mathrm{D}+B^3\,\mathrm{D}\,H-17\,C\,H\,B^3-40\,C\,B^2\,\mathrm{D}\,H \\
&\quad +36\,C\,H^2\,\mathrm{D}\,B+24\,C\,\mathrm{D}^2\,H\,B-6\,H^3\,C^2-4\,H^3\,\mathrm{D}^2-2\,H^4\,B-9\,C^2\,B^2\,H \\
&\quad +30\,C\,B^2\,H^2-14\,C\,B\,H^3-12\,C\,\mathrm{D}^2\,H^2+18\,H^2\,C^2\,B+6\,\mathrm{D}^2\,H^2\,B-7\,H\,\mathrm{D}^2\,B^2 \\
&\quad -6\,\mathrm{D}\,B^2\,H^2+4\,\mathrm{D}\,B\,H^3)\,/\,(4\,(-72\,H^2\,C^2\,B^2\,\mathrm{D}-36\,H^2\,C^2\,\mathrm{D}^2\,B+36\,H^3\,C\,\mathrm{D}^2\,B \\
&\quad -72\,H^2\,C\,\mathrm{D}^2\,B^2+48\,H^3\,C\,\mathrm{D}\,B^2-24\,H^2\,C^3\,\mathrm{D}\,B-24\,H^2\,C\,B\,\mathrm{D}^3+36\,H^3\,\mathrm{D}\,C^2\,B \\
&\quad -24\,B\,C\,H\,\mathrm{D}^4+42\,B^3\,C^2\,\mathrm{D}\,H+18\,B^2\,C^2\,\mathrm{D}^2\,H+42\,B^3\,C\,H\,\mathrm{D}^2-96\,B^3\,C\,\mathrm{D}\,H^2 \\
&\quad +16\,B^2\,C^3\,\mathrm{D}\,H-24\,B\,C^4\,\mathrm{D}\,H+16\,B^2\,C\,H\,\mathrm{D}^3+7\,H^4\,C\,B^2+12\,H^2\,C\,\mathrm{D}^4 \\
&\quad +12\,H^2\,C^4\,\mathrm{D}-6\,H^2\,C^4\,B+16\,H^3\,C\,\mathrm{D}^3+6\,H^4\,C^2\,B+6\,H^4\,\mathrm{D}^2\,B+7\,H^4\,\mathrm{D}\,B^2 \\
&\quad +16\,H^3\,C^3\,\mathrm{D}+12\,H^3\,C^2\,\mathrm{D}^2-6\,B^3\,C\,H^3+6\,B^3\,C^3\,H+7\,B^2\,C^4\,H-6\,B\,H^2\,\mathrm{D}^4 \\
&\quad -6\,B^3\,H^3\,\mathrm{D}+7\,H\,\mathrm{D}^4\,B^2-2\,C^2\,B^2\,\mathrm{D}^3+17\,C\,B^2\,\mathrm{D}^4+17\,\mathrm{D}\,B^2\,C^4-2\,\mathrm{D}^2\,B^2\,C^3 \\
&\quad +4\,H^3\,C^4+4\,B^4\,H\,\mathrm{D}^2+4\,B^4\,\mathrm{D}\,H^2+B^2\,\mathrm{D}^5+6\,H\,\mathrm{D}^3\,B^3+H^5\,B^2+4\,H^3\,\mathrm{D}^4 \\
&\quad +4\,H^4\,C^3+4\,H^4\,\mathrm{D}^3+56\,C\,B^4\,\mathrm{D}\,H+B^2\,C^5+4\,C^2\,B^4\,H+4\,C\,B^4\,H^2))
\end{aligned}
\tag{7.1.2.4}
$$

When the expressions for the shear center were derived, the assumption was that the cross section would behave like in Figure 7.1.2.3. Here the clamped ends correspond to the location of the nitrogen springs or air cushion pins. However, during the work of this thesis the original plan to verify the analytical expressions with measurements in physical dies, was altered to verify the expressions with finite element calculations. According to the finite element calculation, presented in section 9.1.2, the sections of the blank holder twist independently, in a way corresponding to Figure 7.1.2.4, i.e. in the opposite way to what is indicated in Figure 7.1.2.3. The split lines between the sections are indicated in the plan view in Figure 7.1.2.1 together with the lengths denoted *I* and *J*. Since the input, boundary conditions and the magnitude and location of load, is user defined, an uncertainty exists of the true behavior and therefore shear center calculations is, despite the result from the finite element calculation, included in this work.

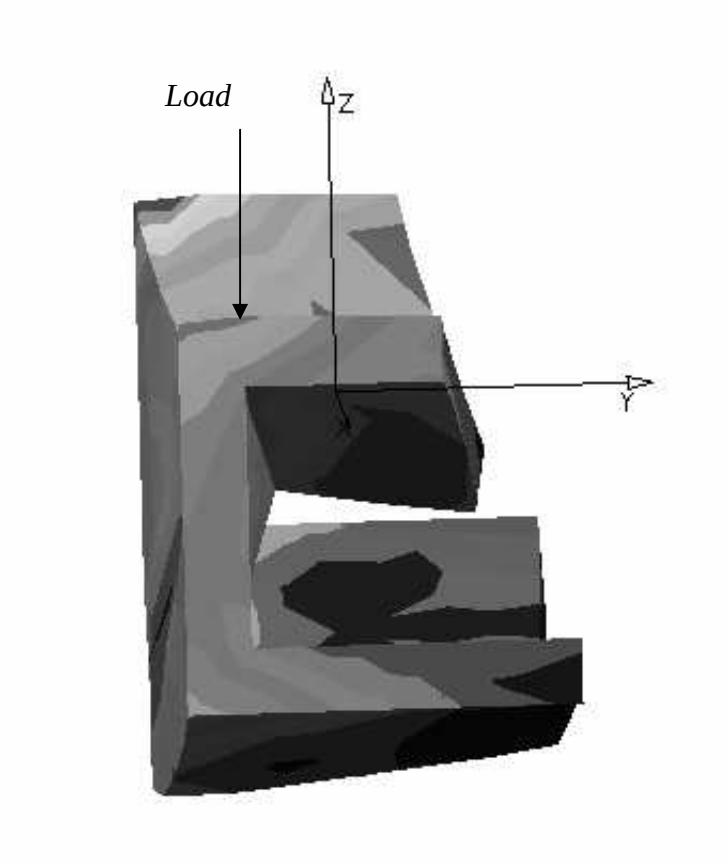

Figure 7.1.2.3. U-shaped profile loaded vertically with both ends clamped.

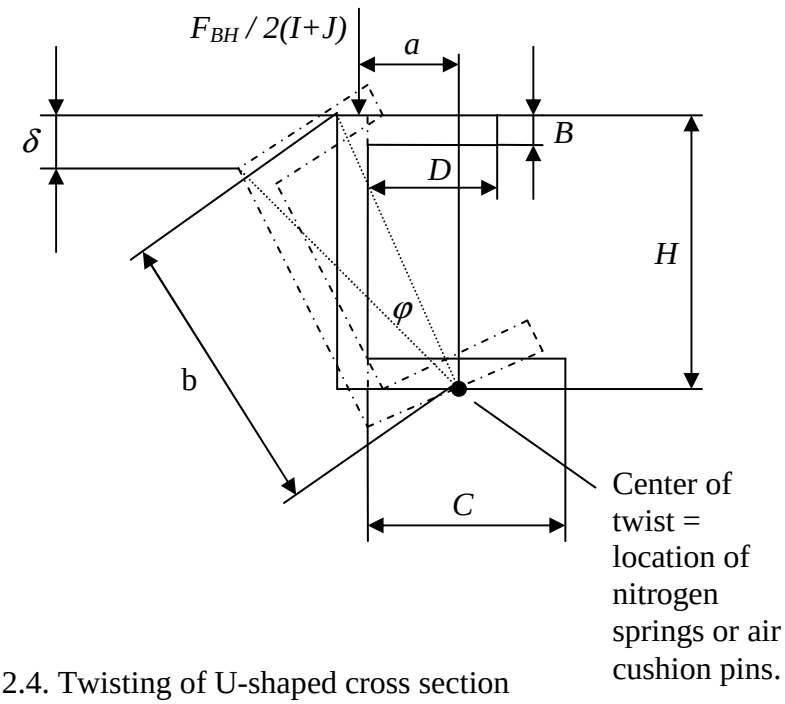

Figure 7.1.2.4. Twisting of U-shaped cross section according to finite element calculation.

Instead of using the shear center, the deflection due to torsion is calculated in the following manner. If the thickness is small compared with the width of the waist and flanges the expression for the angle of twist, φ, reads [2]

$$\varphi = \frac{2M_t(1+\nu)}{EK_t}L \tag{7.1.2.5}$$

where M_t denotes the torsion moment, L the length of the section subjected to torsion and K_t a geometric quantity, the torsion constant, which for a section consisting of n thin walled strips reads [2]

$$K_t = \frac{1}{3}\sum_{i=1}^{n} t_i^3 l_i \tag{7.1.2.6}$$

where t denotes the thickness and l the length of the strip. Assuming the side with length I in Figure 7.1.2.1, with the ends clamped, being subjected to torsion under the conditions stated in Figure 7.1.2.4, then angle of twist, in radians, at the half of the length of the section can be expressed as

$$\varphi = \int_0^{I/2} \frac{2M_t(1+\nu)}{EK} dl = \frac{(1+\nu)}{E}\frac{I}{2}\frac{F_{BH}}{(I+J)}a\frac{3}{B^3}\frac{1}{(C+D+H)} \tag{7.1.2.7}$$

It has been assumed that the torsion moment, M_t, is constant through the whole section, which implies that the section is assumed to be fully supported along the whole length at the center of twist. Finally, using geometrical arguments, the deflection δ from Figure 7.1.2.4 is calculated

$$\boxed{\delta = H - b\sin\left(\arcsin\frac{H}{b} - \frac{(1+\nu)}{E}\frac{I}{2}\frac{F_{BH}}{(I+J)}a\frac{3}{B^3}\frac{1}{(C+D+H)}\right)} \tag{7.1.2.8}$$

7.2. Load cases when the punch hits the blank - analytical expressions (Load case VI and VII)

Load case VI and VII, Area 2

In this section that load case is treated, which is assumed to reflect what is happening in that moment when the punch hits the blank. The aim is to calculate the deflection of the blank holder and the lower die due to bending forces, which arise when the blank is dragged towards the center of the die. It is assumed that the blank is clamped between the lower die and the blank holder. The force transmitted from the punch, is applied as an equally distributed force over the cross section of the blank, acting normal to this (see Figure 7.2.1).

In order to determine the deflection, indicated in section A-A in Figure 7.2.1, only the indicated geometry is considered, i.e. reinforcement walls and vertical walls are neglected. Since the distance plates are in contact, deformation arises only due to bending with respect to

the z-axis. With other words, the load case is considered as bending of a beam clamped in both ends. In [3] following expression found

$$\delta = \frac{Ql^4}{384EI_z} = \frac{\sigma t_b l^4}{384EI_z} \tag{7.2.1}$$

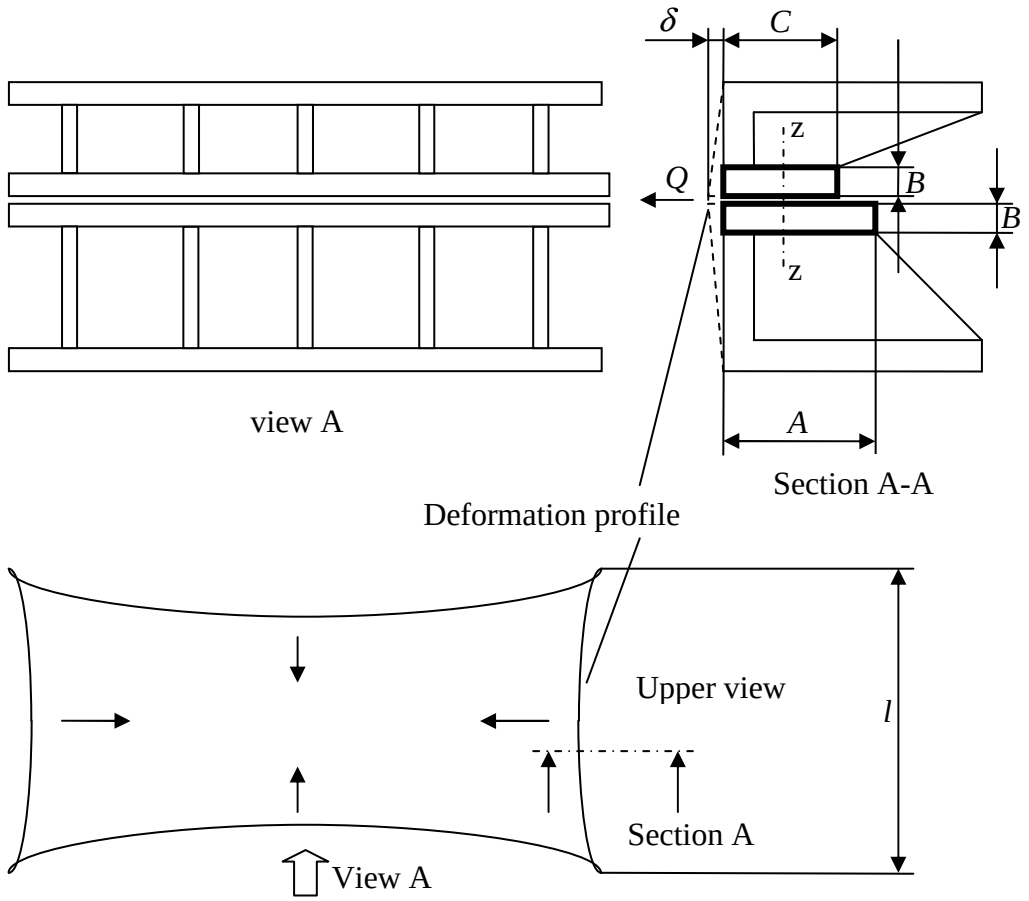

Fig. 7.2.1. Deformations in blank holder and lower die when the punch hits the blank.

Here δ denotes the deflection, Q the load per unit length, σ the yield stress of the blank, t the thickness of the blank, l the length of the section, E Youngs modulus of elasticity and I_z the moment of inertia with respect to the z-axis. See designations in Figure 7.2.1. That part of the section subjected to bending consists of two rectangular profiles. Due to the non-symmetry, the shear center does not coincide with the line of action of the applied force. The expected torsion is however prevented, since the distance plates are in contact. Besides, the torsion moment is small, since the distance between the shear center and the line of action, i.e the moment arm, is small. Under these circumstances, the parameter of interest is I_z, which is calculated by adding the contributions from the rectangular profiles. With help from (B.5) and the designations in section A-A, the moment of inertia is calculated as

$$I_z = \frac{B\left(A^3 + C^3\right)}{12} \tag{7.2.2}$$

which inserted in (7.2.1) yields

$$\delta = \frac{Ql^4}{384EI_z} = \frac{\sigma tl^4}{384EI_z} = \frac{\sigma tl^4}{32EB\left(A^3 + C^3\right)} \tag{7.2.3}$$

Regarding V-shaped profiles, by considering the two extremes shown in Figure 7.2.2, it is assumed that both the moment of inertia and the length vary sinusoidal with the angle.

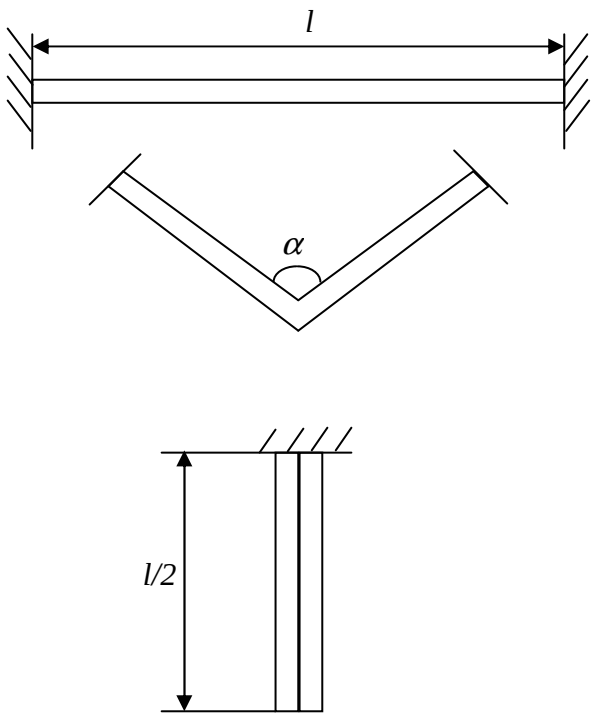

Fig. 7.2.2. Variation of geometry with angle in profile subjected to bending.

Except from that, the type of load case vary, from clamped in both ends to only one end clamped. The expression for a beam with one end free and an equally distributed load read [3]

$$\delta = \frac{Ql^4}{8EI_z} \tag{7.2.4}$$

where δ is measured at the free end. If also the transformation of the load case is assumed be sinusoidal, a suggested expression for the structure in Figure 7.2.2 reads

$$\boxed{\delta = \frac{Q\left(\frac{l}{2}\left(1+\sin\left(\frac{\alpha}{2}\right)\right)\right)^4}{\left(8+376\sin\left(\frac{\alpha}{2}\right)\right)EI_z\left(2-\sin\left(\frac{\alpha}{2}\right)\right)}} \tag{7.2.5}$$

7.3. Load cases when the die is closed - analytical expressions

In the following are load cases treated, which are assumed to reflect the situation when the die is closed or close to be. Considering the lower die, the load is transmitted from the punch and the blank holder, which are assumed to be rigid. When the punch is considered, the load is transmitted form the lower die, which in this case is assumed to be rigid. Consequently the lower die is assumed to be rigid when the blank holder is considered.

7.3.1. Lower die - analytical expressions (Load case VIII, IX, X, XI, XII, XIII and XIV)

Both the influence from the load transmitted from the blank holder and the punch are considered. The blank holder load is assumed to be equally distributed over the distance plates and so is the punch load over each area segment.

Load case VIII, Area 6 Load case IX, Area 4

In dies with V-shape forces are transmitted from the punch acting horizontally as well as vertically, the former trying to tear the lower die apart approximately at the section S-S in Figure 7.3.1.1 and the latter by compressing the walls. In the current load case only the horizontally acting forces are needed. It is firstly necessary to determine the portion of load transmitted from the upper die and secondly determine the area over which the load is distributed. To solve the first problem the section shown in Figure 7.3.1.1 is considered. Three unknowns, F_A, F_B and F_C, imply that three equations are required to solve the problem: horizontal equilibrium of forces, vertical equilibrium of forces and equilibrium of moment with point O as moment centre. It is assumed that the shape of the part is rectangular which means that the line of action of F_A, F_B and F_C is located at midpoint of A, B and C.

$$\left[\sum F_x = 0\right] \quad -F_A \cos\alpha + F_B \cos\beta = 0 \tag{7.3.1.1}$$

$$\left[\sum F_z = 0\right] \quad F_A \sin\alpha + F_C + F_B \sin\beta - F_P = 0 \tag{7.3.1.2}$$

$$\begin{aligned}\left[\sum M_O = 0\right] \; & -F_A \frac{A}{2} \\ & + F_B\left(\cos\beta\left(A\cos\alpha - B\frac{\cos\beta}{2}\right) - \sin\beta\left(A\sin\alpha + C + B\frac{\sin\beta}{2}\right)\right) \\ & - F_C\left(A\sin\alpha + \frac{C}{2}\right) + F_P\left(\frac{\mathrm{A}\sin\alpha + \mathrm{C} + B\sin\beta}{2}\right) = 0\end{aligned} \tag{7.3.1.3}$$

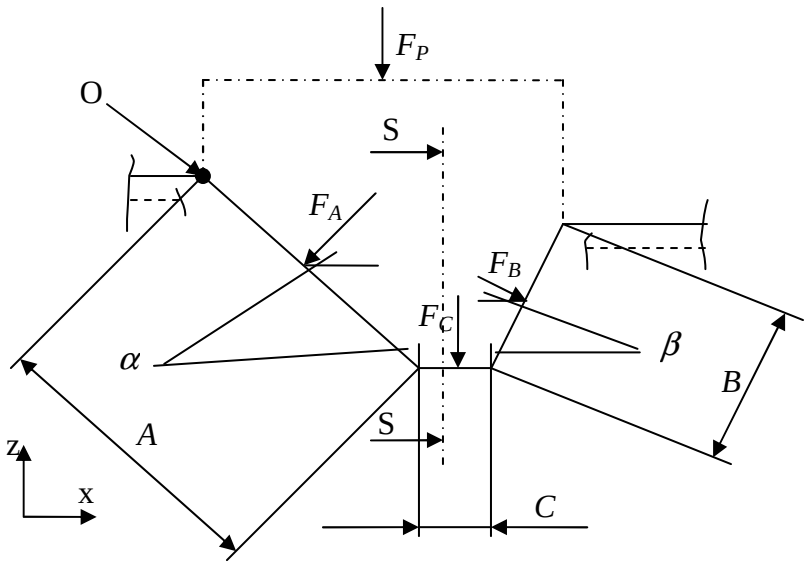

Fig. 7.3.1.1 Cross section of lower die.

Solving the system of equations yields

$$F_A = F_P \cos\beta \left(\frac{A\sin\alpha - B\sin\beta}{-B\cos\alpha - C\sin\beta\cos\alpha + A\cos\beta + C\cos\beta\sin\alpha} \right) \tag{7.3.1.4}$$

$$F_B = F_P \cos\alpha \left(\frac{A\sin\alpha - B\sin\beta}{-B\cos\alpha - C\sin\beta\cos\alpha + A\cos\beta + C\cos\beta\sin\alpha} \right) \tag{7.3.1.5}$$

$$\boxed{\begin{aligned} F_C = {} & -F_P(-A\cos\beta\cos(\alpha)^2 - B\cos\beta\sin\alpha\sin\beta + A\sin\beta\sin\alpha\cos\alpha + \\ & B\cos(\beta)^2\cos\alpha + C\sin\beta\cos\alpha - C\cos\beta\sin\alpha) / \\ & (-B\cos\alpha - C\sin\beta\cos\alpha + A\cos\beta + C\cos\beta\sin\alpha) \end{aligned}} \tag{7.3.1.6}$$

The horizontal force can be expressed using F_A or F_B

$$\boxed{\begin{aligned} F_H = {} & F_A\cos\alpha = F_B\cos\beta = F_P\cos\alpha\cos\beta(A\sin\alpha - B\sin\beta) / \\ & (A\cos\beta - B\cos\alpha - C\sin\beta\cos\alpha + C\cos\beta\sin\alpha) \end{aligned}} \tag{7.3.1.7}$$

If the cross section is a simple V-shape, i.e C=0 then only two force equations are required. Using (7.3.1.1) and (7.3.1.2) with F_C=0 yields

$$\boxed{F_A = F_P\cos\beta / (\cos\alpha\sin\beta + \cos\beta\sin\alpha)} \tag{7.3.1.8}$$

$$\boxed{F_B = F_P\cos\alpha / (\cos\alpha\sin\beta + \cos\beta\sin\alpha)} \tag{7.3.1.9}$$

From the expressions above and Figure (7.3.1.1) the horizontal force is calculated.

$$\boxed{F_H = F_P \cos\alpha \cos\beta / (\cos\alpha \sin\beta + \cos\beta \sin\alpha)} \qquad (7.3.1.10)$$

The horizontal force, F_H, and the vertical force, F_V, are assumed to affect the die in different ways, the former by trying to separate under influence of stresses acting in the x-direction and the latter by giving rise to compressive stresses in the z-direction in the walls. In order to obtain an expression for the stresses acting in the x-direction Figure 7.3.1.2 is considered.
Under assumption that F_H is equally distributed over the length L, which is the length that corresponds to the extension of the form surfaces, and half the thickness B the expression for the stress in the x-direction reads

$$\boxed{\sigma_{xx} = \frac{2F_H}{BL}} \qquad (7.3.1.11)$$

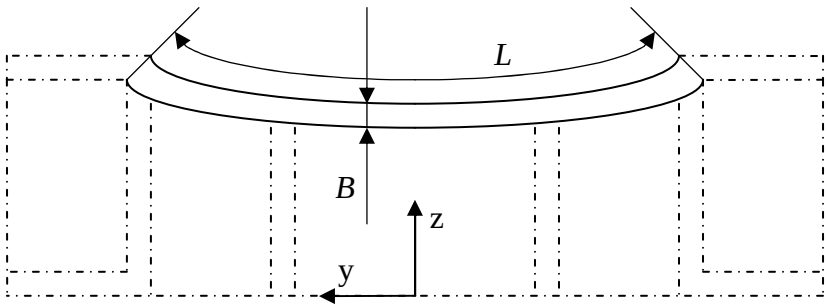

Fig. 7.3.1.2. Section S-S referring to fig. 7.3.1.1

Except from the stress in the x-direction, stresses are assumed to arise in the y- and z-directions as well, and this is due to constrains preventing the Poisson contraction. The stresses, which consequently will be tensile, are obtained as

$$\boxed{\sigma_{yy} = \sigma_{zz} = E\varepsilon_x \nu = \sigma_{xx} \nu} \qquad (7.3.1.12)$$

Since the stress state consists of three components some kind of criteria, which tells when yielding occurs, is required. An example of such criteria is that stated by von Mises, valid for mild steels. In this case it is dealt with cast iron, which is isotropic, but has different yield limits depending if the load is tensile or compressive. The simplest criterion that consider the hydrostatic dependence is proposed by Drucker and Prager, in which the hydrostatic stress state varies linearly with the deviatoric, given by

$$\sqrt{3J_2} + kI_1 - m = 0 \qquad (7.3.1.13)$$

Generally the yield criteria is stated as

$$F(\sigma_1, \sigma_2, \sigma_3) = 0 \qquad (7.3.1.14)$$

(7.3.1.14) shall be interpreted as a contour surface to a function of three variables, the principal stresses $\sigma_1, \sigma_2, \sigma_3$. Instead of using the principal stresses the yield surface can be described with help from the invariants I_1, J_2 and $\cos 3\theta$, since it can be shown [4] that the principal stresses uniquely determines these variables. Using tensor notation I_1 and J_2 are defined as

$$I_1 = \sigma_{ii} \;\; ; \;\; J_2 = \frac{1}{2} S_{ij} S_{ji} \;\; \text{where} \;\; S_{ij} = \sigma_{ij} - \frac{\sigma_{kk}}{3} \delta_{ij} \qquad (7.3.1.15)$$

I_1, J_2 and $\cos 3\theta$ has geometrical interpretations in the stress space according to Figure 7.3.1.4 and by using these variables the hydrostatic influence, determined by I_1, is separated from the deviatoric, determined by J_2 and $\cos 3\theta$. J_2 contains information about the magnitude of the deviatoric stresses whilst $\cos 3\theta$ informs about the direction. The deviatoric plane is defined by I_1 = constant and with (7.3.1.13) in mind $\sqrt{3J_2} = \text{constant}$ results, i.e. the trace in the deviatoric plane is described by a circle, since no notice is taken to the variable $\cos 3\theta$. The deviatoric plane and the linear relation between the hydrostatic and deviatoric stresses are shown in Figure 7.3.1.5. With this information it is concluded that the yield surface is represented by a circular cone in the stress space, see Figure 7.3.1.6. [4]

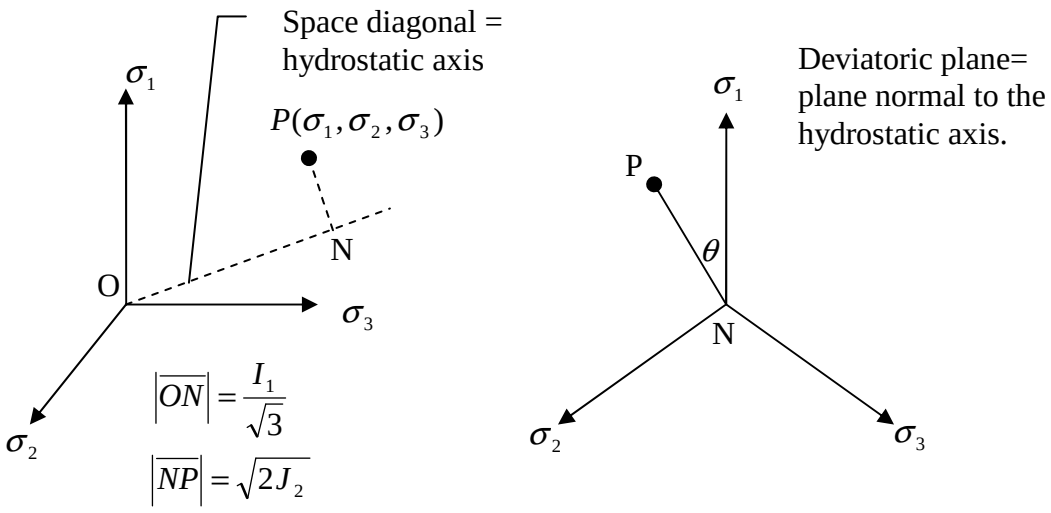

Figure 7.3.1.4. Interpretation of I_1, J_2 and $\cos 3\theta$ in stress space.

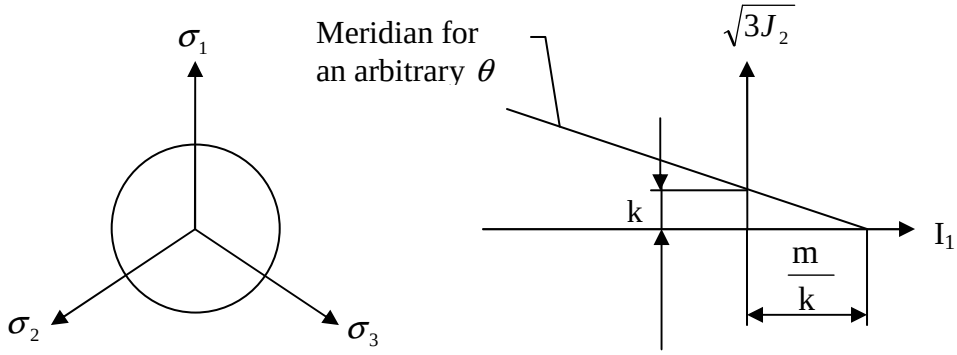

Figure 7.3.1.5. Drucker-Prager criterion. Deviatoric plane to the left and meridian plane to the right.

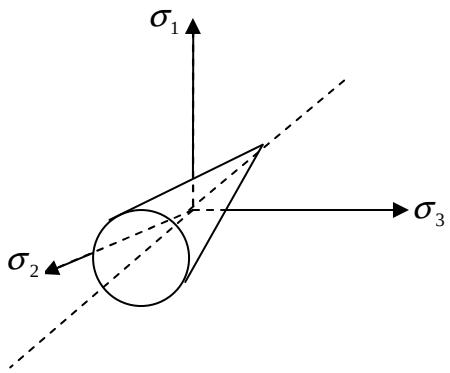

Figure7.3.1.6. Drucker-Prager criterion in the stress space-

I order to obtain a better understanding of the model, a stress state with only two components, $\sigma_{xx}$and σ_{yy} , is considered.

$$I_1^{Bi} = \sigma_{ii} = \sigma_{xx} + \sigma_{yy} \tag{7.3.1.16}$$

$$\left[S_{ij}^{Bi}\right] = \begin{bmatrix} \sigma_{xx} - \dfrac{\sigma_{xx}+\sigma_{yy}}{3} & 0 & 0 \\ 0 & \sigma_{yy} - \dfrac{\sigma_{xx}+\sigma_{yy}}{3} & 0 \\ 0 & 0 & -\dfrac{\sigma_{xx}+\sigma_{yy}}{3} \end{bmatrix} \tag{7.3.1.17}$$

To make the derivation more clear following tensor expression is developed

$$S_{ij}S_{ij} = S_{xj}S_{xj} + S_{yj}S_{yj} + S_{zj}S_{zj} = S_{xx}S_{xx} + S_{xy}S_{xy} + S_{xz}S_{xz} + S_{yx}S_{yx} + S_{yy}S_{yy} + S_{yz}S_{yz} + S_{zx}S_{zx} + S_{zy}S_{zy} + S_{zz}S_{zz} \tag{7.3.1.18}$$

Applying (7.3.1.18) to the stress state in question yields

$$S_{ij}S_{ij} = \left(\frac{2}{3}\sigma_{xx} - \frac{\sigma_{yy}}{3}\right)^2 + \left(\frac{2}{3}\sigma_{yy} - \frac{\sigma_{xx}}{3}\right)^2 + \left(\frac{\sigma_{xx}}{3} + \frac{\sigma_{yy}}{3}\right)^2 = \frac{2}{3}\sigma_{xx}{}^2 + \frac{2}{3}\sigma_{yy}{}^2 - \frac{2}{3}\sigma_{xx}\sigma_{yy} \tag{7.3.1.19}$$

and

$$\sqrt{3J_2} = \sqrt{\frac{3}{2}S_{ij}S_{ij}} = \sqrt{\sigma_{xx}{}^2 + \sigma_{yy}{}^2 - \sigma_{xx}\sigma_{yy}} \tag{7.3.1.20}$$

If (7.3.1.16) and (7.3.1.20) are inserted in (7.3.1.13) following expression is obtained:

$$\sqrt{\sigma_{xx}{}^2 + \sigma_{yy}{}^2 - \sigma_{xx}\sigma_{yy}} + \alpha(\sigma_{xx} + \sigma_{yy}) - \beta = \sqrt{\sigma_1{}^2 + \sigma_2{}^2 - \sigma_1\sigma_2} + \alpha(\sigma_1 + \sigma_2) - \beta = 0 \tag{7.3.1.21}$$

which represents a off-centre ellipse in the in the $\sigma_1\sigma_2$ - plane as shown in Figure 7.3.1.7. In (7.3.1.21) it has been used that the stress components correspond to the principal stresses, since no shear stresses are present. It is seen that the material is able to carry a heavier load compressive compared to tensile mode before yielding occurs, as desired when to model the behaviour of cast iron.

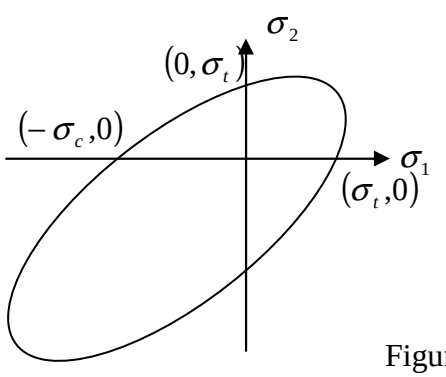

Figure7.3.1.7. Biaxial stress state.

Before (7.3.1.13) can be used to determine whether the stress state is within the allowed area or not, the parameters *k* and *m* have to be determined. It can be done by using the uniaxial tensile yield stress σ_t and the uniaxial compressive yield stress σ_c separately in (7.3.1.13) where after two equations are obtained.

$$\sigma_t = \frac{k}{1+m}, \sigma_c = \frac{k}{1-m} \tag{7.3.1.22}$$

If solved for k and m the result reads

$$k = -\frac{\sigma_t - \sigma_c}{\sigma_t + \sigma_c}, m = \frac{2\sigma_t \sigma_c}{\sigma_t + \sigma_c} \tag{7.3.1.23}$$

Returning to the current triaxial load case, it is necessary to determine I_1 and J_2. With help from (7.3.1.15) is it concluded that

$$I_1^{Tri} = \sigma_{ii} = \sigma_{xx} + \sigma_{yy} + \sigma_{zz} \tag{7.3.1.24}$$

$$\left[S_{ij}^{Tri}\right] = \begin{bmatrix} \sigma_{xx} - \frac{\sigma_{xx}+\sigma_{yy}+\sigma_{zz}}{3} & 0 & 0 \\ 0 & \sigma_{yy} - \frac{\sigma_{xx}+\sigma_{yy}+\sigma_{zz}}{3} & 0 \\ 0 & 0 & \sigma_{zz} - \frac{\sigma_{xx}+\sigma_{yy}+\sigma_{zz}}{3} \end{bmatrix} \tag{7.3.1.25}$$

If (7.3.1.23), (7.3.1.24) and (7.3.1.25) with help from (7.3.1.18) are inserted in (7.3.1.13) the initial yield criteria reads

$$\boxed{\begin{aligned} &\sqrt{\sigma_{xx}^2 - \sigma_{xx}\sigma_{yy} - \sigma_{xx}\sigma_{zz} + \sigma_{yy}^2 - \sigma_{yy}\sigma_{zz} + \sigma_{zz}^2} \\ &+ \frac{(\sigma_c - \sigma_t)(\sigma_{xx} + \sigma_{yy} + \sigma_{zz}) - 2\sigma_c\sigma_t}{\sigma_c + \sigma_t} = \\ &\sqrt{\sigma_1^2 - \sigma_1\sigma_2 - \sigma_1\sigma_3 + \sigma_2^2 - \sigma_2\sigma_3 + \sigma_3^2} \\ &+ \frac{(\sigma_c - \sigma_t)(\sigma_1 + \sigma_2 + \sigma_3) - 2\sigma_c\sigma_t}{\sigma_c + \sigma_t} = 0 \end{aligned}} \tag{7.3.1.26}$$

In (7.3.1.26) the fact that the stress components corresponds to principal stresses has been used.

Load case IX, Area 4

The vertically acting load gives rise to a compressive load in the walls. This can be derived from the expressions for F_A and F_B stated by (7.3.1.4) and (7.3.1.5)

$$\boxed{F_{VA} = F_A \sin\alpha = F_P \cos\beta \sin\alpha \left(\frac{A\sin\alpha - B\sin\beta}{-B\cos\alpha - C\sin\beta\cos\alpha + A\cos\beta + C\cos\beta\sin\alpha} \right)} \tag{7.3.1.27}$$

$$\boxed{F_{VB} = F_B \sin\beta = F_P \cos\alpha \sin\beta \left(\frac{A\sin\alpha - B\sin\beta}{-B\cos\alpha - C\sin\beta\cos\alpha + A\cos\beta + C\cos\beta\sin\alpha} \right)} \tag{7.3.1.28}$$

The contribution from F_C is given directly by (7.3.1.6). If the form is a simple V-shape (7.3.1.8) and (7.3.1.9) are used to obtain

$$\boxed{F_{VA} = F_A \sin\alpha = F_P \cos\beta \sin\alpha / (\cos\alpha \sin\beta + \cos\beta \sin\alpha)} \tag{7.3.1.29}$$

$$\boxed{F_{VB} = F_B \sin\beta = F_P \cos\alpha \sin\beta / (\cos\alpha \sin\beta + \cos\beta \sin\alpha)} \tag{7.3.1.30}$$

Figure 7.3.1.8, which shows the lower die seen in the press direction, indicates the areas over which the forces are distributed. Since it is assumed that F_{VA}, F_{VB} and F_C affect three different areas equilibrium yields

$$F_{VA} = \sigma_{WA}\left(A_{PA} - n_A (I - B_A)(J - B_A)\right) \tag{7.3.1.31}$$

$$F_{VB} = \sigma_{WB}\left(A_{PB} - n_B (E - B_B)(F - B_B)\right) \tag{7.3.1.32}$$

$$F_C = \sigma_{WC}\left(A_C - n_C (G - B_C)(H - B_C)\right) \tag{7.3.1.33}$$

where n_A, n_B and n_C denotes the number of frames in area A_{PA}, A_{PB} and A_C respectively.
If these equations are solved for the wall thicknesses following expressions are obtained

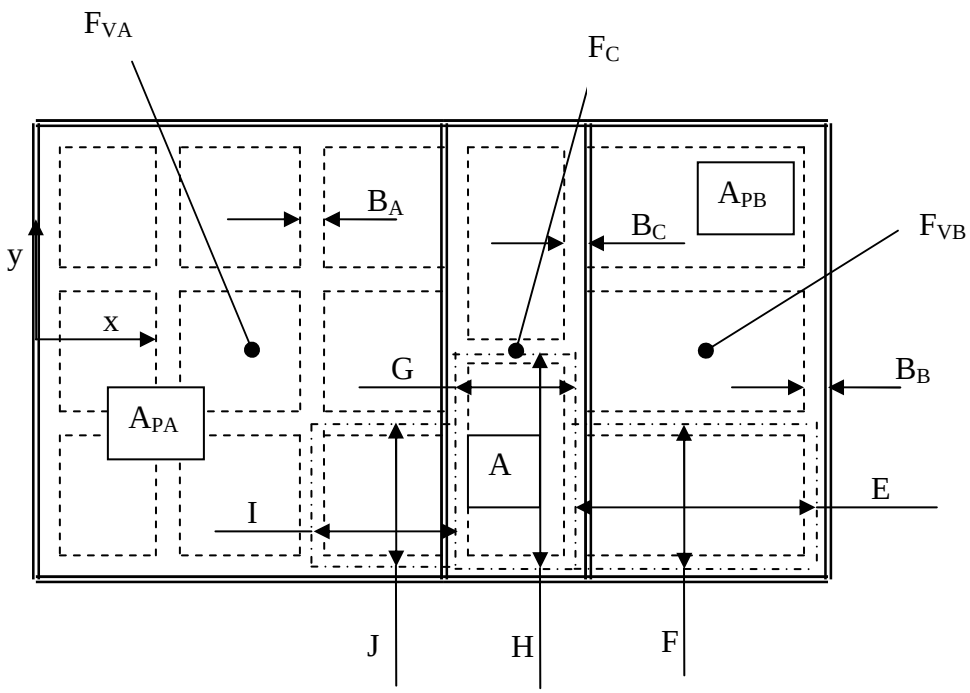

Figure 7.3.1.8. Lower die seen in the press direction

$$B_A = \frac{I+J}{2} + \sqrt{\left(\frac{I+J}{2}\right)^2 - \left(IJ + \frac{\frac{F_{VA}}{\sigma_{WA}} - A_{PA}}{n_A}\right)} \tag{7.3.1.34}$$

$$B_B = \frac{E+F}{2} + \sqrt{\left(\frac{E+F}{2}\right)^2 - \left(EF + \frac{\frac{F_{VB}}{\sigma_{WB}} - A_{PB}}{n_B}\right)} \tag{7.3.1.35}$$

$$B_C = \frac{G+H}{2} + \sqrt{\left(\frac{G+H}{2}\right)^2 - \left(GH + \frac{\frac{F_C}{\sigma_{WC}} - A_C}{n_C}\right)} \tag{7.3.1.36}$$

With this approach the thicknesses of the walls are dependent of the design of the casting structure, which seems to be reasonable.

Load case X, Area 1 and 5

When the die is closed the load transmission from the blank holder is imagined to occur at the distance plates. This means that the main task for the blank holder is to prevent wrinkles and in the case the blank needs to be stretched, draw beads are required. In most cases the distance plates are located at or near a point where two walls meet. It may be near one of the outer sides or close to the cavity. Figure 7.3.1.10 shows the most common variants. Since each distance plate is assumed to carry the same load, the stress in the vertically walls is determined from

$$\sigma_W = \frac{F_{BH}}{nB(A+C)} \tag{7.3.1.37}$$

where F_{BH} denotes the blank holder load, n denotes the number of distance plates. The designations from fig 7.3.1.10 have been used. Apart from the stress it is of interest to determine the displacement of the walls, since this affects the surface pressure. With help from Hooke´s law the expression for the displacement reads

$$u_z = \frac{\sigma_w}{E} H \tag{7.3.1.38}$$

where E is the modulus of elasticity and H the height shown in Figure 7.3.1.9.

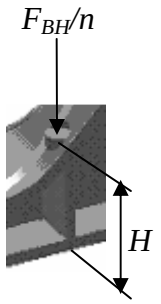

Fig. 7.3.1.9. Definition of the height *H*

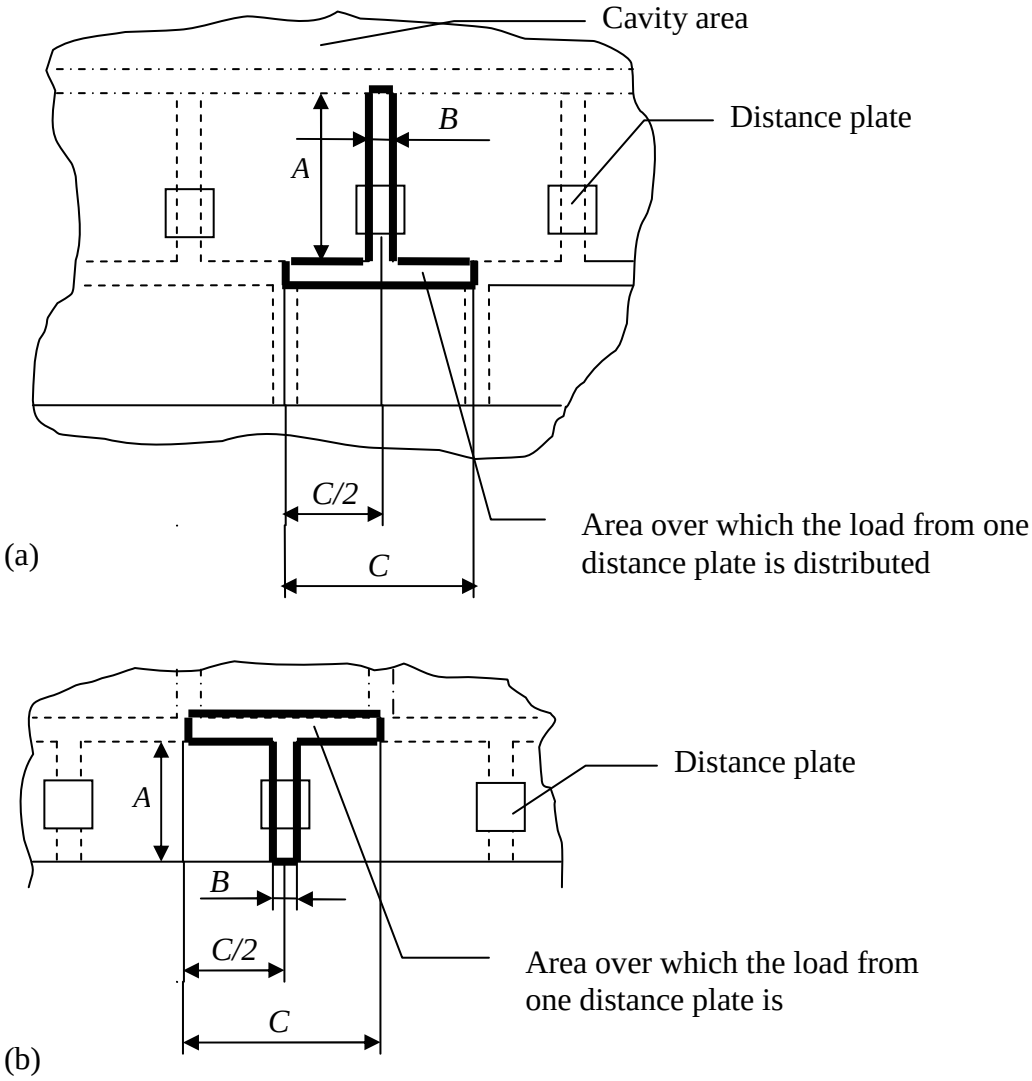

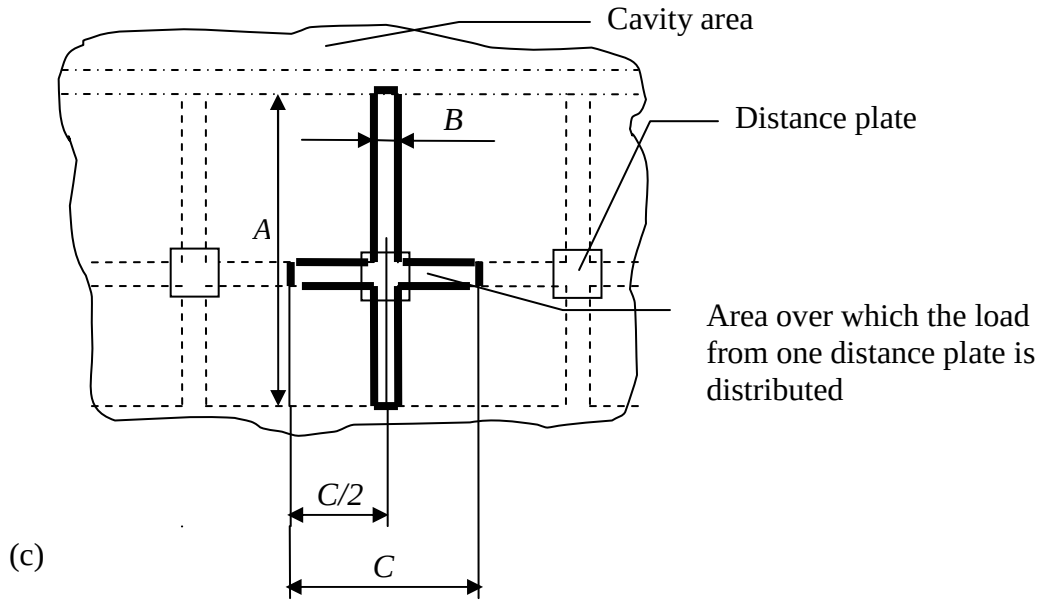

Fig. 7.3.1.10. Different possibilities for positioning of distance plates.

Load case XI, Area 3

Except from the stresses in the walls it is also of interest to determine the deflection in the area between the walls, which is illustrated in Figure 7.3.1.11. The problem is transferred to a plate problem with all four boundaries clamped. Under assumption that Kirchhoff plate theory is valid, i.e. the plate is thin meaning plane stress condition is valid, the equation to be solved can be shown [5] to read

$$\Delta\Delta w(x,y) = \left(\frac{\partial^2}{\partial x^2} + \frac{\partial^2}{\partial y^2}\right)\left(\frac{\partial^2 w}{\partial x^2} + \frac{\partial^2 w}{\partial y^2}\right) = \frac{\partial^4 w}{\partial x^4} + 2\frac{\partial^4 w}{\partial x^2 \partial y^2} + \frac{\partial^4 w}{\partial y^4} = \frac{12\left(1-\nu^2\right)}{Et^3} q \qquad (7.3.1.39)$$

which can be reformulated

$$\frac{\partial^2 M_{xx}}{\partial x^2} + 2\frac{\partial^2 M_{xy}}{\partial x \partial y} + \frac{\partial^2 M_{yy}}{\partial y^2} + q = 0 \qquad (7.3.1.40)$$

The quantities are defined in appendix A.

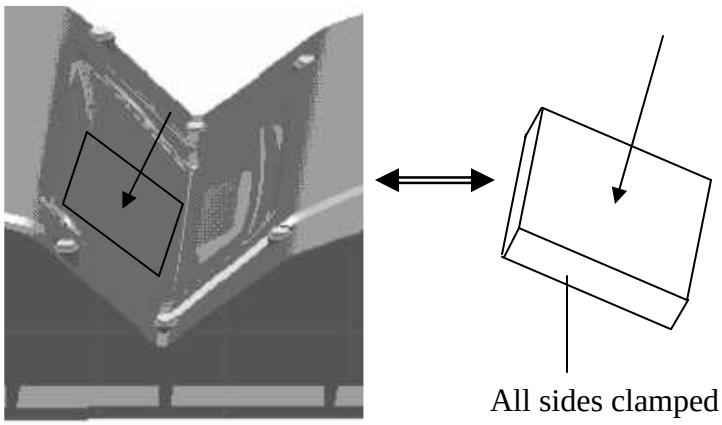

Fig. 7.3.1.11. Plate used to calculate deflections.

(7.3.1.40) with all sides clamped is solved in the mathematical appendix part A with the result

$$\boxed{u = \frac{15q\left(1-\nu^2\right)}{32Et^3}\frac{A^4B^4}{7A^2B^2 - 2A^2B^2\nu + 10A^4 + 10B^4}} \qquad (7.3.1.41)$$

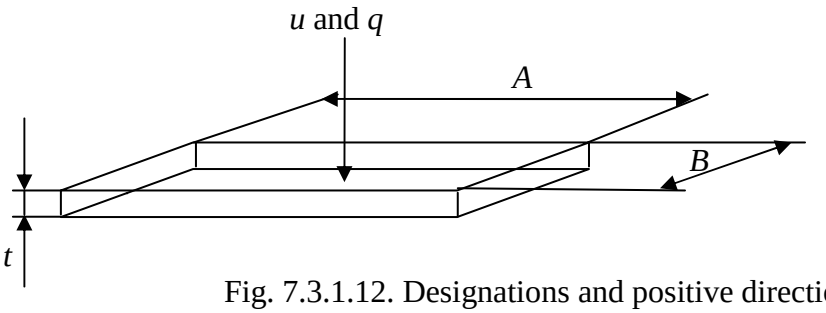

Fig. 7.3.1.12. Designations and positive directions

u denotes the deflection at the centre of the plate and q is a equally distributed load (force per unit area). The designations are explained in Figure 7.3.1.12. It was concluded in the derivation of (7.3.1.41), that it seems to predict deflections well in plates where the length of the smallest side corresponds to one tenth of the thickness. If the plate is thicker the expression has to be used with care.

Load case XII, XIII and XIV, Area 1, 3, 4 and 5

Regarding flat dies, they are assumed to be exposed only to stresses in the z-direction. In order to derive an expression for the stresses in the walls in the lower die due to the load from the punch, the load is assumed to be equally distributed over the vertically walls. Following the same procedure as in the derivation of (7.3.1.34), (7.3.1.35) and (7.3.1.36), the expression reads

$$B = \frac{G+H}{2} + \sqrt{\left(\frac{G+H}{2}\right)^2 - \left(GH + \frac{\frac{F_P}{\sigma_W} - A_C}{n}\right)} \qquad (7.3.1.42)$$

Here A_C denotes the area of the punch, defined in Figure 7.3.1.8. Since the body considered is flat, A_{PA} and A_{PB} are not taken into account. Regarding stresses in the walls in flat lower dies due to load on the distance plates transmitted from the blank holder, the same expressions, (7.3.1.37) and (7.3.1.38), derived for V-shaped lower dies, is applicable. Also the expression for calculation of the deflection in the area between the walls in V-shaped dies, (7.3.1.41), is applicable for flat dies.

7.3.2. Punch - analytical expressions (Load case XV, XVI, XVII and XVIII)

Forces acting on the punch when the die is closed arise from the lower die. This means that many of the expressions derived in section 7.3.1 is applicable in this section as well.

Load case XV and XVI, Area 3 and 4

Regarding V-shaped dies, the forces acting on the punch when the die is closed, are shown in Figure 7.3.2.1. The correspondence to the forces trying to tear the lower die apart is the horizontal compressive components of the forces acting on the punch. Since cast iron is able to carry a higher load compressive compared to tensile, and the area over which the compressive load is distributed is larger than the corresponding area in the lower die for the tensile load, a load case similar to that derived in section 7.3.1 regarding forces trying to tear the lower die apart, is omitted regarding the punch.

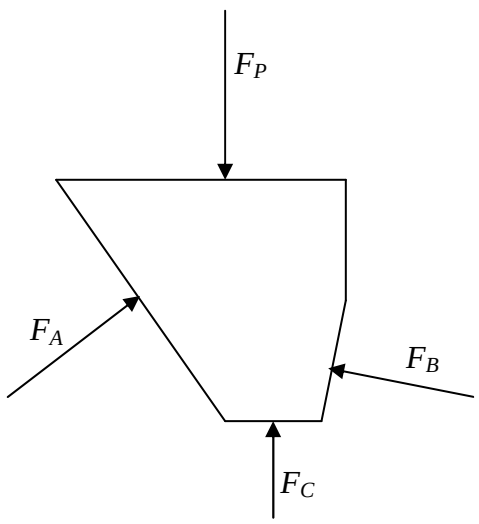

Fig. 7.3.2.1. Forces acting on the punch when the die is closed.

(7.3.1.34), (7.3.1.35) and (7.3.1.36) are applicable also for calculations of stresses in the wall due to the lower die load and so is (7.3.1.41) regarding deflection in the area between the walls.

Load case XVII and XVIII, Area 3 and 4

In a flat die the conditions regarding the forces acting on the punch are the same as in the lower die, which means that the expressions used in section 7.3.1 is applicable. Regarding forces acting compressive at the vertically walls due to the lower die load, (7.3.1.42) is applicable. (7.3.1.41) applies for calculation of deflection in the area between the walls.

7.3.3. Blank holder – analytical expressions (Load case XIX and XX)

When the die is closed the load transmission from the lower die is assumed to take place only at the distance plates. Of interest is, except from being able to calculate the stress in the walls, the possibility to calculate the deflection, since this affects the surface pressure on the blank.

Load case XIX and XX, Area 1 and 5

In order to calculate the stress and deflection in the walls beneath the distance plates, (7.3.1.37) and (7.3.1.38) derived in section 7.3.1 are applicable for V-shaped as well as flat blank holders.

8. Derivation of analytical expressions for some other situations of interest

8.1. Two blanks accidentally at the same time

Sometimes two blanks accidentally are placed in the die at the same time. Since the gap between the upper and lower die corresponds to the thickness of one blank, very large forces arise in regions with nearly vertical surfaces. Neither a finite element calculation has been carried out nor a derivation of an analytical expression. The reason for this is that the problem requires software more advanced than the used. However, a suggested approach is to consider the friction forces, F_i, according to Figure 8.1.1. N_i denotes the normal forces, R_i the resultants and F_p the punch force. Four unknown require four equations

$$\begin{aligned} &F_1 = \mu N_1 \\ &F_2 = \mu N_2 \\ &F_1 \cos\alpha + F_2 \cos\beta + N_1 \sin\alpha + N_2 \sin\beta = F_p \\ &-F_1 \sin\alpha + F_2 \sin\beta + N_1 \cos\alpha - N_2 \cos\beta = 0 \end{aligned} \tag{8.1.1}$$

from which all acting forces can be obtained. The horizontal force, trying to split the die, is then obtained from horizontal equilibrium.

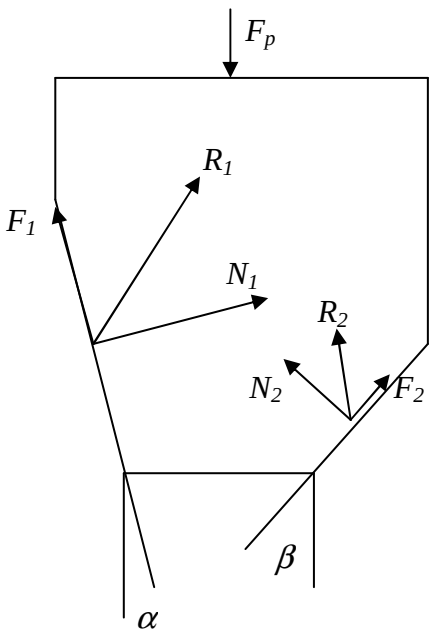

Figure 8.1.1. Forces acting on a V-shaped punch when two blanks accidentally are put in the die

8.2. Die on trestles (Load case XXI and XXII)

In this section that load case is treated, which covers what happens when the die is placed on trestle, for example in connection with maintenance. Experience has shown that if the die is

long, problem may arise to put the upper and lower die together, due to displacement of the guidings. The problem mainly arises in dies where guide pins are used. Draw dies uses wear plates, but this load case also serves as an indication on the general bending stiffness.

The deflection at mid-span for a simply supported beam is given as [3]

$$\delta = \frac{5Wl^3}{384EI_y} \tag{8.2.1}$$

Here δ denotes the deflection, W the mass of the part, l the length of the part, E Youngs modulus of elasticity and I_y the moment of inertia with respect to the y-axis. In order to calculate the moment of inertia use of Figure 8.2.1 is made.

The distance between the walls and the height of the cross section is assumed to be constant. Symmetry is said to exist with respect to the xz- and yz-plane. The influence of the walls perpendicular to the bending plane is neglected. In order to calculate the moment of inertia, knowledge about the neutral axis is required. Since the neutral axes passes through the center of mass, the calculations starts with finding an expression for the position in the z-direction. The center of mass is located at that point where the moment of the whole area equals the sum of the moments of all elements, i.e.

$$\begin{aligned}&\left(B(C+H+A)+\frac{JD}{2}+J\frac{n}{2}D+F\frac{n}{2}h\right)z_{tp} = \\ &B\left(\frac{BC}{2}+\frac{H^2}{2}+A\left(H-\frac{B}{2}\right)\right)+\left(\frac{JD}{2}+J\frac{n}{2}D\right)\left(h-\frac{J}{2}\right)+\frac{Fnh^2}{4}\end{aligned} \tag{8.2.2}$$

where n denotes the total number of pockets with width D. The pocket located at the center line shall not be included. In Figure 8.2.1 n = 4.

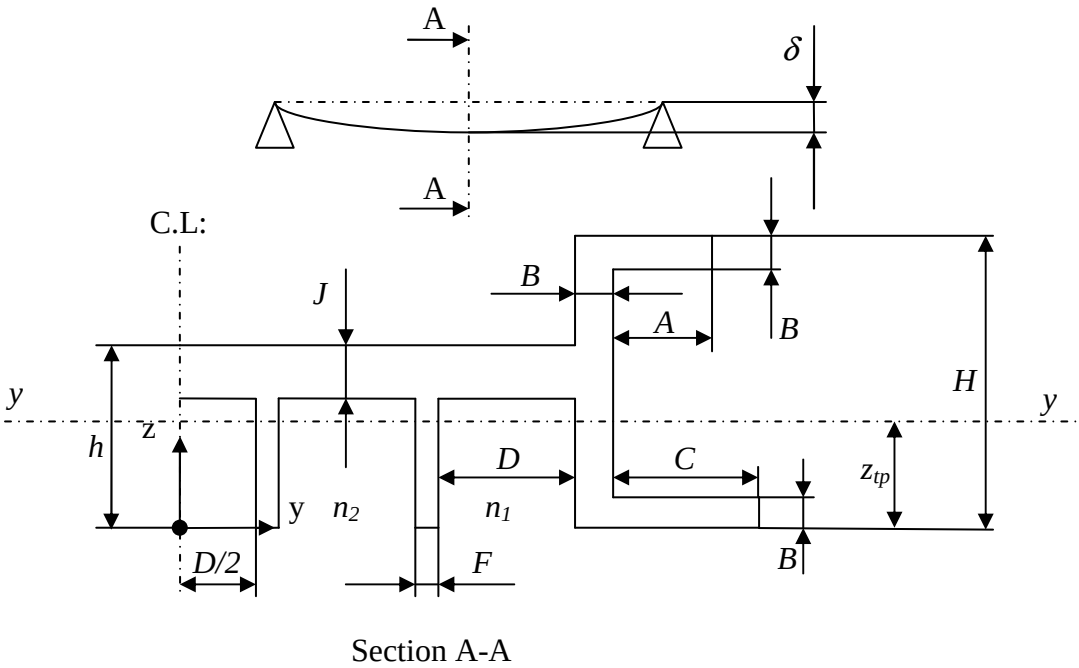

Fig. 8.2.1. Cross section of die used in analysis of bending with respect to the y-axis. Only one half is shown.

With help from the parallel axis theorem, (B.7), the expression for the moment of inertia for the section reads

$$I_y = 2\left(\begin{array}{l} \dfrac{CB^3}{12} + BC\left(z_{tp} - \dfrac{B}{2}\right)^2 + \dfrac{BH^3}{12} + BH\left(\dfrac{H}{2} - z_{tp}\right)^2 + \dfrac{AB^3}{12} + AB\left(H - \dfrac{B}{2} - z_{tp}\right)^2 + \\ \dfrac{DJ^3}{24} + \dfrac{JD}{2}\left(h - \dfrac{J}{2} - z_{tp}\right)^2 + \dfrac{n}{2}\left(\dfrac{DJ^3}{12} + JD\left(h - \dfrac{J}{2} - z_{tp}\right)^2\right) + \\ \dfrac{n}{2}\left(\dfrac{Fh^3}{12} + Fh\left(z_{tp} - \dfrac{h}{2}\right)^2\right) \end{array}\right) \tag{8.2.3}$$

If (8.2.2) is solved for z_{tp} and inserted in (8.2.3), the final expression for the deflection at mid-span is obtained after insertion in (8.2.1)

$$\delta := \frac{5}{384} Q\, l^3 \Big/ \left(E \left(\frac{1}{6} C\, B^3 + 2\, B\, \mathrm{C} \left(\frac{B\left(\frac{1}{2} B\, C + \frac{1}{2} H^2 + A\left(H - \frac{1}{2} B\right)\right) + \left(\frac{1}{2} J\, D + \frac{1}{2} J\, n\, \mathrm{D}\right)\left(h - \frac{1}{2} J\right) + \frac{1}{4} F\, n\, h^2}{B\,(C + H + A) + \frac{1}{2} J\, D + \frac{1}{2} J\, n\, \mathrm{D} + \frac{1}{2} F\, n\, h} - \frac{1}{2} B \right)^2 \right.\right.$$

$$+ \frac{1}{6} B\, H^3 + 2\, B\, H \left(\frac{1}{2} H - \frac{B\left(\frac{1}{2} B\, C + \frac{1}{2} H^2 + A\left(H - \frac{1}{2} B\right)\right) + \left(\frac{1}{2} J\, D + \frac{1}{2} J\, n\, \mathrm{D}\right)\left(h - \frac{1}{2} J\right) + \frac{1}{4} F\, n\, h^2}{B\,(C + H + A) + \frac{1}{2} J\, D + \frac{1}{2} J\, n\, \mathrm{D} + \frac{1}{2} F\, n\, h} \right)^2$$

$$+ \frac{1}{6} A\, B^3 + 2\, A\, B \left(H - \frac{1}{2} B - \frac{B\left(\frac{1}{2} B\, C + \frac{1}{2} H^2 + A\left(H - \frac{1}{2} B\right)\right) + \left(\frac{1}{2} J\, D + \frac{1}{2} J\, n\, \mathrm{D}\right)\left(h - \frac{1}{2} J\right) + \frac{1}{4} F\, n\, h^2}{B\,(C + H + A) + \frac{1}{2} J\, \mathrm{D} + \frac{1}{2} J\, n\, \mathrm{D} + \frac{1}{2} F\, n\, h} \right)^2$$

$$+ \frac{1}{12} D\, J^3 + J\, D \left(h - \frac{1}{2} J - \frac{B\left(\frac{1}{2} B\, C + \frac{1}{2} H^2 + A\left(H - \frac{1}{2} B\right)\right) + \left(\frac{1}{2} J\, \mathrm{D} + \frac{1}{2} J\, n\, \mathrm{D}\right)\left(h - \frac{1}{2} J\right) + \frac{1}{4} F\, n\, h^2}{B\,(C + H + A) + \frac{1}{2} J\, \mathrm{D} + \frac{1}{2} J\, n\, \mathrm{D} + \frac{1}{2} F\, n\, h} \right)^2 + n$$

$$\left(\frac{1}{12} \mathrm{D}\, J^3 + J\, \mathrm{D} \left(h - \frac{1}{2} J - \frac{B\left(\frac{1}{2} B\, C + \frac{1}{2} H^2 + A\left(H - \frac{1}{2} B\right)\right) + \left(\frac{1}{2} J\, \mathrm{D} + \frac{1}{2} J\, n\, \mathrm{D}\right)\left(h - \frac{1}{2} J\right) + \frac{1}{4} F\, n\, h^2}{B\,(C + H + A) + \frac{1}{2} J\, \mathrm{D} + \frac{1}{2} J\, n\, \mathrm{D} + \frac{1}{2} F\, n\, h} \right)^2 \right) +$$

$$
n\left(\frac{1}{12}F\,h^3 + F\,h\right.
$$

$$
\left(\frac{B\left(\frac{1}{2}B\,C + \frac{1}{2}H^2 + A\left(H - \frac{1}{2}B\right)\right) + \left(\frac{1}{2}J\,\mathrm{D} + \frac{1}{2}J\,n\,\mathrm{D}\right)\left(h - \frac{1}{2}J\right) + \frac{1}{4}F\,n\,h^2}{B\,(C + H + A) + \frac{1}{2}J\,\mathrm{D} + \frac{1}{2}J\,n\,\mathrm{D} + \frac{1}{2}F\,n\,h} - \frac{1}{2}h\right)^2
$$

$$
\left.\right)\right)\right) \qquad (8.2.4)
$$

A second alternative regarding the casting structure exist, which is shown in Figure 8.2.2.

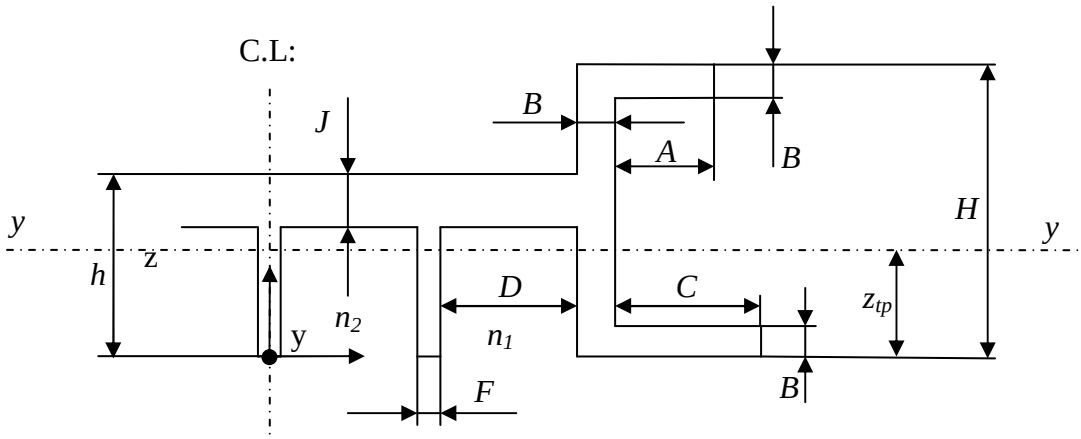

Fig. 8.2.2. A second alternative to cross section of die used in analysis of bending with respect to the y-axis. Only one half is shown.

In this case the expression for the center of mass reads

$$
\left(B(C + H + A) + J\,\frac{n}{2}D + F\,\frac{n-1}{2}h\right)z_{tp} =
$$

$$
B\left(\frac{BC}{2} + \frac{H^2}{2} + A\left(H - \frac{B}{2}\right)\right) + J\,\frac{n}{2}D\left(h - \frac{J}{2}\right) + \frac{F(n-1)h^2}{4} \qquad (8.2.5)
$$

and the expression for the moment of inertia

$$I_y = 2\left(\begin{array}{l}\dfrac{CB^3}{12} + BC\left(z_{tp} - \dfrac{B}{2}\right)^2 + \dfrac{BH^3}{12} + BH\left(\dfrac{H}{2} - z_{tp}\right)^2 + \dfrac{AB^3}{12} + AB\left(H - \dfrac{B}{2} - z_{tp}\right)^2 + \\ + \dfrac{n}{2}\left(\dfrac{DJ^3}{12} + JD\left(h - \dfrac{J}{2} - z_{tp}\right)^2\right) + \dfrac{n-1}{2}\left(\dfrac{Fh^3}{12} + Fh\left(z_{tp} - \dfrac{h}{2}\right)^2\right)\end{array}\right) \tag{8.2.6}$$

and after insertion, finally the deflection at mid-span

$$\delta := \frac{5}{384} Q\, l^3 \Big/ \Bigg(E \Bigg(\frac{1}{6} C\, B^3 + 2\, B$$

$$\mathrm{C}\left(\frac{B\left(\frac{1}{2} B\, C + \frac{1}{2} H^2 + A\left(H - \frac{1}{2} B\right)\right) + \frac{1}{2} J\, n\, D\left(h - \frac{1}{2} J\right) + \frac{1}{4} F\,(n-1)\, h^2}{B\,(C + H + A) + \frac{1}{2} J\, n\, \mathrm{D} + \frac{1}{2} F\,(n-1)\, h} - \frac{1}{2} B\right)^2$$

$$+ \frac{1}{6} B\, H^3 + 2\, B\, H$$

$$\left(\frac{1}{2} H - \frac{B\left(\frac{1}{2} B\, C + \frac{1}{2} H^2 + A\left(H - \frac{1}{2} B\right)\right) + \frac{1}{2} J\, n\, \mathrm{D}\left(h - \frac{1}{2} J\right) + \frac{1}{4} F\,(n-1)\, h^2}{B\,(C + H + A) + \frac{1}{2} J\, n\, \mathrm{D} + \frac{1}{2} F\,(n-1)\, h}\right)^2$$

$$+ \frac{1}{6} A\, B^3 + 2\, A\, B$$

$$\left(H - \frac{1}{2} B - \frac{B\left(\frac{1}{2} B\, C + \frac{1}{2} H^2 + A\left(H - \frac{1}{2} B\right)\right) + \frac{1}{2} J\, n\, \mathrm{D}\left(h - \frac{1}{2} J\right) + \frac{1}{4} F\,(n-1)\, h^2}{B\,(C + H + A) + \frac{1}{2} J\, n\, \mathrm{D} + \frac{1}{2} F\,(n-1)\, h}\right)^2$$

$$+ n \Bigg(\frac{1}{12} \mathrm{D}\, J^3 + J\, \mathrm{D}$$

$$\left(h - \frac{1}{2} J - \frac{B\left(\frac{1}{2} B\, C + \frac{1}{2} H^2 + A\left(H - \frac{1}{2} B\right)\right) + \frac{1}{2} J\, n\, \mathrm{D}\left(h - \frac{1}{2} J\right) + \frac{1}{4} F\,(n-1)\, h^2}{B\,(C + H + A) + \frac{1}{2} J\, n\, \mathrm{D} + \frac{1}{2} F\,(n-1)\, h}\right)^2$$

$$\Bigg) + (n-1) \Bigg(\frac{1}{12} F\, h^3 +$$

$$F\,h\left(\frac{B\left(\frac{1}{2}B\,C+\frac{1}{2}H^2+A\left(H-\frac{1}{2}B\right)\right)+\frac{1}{2}J\,n\,\mathrm{D}\left(h-\frac{1}{2}J\right)+\frac{1}{4}F\,(n-1)\,h^2}{B\,(C+H+A)+\frac{1}{2}J\,n\,\mathrm{D}+\frac{1}{2}F\,(n-1)\,h}-\frac{1}{2}h\right)^2 \tag{8.2.7}$$

9. Evaluation of the analytical expressions using finite element calculations

In the finite element calculations the *Catia* built-in finite element solver *Ansolid* has been used. Without exception ten-node tetrahedral elements have been used. The bodies have been considered one by one. For example when the load from the blank holder on the lower die is considered, only the mesh of the lower die is used and the influence from the blank holder is considered as an applied load. This means that it has not been dealt with contact problems. If not otherwise stated, surfaces towards bolster or slide have been clamped in the z-direction and the wear plates clamped in the x- and y-directions. Throughout the analytical calculations as well as in the FE-calculations, following values have been used

- Poisson's ratio $\nu = 0{,}28$
- Density $\rho = 7200$ kg/m^3
- Youngs modulus of elasticity $E = 165$ GPa
- Blank holder load $F_{BH} = 1.2$ MN
- Punch load $F_P = 6$ MN
- Acceleration of gravity $g = 9.81$ m/s^2

The material parameters are valid for spheroidal graphite iron (ref, Volvo standard VOV 1107,391). The applied loads are representative for deep drawing operations. The results from the FE-calculations are shown in colour maps. In the analytical calculations the inserted values are taken from the CAD-models.

9.1. Load cases when the blank holder hits the lower die-evaluation

In this section the results based on the expression derived in section 7.1 are accounted and compared with finite element calculations.

9.1.1. Lower die – evaluation (Load case I and II)

The load is applied in two different ways depending on the shape of the lower die. If the lower die is flat, a body corresponding to the lower die is merged with the lower die in those areas where the load transmission is assumed to occur. Figure 9.1.2.4 illustrates an example. The load from the blank holder is applied as a contact load. The method merging a body corresponding to a blank holder to the lower die is not applicable regarding V-shaped dies, since such approach would give rise to erroneous stress distributions. Merging two bodies with inclined surfaces, makes an applied vertical load to be transmitted vertically. Instead the load from the blank holder is applied as a pressure over the draw bead areas, i.e. the load is applied perpendicular to the surface of the draw beads. The difference between the approaches is shown in Figure 9.1.1.1.

Load case I, Area 1

Regarding V-shaped dies, in the analytical expressions derived in section 7.1.1, only the vertical stress component is considered. The result from these expressions are compared to the von Mises stress from the finite element calculations in order to find out if it is acceptable to consider only the vertical stress component.

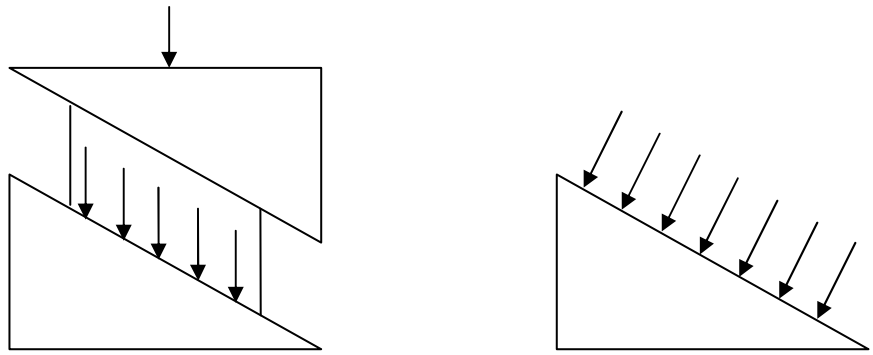

Blank holder and lower die merged. Load applied on the blank holder.

Load form the blank holder applied as a pressure on the lower

Figure 9.1.1.1. Different stress distributions in the lower die depending on how the load from the blank holder is applied.

Figure 9.1.1.2 shows the V-shaped lower die and the areas where the load from the blank holder is transmitted. In this case draw beads are located only at the inclined surfaces. With use of (7.1.1.9) and (7.1.1.10) the stresses in the walls beneath the draw beads are calculated.

$$\sigma_{WA} = \frac{F_{BH}^{VA}}{(2H+I)L} = \frac{F_{BH}\cos\beta\sin\alpha}{(\cos\alpha\sin\beta+\cos\beta\sin\alpha)}\frac{1}{(2H+I)L} = \frac{1.20\cdot 10^6\cos 52°\sin 45°}{(\cos 45°\sin 52°+\cos 52°\sin 45°)}\frac{1}{(2\cdot 640\cdot 40)}\,\text{MPa} = 10\,\text{MPa} \qquad (9.1.1.1)$$

$$\sigma_{WB} = \frac{F_{BH}^{VB}}{(2K+J)L} = \frac{F_{BH}\cos\alpha\sin\beta}{(\cos\alpha\sin\beta+\cos\beta\sin\alpha)}\frac{1}{(2K+J)L} = \frac{1.20\cdot 10^6\cos 45°\sin 52°}{(\cos 45°\sin 52°+\cos 52°\sin 45°)}\frac{1}{(2\cdot 480\cdot 40)}\,\text{MPa} = 17\,\text{MPa} \qquad (9.1.1.2)$$

Since the draw beads only are located in the inclined areas, I and J have been set equal to zero. σ_{WA} corresponds to the wall stress at the left hand side and σ_{WB} corresponds to the wall stress at the right hand side in Figure 9.1.1.2.

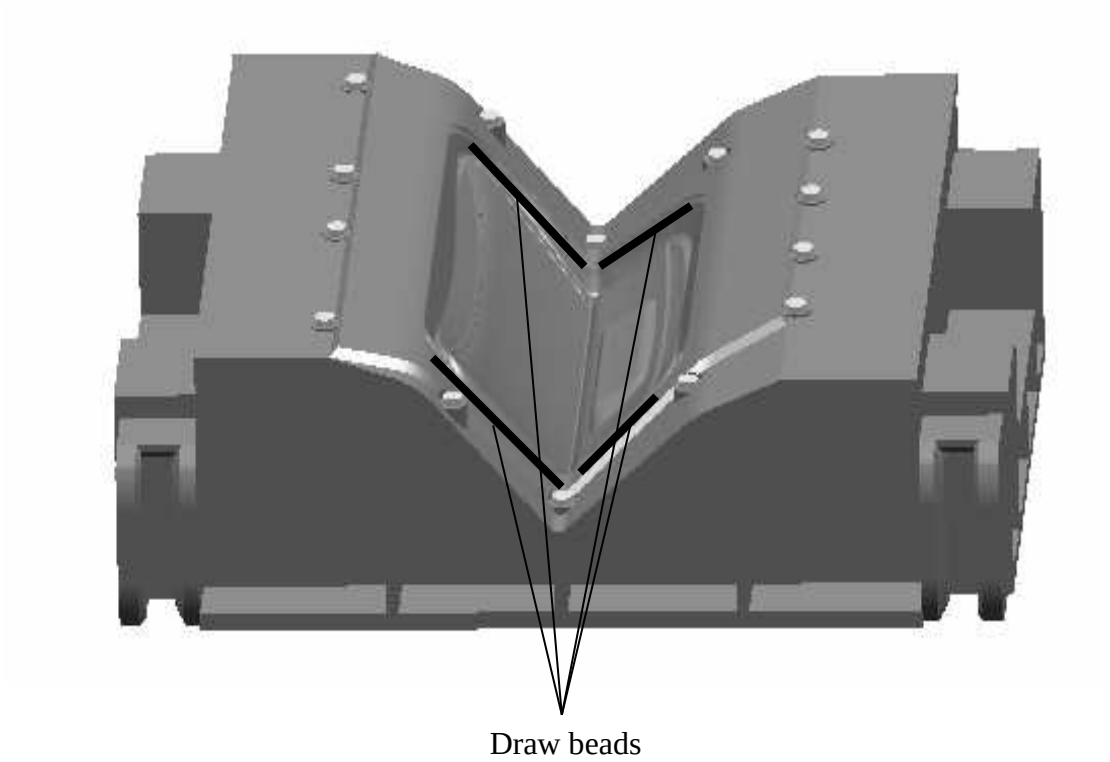

Figure 9.1.1.2. V-shaped lower die with the location of draw beads marked out.

Comments load case I, Area 1

The result of the finite element calculation is shown in Figure 9.1.1.3. σ_{WA} is the stress in the walls with negative x-component and σ_{WB} is the stress in the walls with positive x-component. It is immediately concluded that the stress varies within each of the areas, mainly 4-12 MPa regarding σ_{WA} and 10-14 MPa regarding σ_{WB}. However, the results from the analytical expressions are in fair agreement with the finite element calculations.

Load case II, Area 1

Regarding flat lower dies, the load in the finite element calculation is applied as a pressure in the flat draw bead areas, which gives rise to a stress in the walls, mainly vertically.

Figure 9.1.1.4 shows a flat lower die with the location of the draw beads indicated by thick lines. In order to calculate the stress due to the load from the blank holder (7.1.1.11) is applied

$$\sigma_W = \frac{F_{BH}}{2L(I+J)} = \frac{1{,}2 \cdot 10^6}{2 \cdot 50(1900 \cdot 1170)} = 4\,\text{MPa} \qquad (9.1.1.3)$$

Figure 9.1.1.2. V-shaped lower die. The black lines indicates the position of the draw beads on which the load from the blank holder is distributed

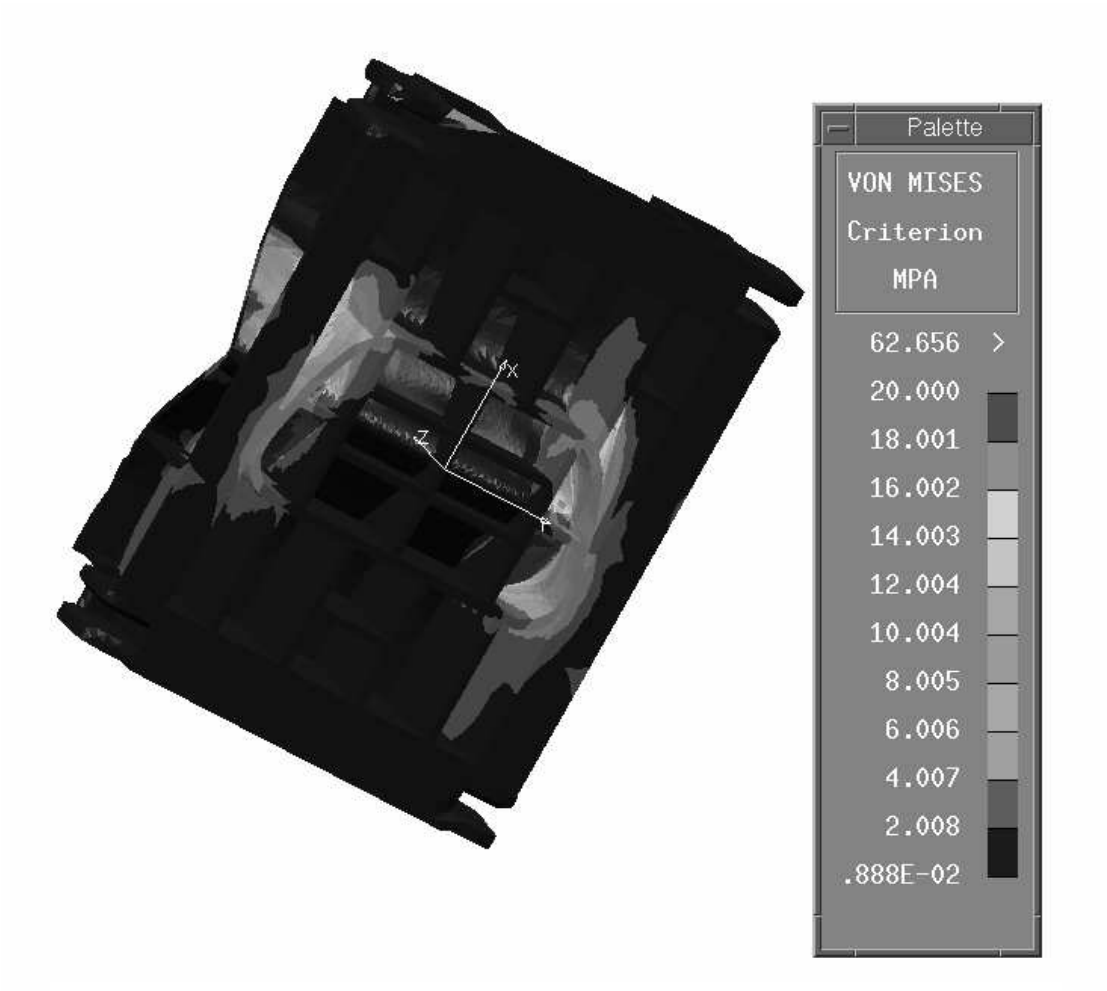

Figure 9.1.1.3. Von Mises stresses in V-shaped lower die the moment after the blank holder hit the lower die

Comments load case II, Area 1

The result from the finite element calculation is shown in Figure 9.1.1.5. The stress takes the same value in the walls irrespective of location, which is expected for a simple load case like this. The fact that the stress level is raised in the horizontal areas in connection to the walls under the draw beads, and the difference between the analytical and numerical calculations, 4 MPa compared to 2 MPa, is probably explained by the way the load is applied. In the model used in the finite element calculations no draw beads exist. Instead the load is applied on the radius encompassing the form area. See Figure 9.1.1.6. If the load would have been applied more vertically, as in the case of draw beads, the agreement between the calculations would have been much better.

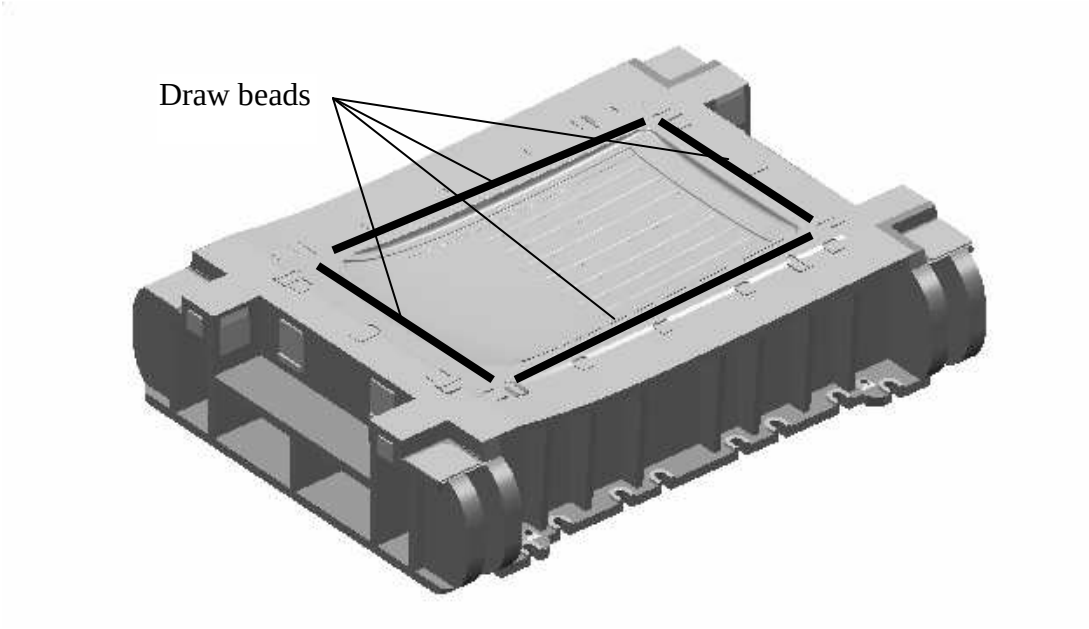

Figure 9.1.1.4. Flat lower die. The black lines indicate the position of the draw beads on which the load from the blank holder is distributed.

9.1.2. Blank holder – evaluation (Load case III, IV and V)

The load is applied according to what has been mentioned in section 9.1.1.

Load case III, Area 1

Regarding forces acting compressive at the vertically walls due to the load from the lower die, Figure 9.1.2.1 shows a V-shaped blank holder and the areas there the load from the lower die is transmitted. These areas correspond to the areas indicated in the lower die in Figure 9.1.1.2. Since the expressions to be used, geometry and load is the same as in section 9.1.1 the results are the same as in (9.1.1.1) and (9.1.1.2), namely 10 MPa and 17 MPa respectively.

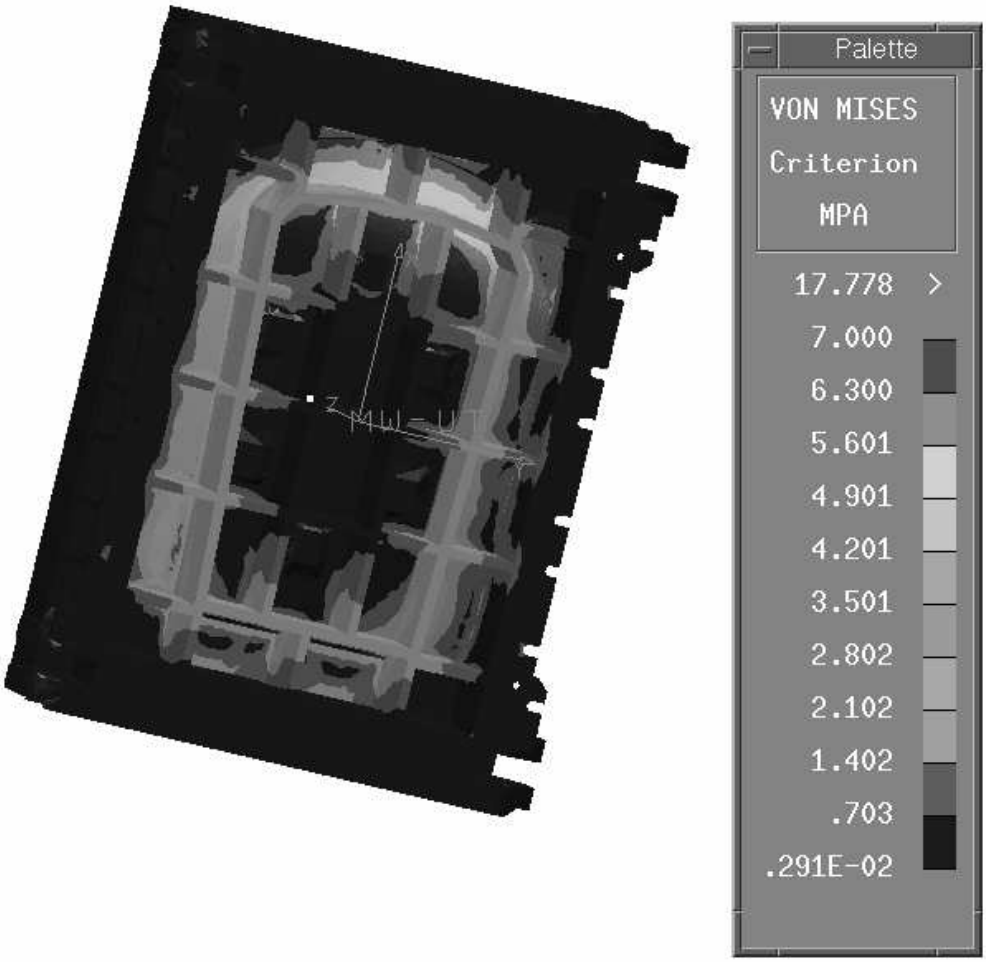

Figure 9.1.1.5. Stress distribution in a die with flat cross section due to the load from the blank holder in the draw beads.

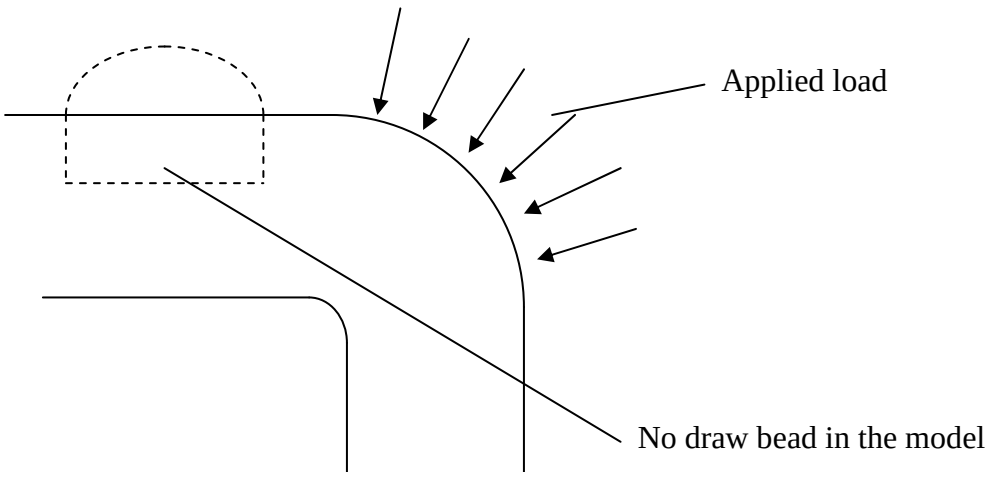

Figure 9.1.1.6. Since no draw beads exist in the model, the load is applied in the radius instead.

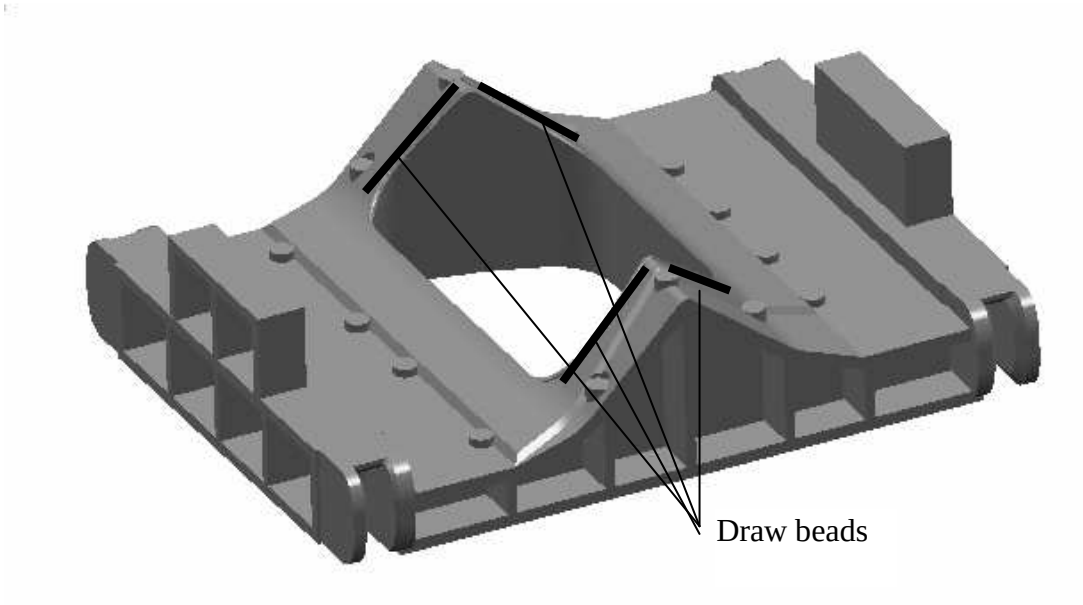

Figure 9.1.2.1. V-shaped blank holder. The black lines indicates the position of the draw beads on which the load from the lower die is distributed

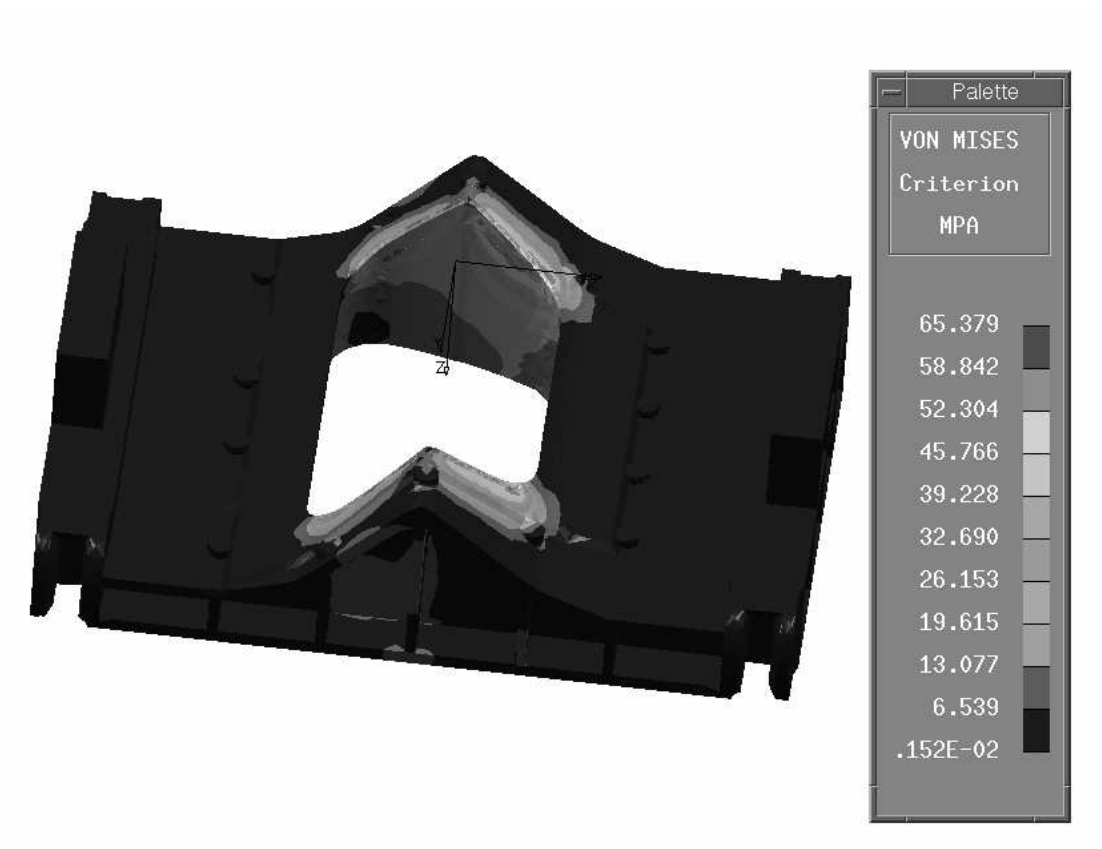

Figure 9.1.2.2. Von Mises stresses in V-shaped blank holder in the moment after the lower die and blank holder has got in touch.

Comments load case III, Area 1

Figure 9.1.2.2 shows the result from the finite element calculation. σ_{WA} corresponds to the stress in the walls with negative x-coordinate and σ_{WB} corresponds to the stress in the walls with positive x-coordinate. The analytically calculated value for σ_{WA} is 10 MPa (see (9.1.1.1)) and for σ_{WB} 17 MPa (see (9.1.1.2)). The values corresponding to σ_{WA} in the finite element calculation varies mainly between 6 and 19 MPa and for σ_{WB} the stress varies between 6 and 40 MPa. The locally higher stresses that vary between 40 and 65 MPa are probably not dependent of the thicknesses of the wall, but a consequence of the position of the draw bead, which is close to the edge. If the influence of the position of the draw bead is not considered, a comparison between the results shows upon a fair agreement. However, there is a potential in refining the model by consider the variation of the stress with the position in the z-direction and also by consider more than the stress component in the vertical direction.

Load case IV, Area 1

In flat dies, the load in the finite element calculation is applied as a pressure in the flat draw bead areas, which gives rise to a stress in the walls, mainly vertically directed.

Figure 9.1.2.3 shows a flat blank holder with the location of the draw beads indicated by thick lines. Since (7.1.1.11) is applied with the same values as in (9.1.1.3) in this case as well the result is 4 MPa.

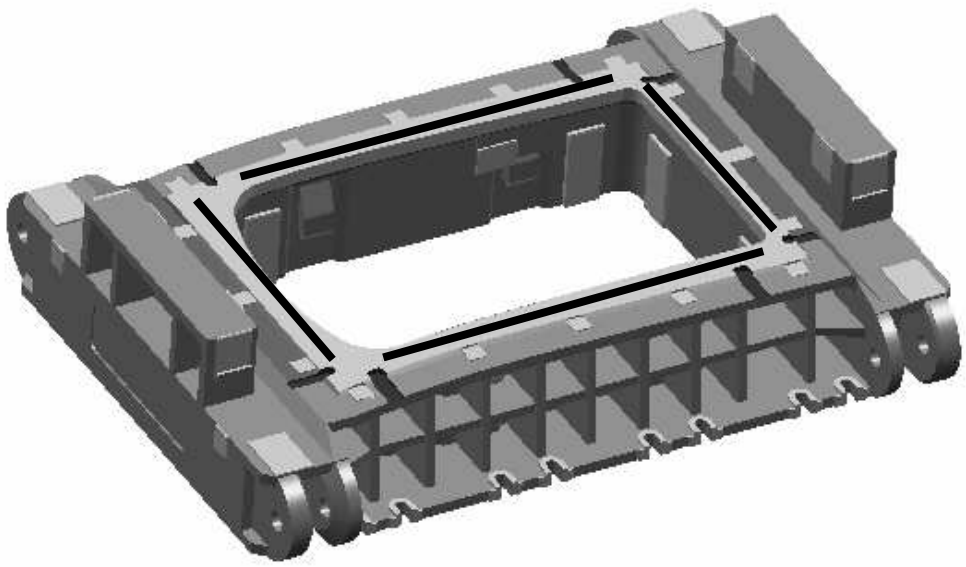

Figure 9.1.2.3. Flat blank holder. The black lines indicate the position of the draw beads on which the load from the blank holder is distributed.

Comments load case IV, Area 1

The result from the finite element calculation is shown in Figure 9.1.2.4. The stress varies in the interval 2-4 MPa, which is in agreement with the result from the analytical expression.

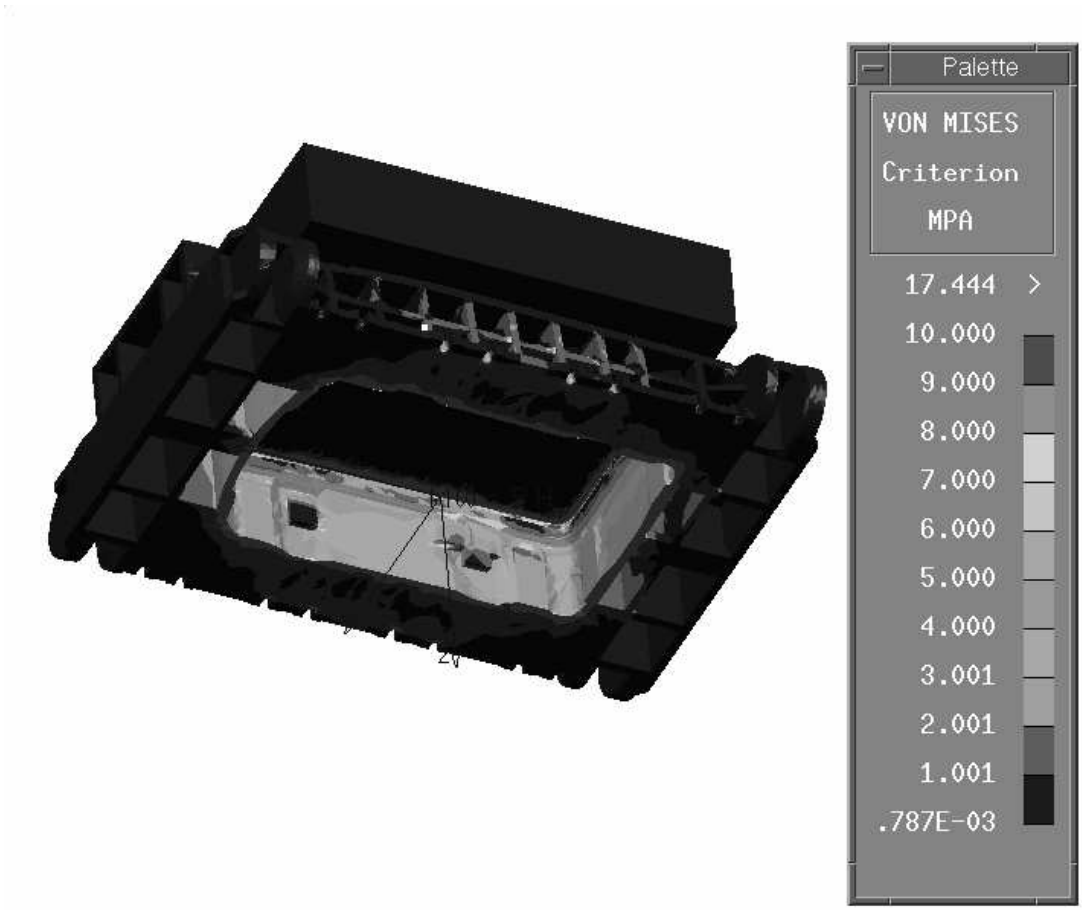

Figure 9.1.2.4. Stress distribution in a die with flat cross section due to the load from the lower die blank holder in the draw beads.

Load case V, Area 2

Figure 9.1.2.5 shows a blank holder, used in a single acting press supported with nitrogen springs, deformed due to load in the draw beads. The section indicated is used in the calculations. The deflection due to torsion is calculated using (7.1.2.8) and the resulting vertical deflection in the middle of the section is

$$\delta = H - b\sin\left(\arcsin\frac{H}{b} - \frac{(1+\nu)}{E}\frac{I}{2}\frac{F_{BH}}{(I+J)}a\frac{3}{B^3}\frac{1}{(C+D+H)}\right)$$

$$300 - 405\cdot\sin\left(\arcsin\left(\frac{300}{405}\right) - \frac{(1+0.28)}{165000}\cdot\frac{1360}{2}\cdot\frac{1.2\cdot 10^6}{1360+1250}\cdot 190\cdot\frac{3}{50^3}\cdot\frac{1}{175+175+300}\right) =$$

$$0.005\,\text{mm}$$

(9.1.2.1)

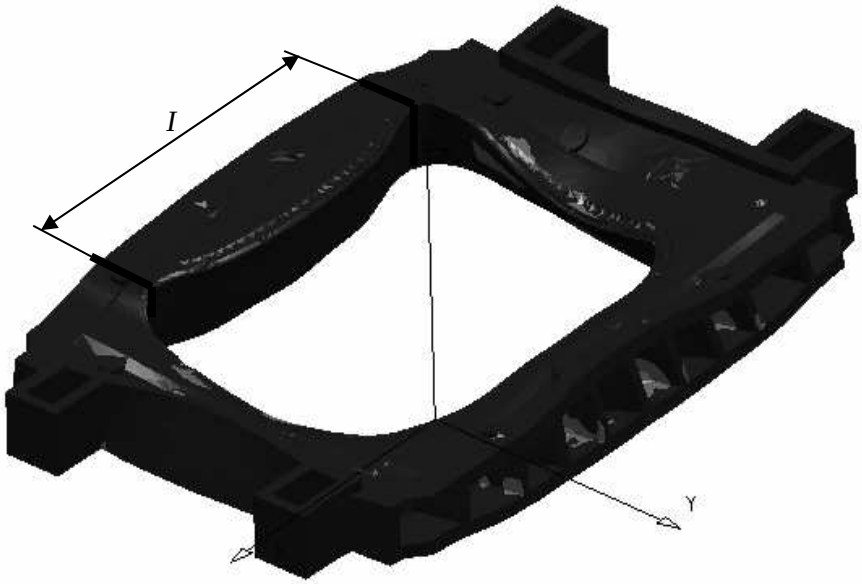

Figure 9.1.2.5. Blank holder in single acting press subjected to torsion.

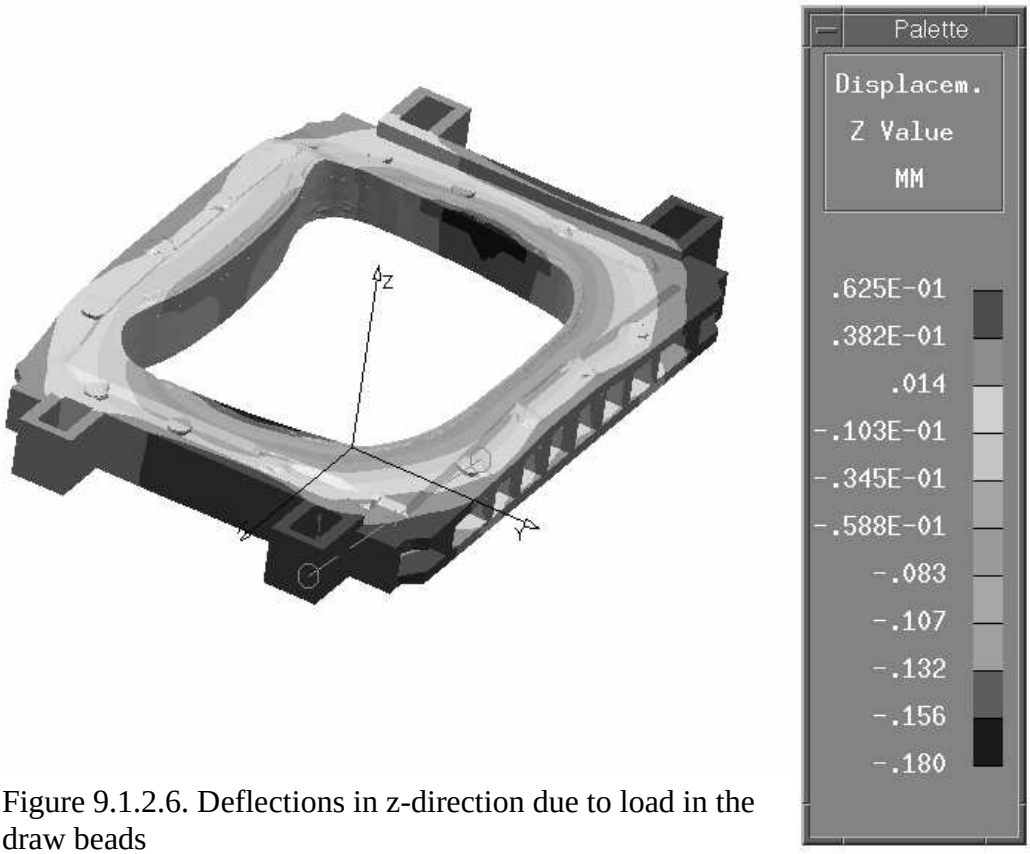

Figure 9.1.2.6. Deflections in z-direction due to load in the draw beads

Comments load case V, Area 2

As can be seen in Figure 9.1.2.6, 0.06 mm from the finite element calculation shall be compared with 0.005 mm from the analytical calculation, i.e. a difference approximately equal to a factor 10. An explanation to the lack of agreement between the results probably lies in the behavior of the ends. In the derivation of the analytical expression it was assumed that the ends are clamped, which is not the case according to the finite element calculation and since the ends are subjected to torsion as well, a larger deflection results.

9.2. Load cases when the punch hits the blank – evaluation (Load case VI and VII)

The deflection was calculated using (7.2.3). The stress in the blank was set equal to 600 MPa and the thickness equal to 1.5 mm. In this case the stress has been chosen to correspond to the yield stress for UHSS (Ultra High Strength Steel).

Load case VI, Area VI

Together with geometrical parameters for the flat die used in the calculations, the result reads

$$\delta = \frac{Ql^4}{384EI_z} = \frac{\sigma\, tl^4}{384EI_z} = \frac{\sigma\, tl^4}{32EB\left(A^3 + C^3\right)} = \frac{600 \cdot 1.5 \cdot 1625^4}{32 \cdot 165000 \cdot 55\left(295^3 + 460^3\right)}\,\text{mm} = 0.2\,\text{mm} \tag{9.2.1}$$

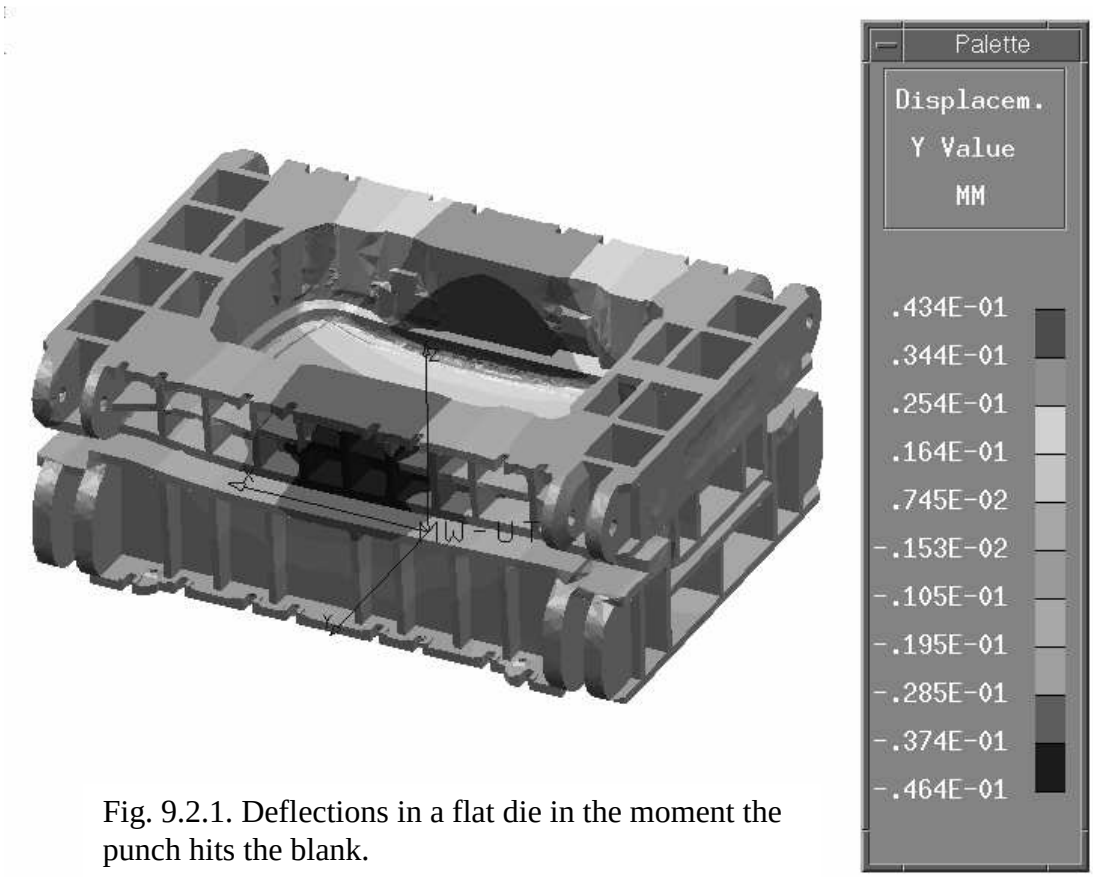

Fig. 9.2.1. Deflections in a flat die in the moment the punch hits the blank.

Comments load case VI, Area 2

As can be seen from Figure 9.2.1, 0.043 mm from the finite element calculations, shall be compared with 0.2 mm, i.e. a difference of about a factor five between the calculations. It seems to be a too coarse approximation only considering the sections marked out in Figure 7.2.1. Especially the forming area contributes to make the cross section stiffer. In the FE-calculation the lower die and the blank holder were prevented to move independently to each other, which probably they will in reality. More dies have to be analysed using FE-calculations with possibility to solve contact problems, before any statement can be made how to refine (7.2.3).

Load case VII, Area 2

After (7.2.3) has been applied on the left side on structure shown in Figure 9.2.2, the result for the deflection at midspan reads

$$\delta = \frac{Ql^4}{384EI_z} = \frac{\sigma\, tl^4}{384EI_z} = \frac{\sigma\, tl^4}{32EB\left(A^3 + C^3\right)} = \frac{600 \cdot 1.5 \cdot 1650^4}{32 \cdot 165000 \cdot 50\left(720^3 + 1000^3\right)}\,\text{mm} = 0.02\,\text{mm}$$

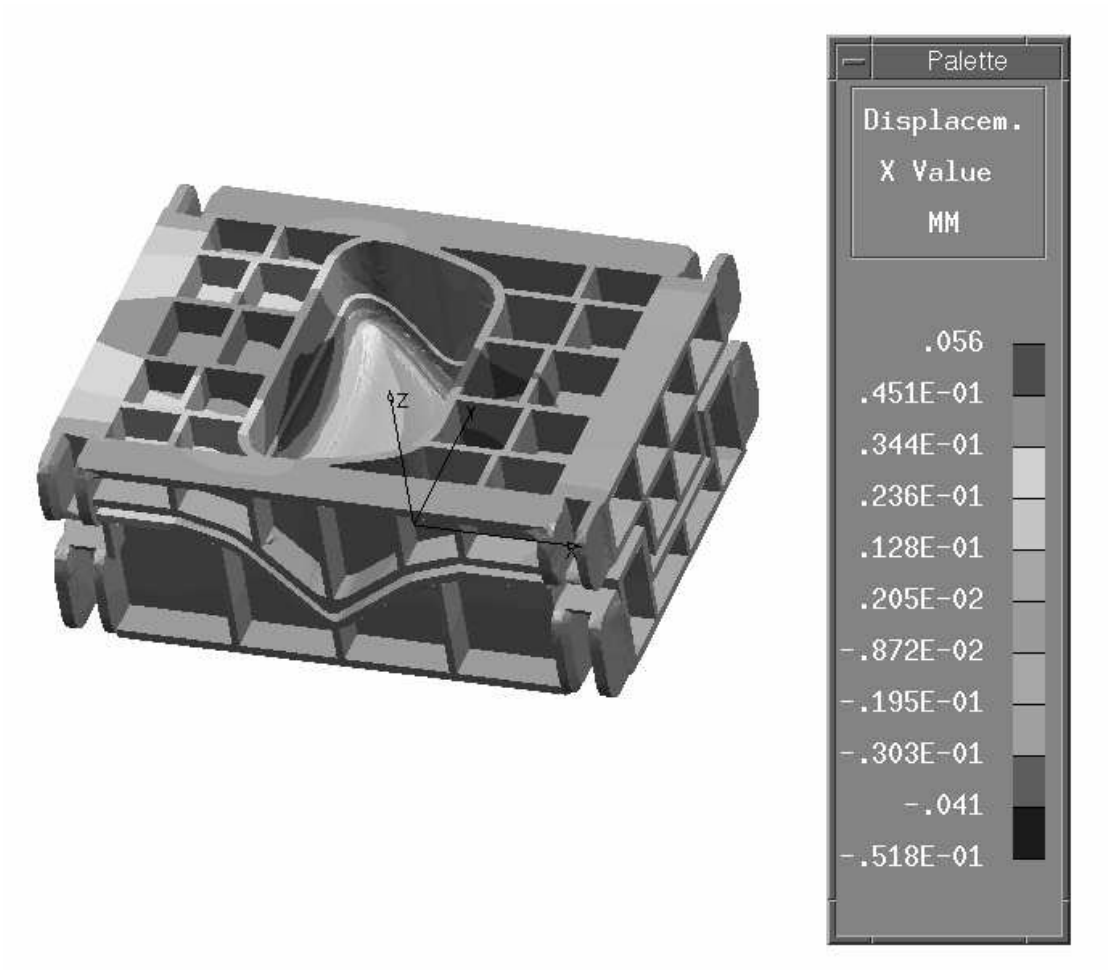

Comments load case VII, Area 2

In this case it differs a factor three between the results, but in contradiction to the previous load case, the deflection according to the FE-calculation is larger compared the analytically calculated.

9.3. Load cases when the die is closed - evaluation

In this section load cases are considered when the die is closed. During forming the areas containing radii are exposed to the forces necessary to deform the blank. In order to simplify the calculations the body not considered is assumed to be rigid. This means, for instance when calculating the deflection under the distance plates, if the lower die is considered, that the blank holder is assumed to be rigid. In this manner the worst case is treated.

9.3.1. Lower die – evaluation (Load case VIII, IX, X, XI, XII, XII and XIV)

Regarding the lower die, the load from the punch slide is in the FE-calculations transmitted to the lower die in two different ways depending on type of die. In the case of flat dies a solid body, corresponding to the punch, is merged with the lower die in the areas where the load transmission is assumed to occur. At the top of the merged body, which corresponds to the area between the punch slide and the punch, a contact load is applied. The benefit from such approach is that the stress distribution in the boundary between the punch and lower die better

reflects the reality compared to if the load would have been applied as an equally distributed pressure over the form surfaces in the lower die. Regarding the V-shaped dies a pressure load is (load normal to the surface) applied at the form surfaces. (7.3.1.8) and (7.3.1.9) are used to calculate the applied pressure. The load over the distance plates, which is assumed to be the same for each plate, is applied as a contact load. Both the load from the punch and the load from the blank holder are applied at the same time.

With reference to what has been mentioned earlier, the loads acting at the V-shaped lower die are shown in Figure 9.3.1.1.

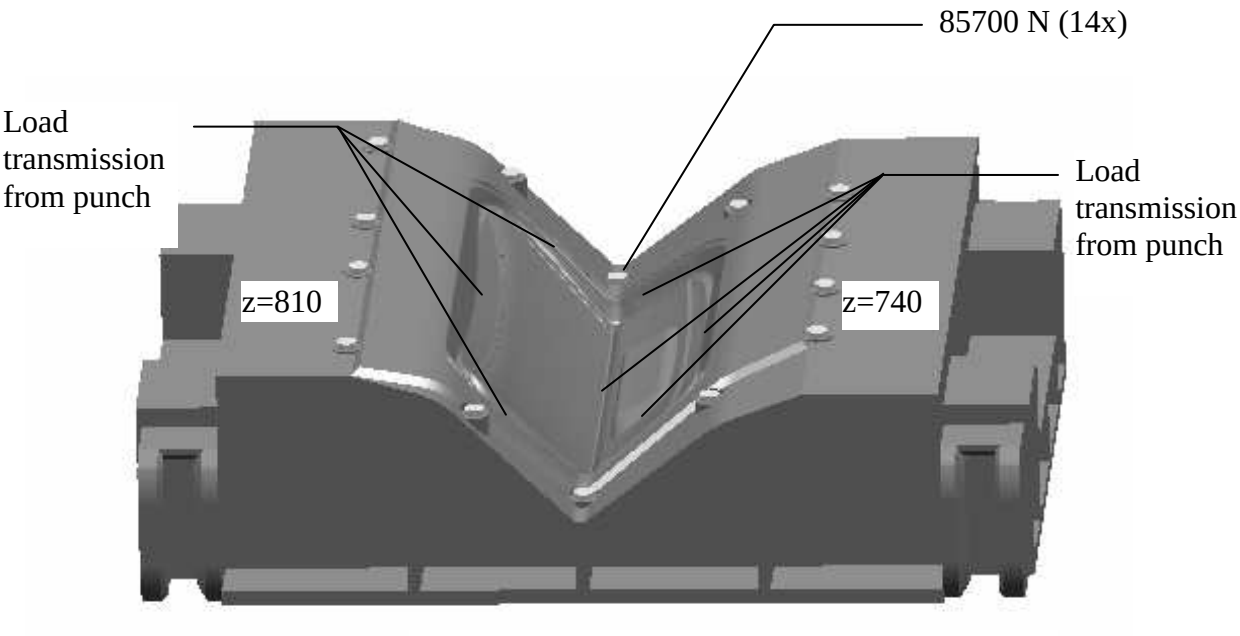

Fig. 9.3.1.1. Load acting at V-shaped lower die when the die is closed.

Load case VIII, Area 6

In order to determine the stress due to the horizontal force transmitted from the punch via the blank, trying to separate the lower die when the die closes, use of (7.3.1.10) is made.

$$\begin{aligned} F_H &= F_P \cos\alpha \cos\beta / (\cos\alpha \sin\beta + \cos\beta \sin\alpha) = \\ &6 \cdot 10^6 \cos 45° \cos 52° / (\cos 45° \sin 52° + \cos 52° \sin 45°) \text{ N} = 2631646.32 \text{ N} \end{aligned} \tag{9.3.1.1}$$

Knowing the horizontal force, (7.3.1.11) and (7.3.1.12) are used to calculate the stress components

$$\begin{aligned} \sigma_{xx} &= \frac{2F_H}{BL} = \frac{2 \cdot 2631646.32}{60 \cdot 1430} = 61.34 \text{ MPa} \\ \sigma_{yy} &= \sigma_{zz} = \sigma_{xx} \nu = 61.34 \cdot 0.28 = 17.18 \text{ MPa} \end{aligned} \tag{9.3.1.2}$$

Finally (7.3.1.26) is used to find out if yielding occurs or not.

$$\sqrt{\sigma_{xx}^2 - \sigma_{xx}\sigma_{yy} - \sigma_{xx}\sigma_{zz} + \sigma_{yy}^2 - \sigma_{yy}\sigma_{zz} + \sigma_{zz}^2} + \frac{(\sigma_c - \sigma_t)(\sigma_{xx} + \sigma_{yy} + \sigma_{zz}) - 2\sigma_c\sigma_t}{\sigma_c + \sigma_t} =$$

$$\sqrt{61.34^2 - 61.34 \cdot 17.18 - 61.34 \cdot 17.18 + 17.18^2 - 17.18 \cdot 17.18 + 17.18^2} + \frac{(414 - 380)(61.34 + 17.18 + 17.18) - 2 \cdot 414 \cdot 380}{414 + 380} = -348 \qquad (9.3.1.3)$$

The negative result tells that the stress state is well contained within the yield surface. To make it possible to compare the analytical result with the FE-calculation it is necessary to convert the stress state to the von Mises criterion which is given as

$$\sqrt{3J_2} - \sigma_{y0} = 0 \qquad (9.3.1.4)$$

σ_{y0} denotes the initial yielding stress and $\sqrt{3J_2}$ is given by (7.3.1.20). Thus the stress state is calculated as

$$\sqrt{3J_2} = \sqrt{\sigma_{xx}^2 - \sigma_{xx}\sigma_{yy} - \sigma_{xx}\sigma_{zz} + \sigma_{yy}^2 - \sigma_{yy}\sigma_{zz} + \sigma_{zz}^2} = \sqrt{61.34^2 - 61.34 \cdot 17.18 - 61.34 \cdot 17.18 + 17.18^2 - 17.18 \cdot 17.18 + 17.18^2} = 44\,\text{MPa} \qquad (9.3.1.5)$$

A section from the FE-result corresponding to section S-S in Figure (7.3.1.1), i.e. in the bottom of the V-shape is shown in Figure 9.3.1.2.

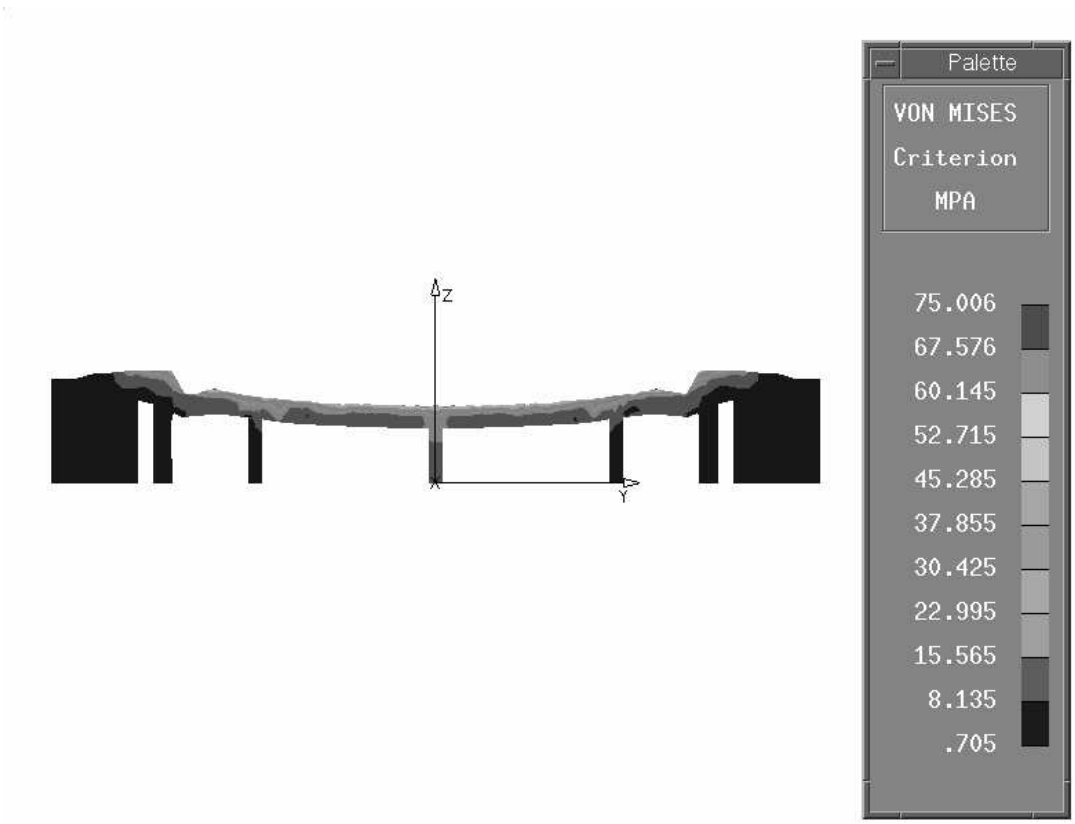

Fig. 9.3.1.2. Cross section corresponding to section S-S in Figure 7.3.1.1, i.e. at the bottom of the V-shape.

Comments load case VIII, Area 6

It is concluded that the analytical calculations is in fair agreement with the FE-calculations. See fig 9.3.1.2. Apart from small local areas with stress levels about 75 MPa the stress varies between 15 and 52 MPa in the upper half of the section. In the deriving of (7.3.1.11) it was assumed that only the upper half carried the load. To obtain a better agreement with the FE-calculation it is possible to assume that the stress decreases over the section according to some suitable function. In that case the right hand side of (7.3.1.11) has to be expressed as an integral. However, it is of greater importance to find out how the distribution varies with the load and the thickness of the section. Finally it must be kept in mind that the lower die at the bottom in the FE-calculation is constrained to any movements in the z-direction while it in reality is only constrained in the negative z-direction. The constraints in the FE-calculations may introduce additional stresses.

Load case IX, Area 4

In order to determine the stress in the walls due to the punch load and since it dealt with a die with a simple V-shape, (7.3.1.29) and (7.3.1.30) are inserted in (7.3.1.34) and (7.3.1.35) respectively to obtain an expression for the wall thickness given geometrical data, punch load, and tension. In order to make a comparison with the FE-calculation the expressions above are solved for σ_{WA} and σ_{WB}, which yields

$$\begin{aligned}\sigma_{WA} &= F_p \tan\alpha / \left((\tan\alpha + \tan\beta)\left(-n\left(IJ + B_a^2 - B_a(I+J)\right) + A_{PA}\right)\right) = \\ &6 \cdot 10^6 \tan 45° / \left((\tan 45° + \tan 52°)\left(-6\left(380 \cdot 250 + 40^2 - 40(380+250)\right) + 802500\right)\right) \text{MPa} = \\ &7 \text{ MPa}\end{aligned} \tag{9.3.1.6}$$

$$\begin{aligned}\sigma_{WB} &= F_p \tan\beta / \left((\tan\alpha + \tan\beta)\left(-n\left(EF + B_b^2 - B_b(E+F)\right) + A_{PB}\right)\right) = \\ &6 \cdot 10^6 \tan 52° / \left((\tan 45° + \tan 52°)\left(-6\left(430 \cdot 155 + 40^2 - 40(430+155)\right) + 608080\right)\right) \text{MPa} = \\ &10 \text{ MPa}\end{aligned} \tag{9.3.1.7}$$

Average values of the size of the casting structure have been inserted. The result from the FE-calculation is shown in Figure 9.3.1.3.

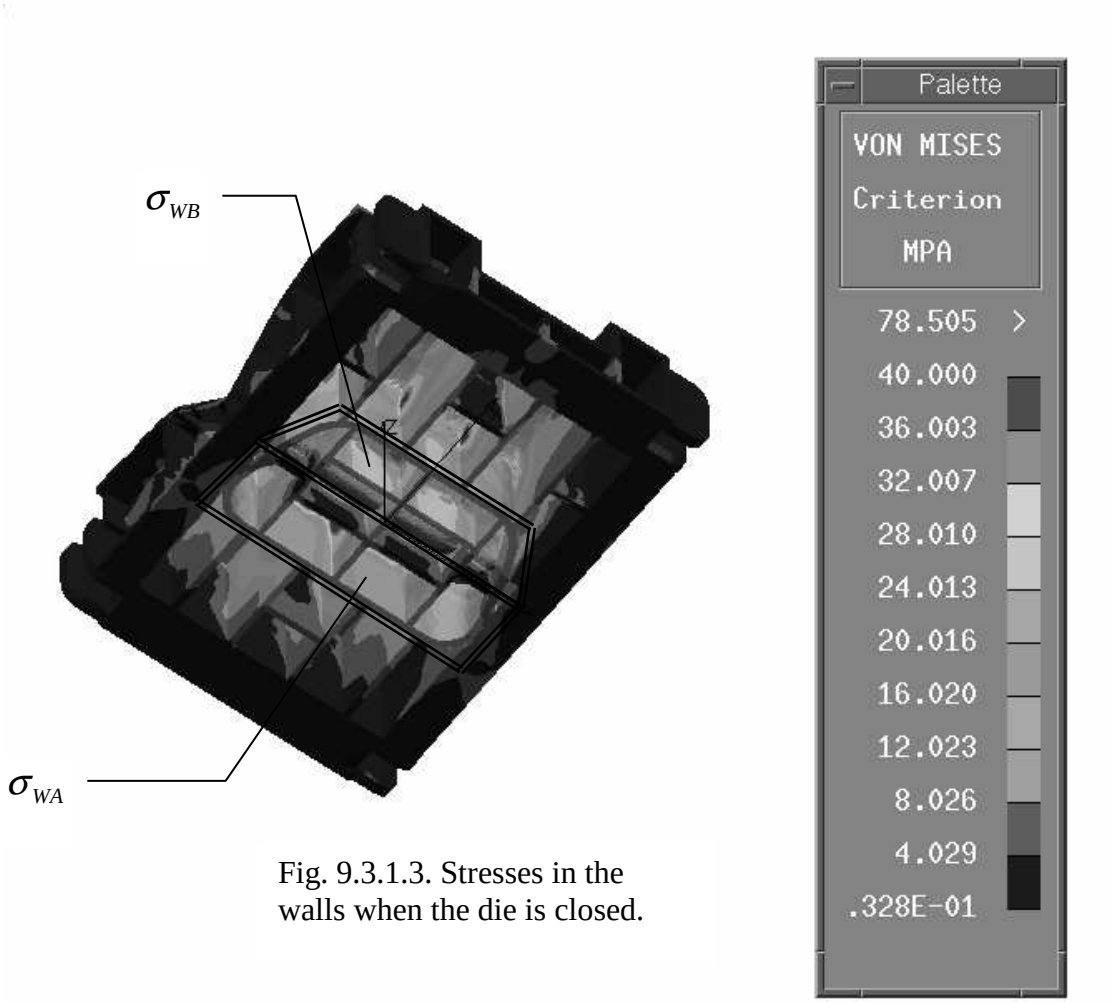

Fig. 9.3.1.3. Stresses in the walls when the die is closed.

Comments load case IX, Area 4

σ_{WA} given by (9.3.1.6) and σ_{WB} given by (9.3.1.7) act in the areas indicated in Figure 9.3.1.3. It is concluded that the assumption that the stress distributions are constant in their respective area are not true. In the area valid for σ_{WA} the stresses vary between a few MPa to 28 MPa and locally even higher. These values are to be compared with the predicted value of 7 MPa. The stresses for the area represented by σ_{WB} vary between a few MPa to 32 MPa with locally higher values and the predicted value is 10 MPa. It seems to be a too coarse assumption assuming the load to be equally distributed over the whole forming area. Instead it is suggested to distribute the load equally over the forming radii. If necessary the expression probably can be refined by taking a bi- or tri-axial stress state into account.

Load case X, Area 1 and 5

With respect to what has been mentioned in section 7.3.1, the stress state in the walls due to the load on the distance plates from the blank holder is calculated from (7.3.1.37). In this calculations the stresses in the areas at the sides with z=740 mm and z=810 mm are considered. As can be seen from Figure 9.3.1.1 and Figure 9.3.1.3, there is difference in geometry between the areas. In the area with z=740 mm is alternative c applicable with *C* substituted for *C*/2 and the same is valid for the two walls closest to the center line at z=810

mm, whilst alternative c with C=0 is valid for the outer walls. Starting with the area for z=740 mm and the distance plates closest to nearest the center line at z=810 mm the result is

$$\sigma_W = \frac{F_{BH}}{nB\left(A + C/2\right)} = \frac{1.2 \cdot 10^6}{14 \cdot 40(400 + 200)} \text{MPa} = 4 \text{ MPa} \qquad (9.3.1.8)$$

For the outer distance plates at z=810 mm is alternative c with *C*=0 applicable which yields

$$\sigma_W = \frac{F_{BH}}{nBA} = \frac{1.2 \cdot 10^6}{14 \cdot 40 \cdot 400} \text{MPa} = 5 \text{ MPa} \qquad (9.3.1.9)$$

The corresponding displacements are calculated with help from (7.3.1.38) which yields

$$\begin{aligned} u_{z,740} &= \frac{\sigma_w}{E} H = \frac{4}{165 \cdot 10^3} 740 \text{ mm} = 0.02 \text{ mm} \\ u_{z,810inner} &= \frac{\sigma_w}{E} H = \frac{4}{165 \cdot 10^3} 810 \text{ mm} = 0.02 \text{ mm} \\ u_{z,810outer} &= \frac{\sigma_w}{E} H = \frac{5}{165 \cdot 10^3} 810 \text{ mm} = 0.02 \text{ mm} \end{aligned} \qquad (9.3.1.10)$$

Comments load case X, Area 1 and 5

From Figure 9.3.1.3 it is immediately concluded that the stress levels vary in the walls. At the distance plates at the height 740 mm the stress varies from a few to about 20 MPa and locally higher. For the distance plates at height 810 are the corresponding values a few MPa to 16 MPa and locally higher. This indicates that the stress due to the punch also influences the areas under the distance plates and the adopted description is too simple. The difference in stress between the analytical and FE-calculated values is reflected in the displacements, 0.02 mm from the analytical expression compared to 0.03-0.045 from the FE-calculations. It should be noted that the shown displacements in Figure 9.3.1.4 are the magnitude of the displacement vector, which means that the displacements in the walls not necessarily are parallel to the z-direction.

Load case XI, Area 3

In order to calculate the deflection in the area between the walls Figure 9.3.1.4 is considered. The two areas having the largest deflections have a maximum deflection of 0.146 mm, but after the deflections of the surroundings, which are about 0.087 mm, have been subtracted, the maximum deflection of the area between the walls is 0.146-0.087=0.059 mm. The thickness varies from 56 to 68 mm and the size of the plate is 255x460 mm. This means, as has been mentioned earlier, that the derived expression may not give a reliable result since the thickness exceeds one tenth of the shortest length of the sides. In the FE-calculation a load of 14 MPa is applied. In (7.3.1.41) the load is calculated with help from the expression for F_B ,(7.3.1.9), i.e. the load is assumed to be equally distributed over the whole area, not only the areas with radii. Finally it is assumed that the plate is deformed mainly normal to the surface. Starting with the calculation of F_B

$$F_B = F_P \cos\alpha / (\cos\alpha \sin\beta + \cos\beta \sin\alpha) =$$

$$\frac{6 \cdot 10^6 \cos 45°}{\cos 45° \sin 52° + \cos 52° \sin 45°} \text{ N} = 4.27 \cdot 10^6 \text{ N} \tag{9.3.1.11}$$

When the force is known, the load is calculated

$$q = \frac{F_B}{S} = \frac{4.27 \cdot 10^6}{685200} \text{ MPa} = 6.23 \text{ MPa} \tag{9.3.1.12}$$

and finally the deflection using (7.3.1.41)

$$u = \frac{15q\left(1-\nu^2\right)}{32Et^3} \frac{A^4 B^4}{7A^2B^2 - 2A^2B^2\nu + 10A^4 + 10B^4} =$$

$$\frac{15 \cdot 6.23\left(1-0.28^2\right)}{32 \cdot 165 \cdot 10^3 \cdot 62^3} \frac{460^4 \cdot 255^4}{7 \cdot 460^2 \cdot 255^2 - 2 \cdot 460^2 \cdot 255^2 \cdot 0.28 + 10 \cdot 460^4 + 10 \cdot 255^4} \text{ mm} = 0.02 \text{ mm} \tag{9.3.1.13}$$

Comments load case XI, Area 3

A deflection of 0.02 mm from the analytical expression compared to 0.059 mm from the FE-calculation means a difference of a factor three, which is not acceptable. The explanation is found in the discussion above. What may reduce the error is the fact that it is not sure that the displacement vector from the FE-calculation is normal to the surface. If this is the case, the component normal to the surface will be less than 0.059 mm.

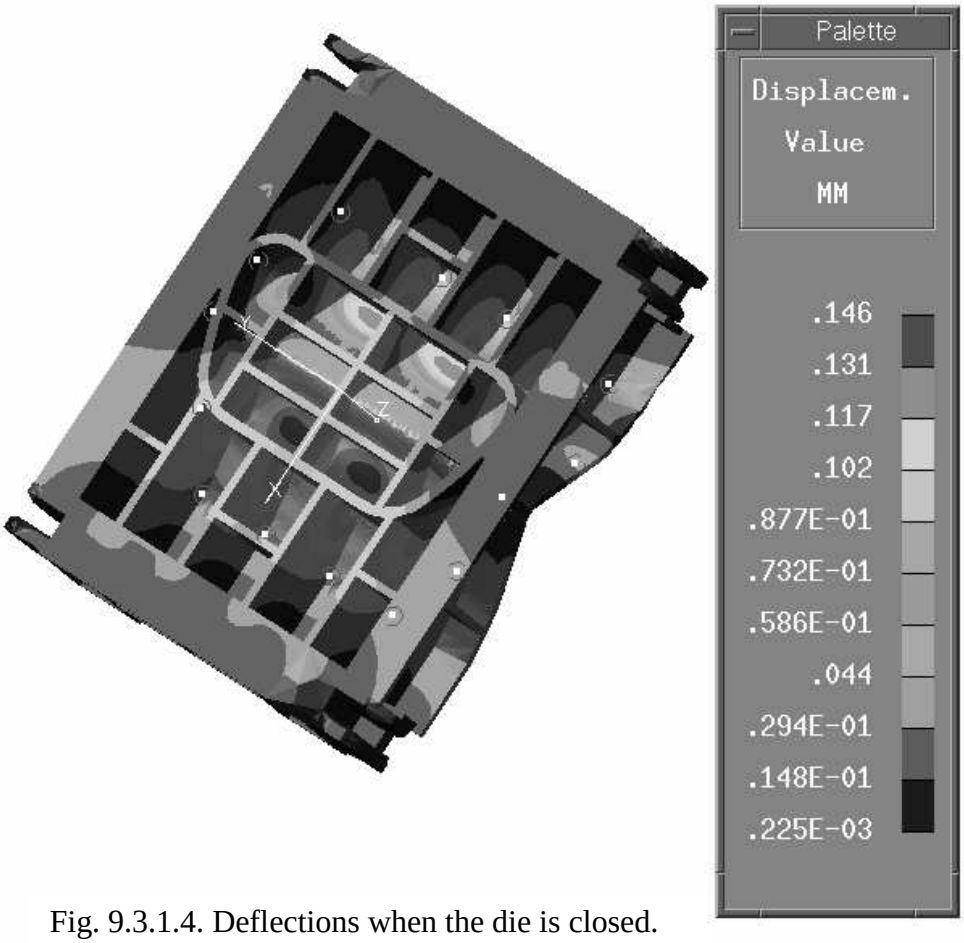

Fig. 9.3.1.4. Deflections when the die is closed.

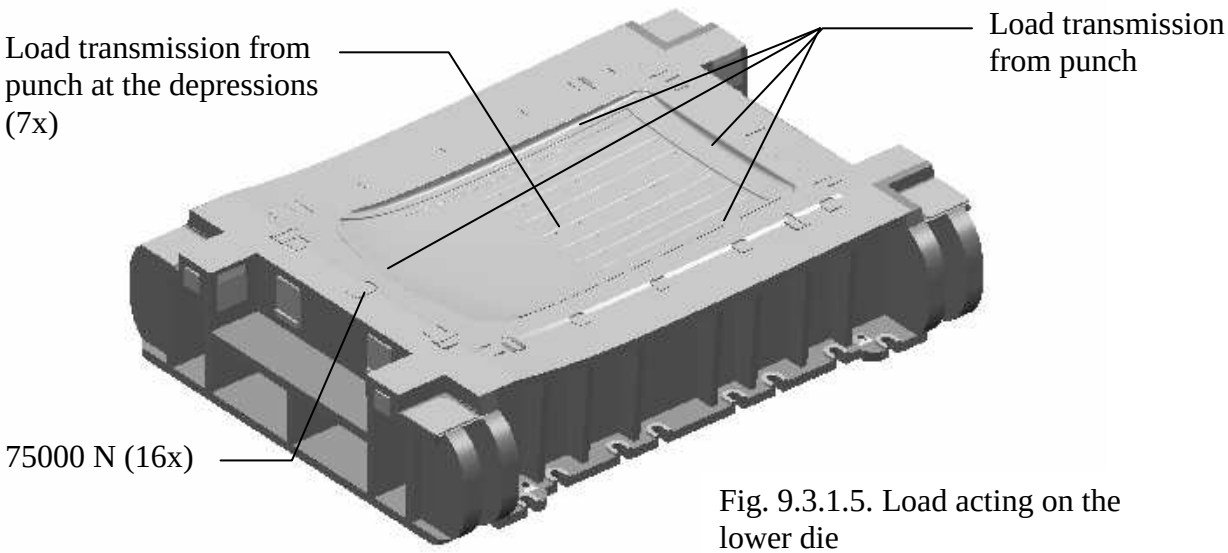

Fig. 9.3.1.5. Load acting on the lower die

Load case XII, Area 4

Figure 9.3.1.5 shows the loads acting in a flat lower die when the die is closed. Just as in the case of V-shaped dies is the load from the blank holder transmitted only at the distance plates.

Using (7.3.1.42) and solving for the stress acting at the walls due to the punch load yields

$$\sigma_W = \frac{F_P}{A + n(G(B-H) + B(H-B))} = \frac{6 \cdot 10^6}{2241360 + 12(490(40-380) + 40(380-40))} \text{MPa} = 15\,\text{MPa} \tag{9.3.1.14}$$

Comments load case XII, Area 4

As can be seen in Figure 9.3.1.6 the analytically calculated result is mainly in agreement with the FE-calculation. Differences are found in the area where no force transmission takes place and the conclusion is that the expression reflects the stress state well as long as the punch load is distributed over the whole forming area. If this is not the case, the area under the locations where the punch load is transmitted has to be used.

Load case XIII, Area 1 and 5

With reference to (7.3.1.37) and Figure 7.3.1.10, alternative **a** is the most suitable description and the stress in the walls due to the load on the distance plates is calculated as

$$\sigma_W = \frac{F_{BH}}{nB(A+C)} = \frac{1.2 \cdot 10^6}{16 \cdot 40(300+440)} \text{MPa} = 3\,\text{MPa} \tag{9.3.1.15}$$

and the deflection, using (7.3.1.38), as

$$u_z = \frac{\sigma_w}{E} H = \frac{3}{165 \cdot 10^3} 640\,\text{mm} = 0.01\,\text{mm} \tag{9.3.1.16}$$

Comments load case XIII, Area 1 and 5

The result from the FE-calculation is seen in Figure 9.3.1.6. The FE-calculation predicts a slightly higher stress level, 2-8 MPa, depending on location. This is due to the influence of the punch load and it is suggested that a parameter that take this into account is incorporated in (7.3.1.37). Regarding the deflections the agreement is satisfactory. See Figure 9.3.1.7.

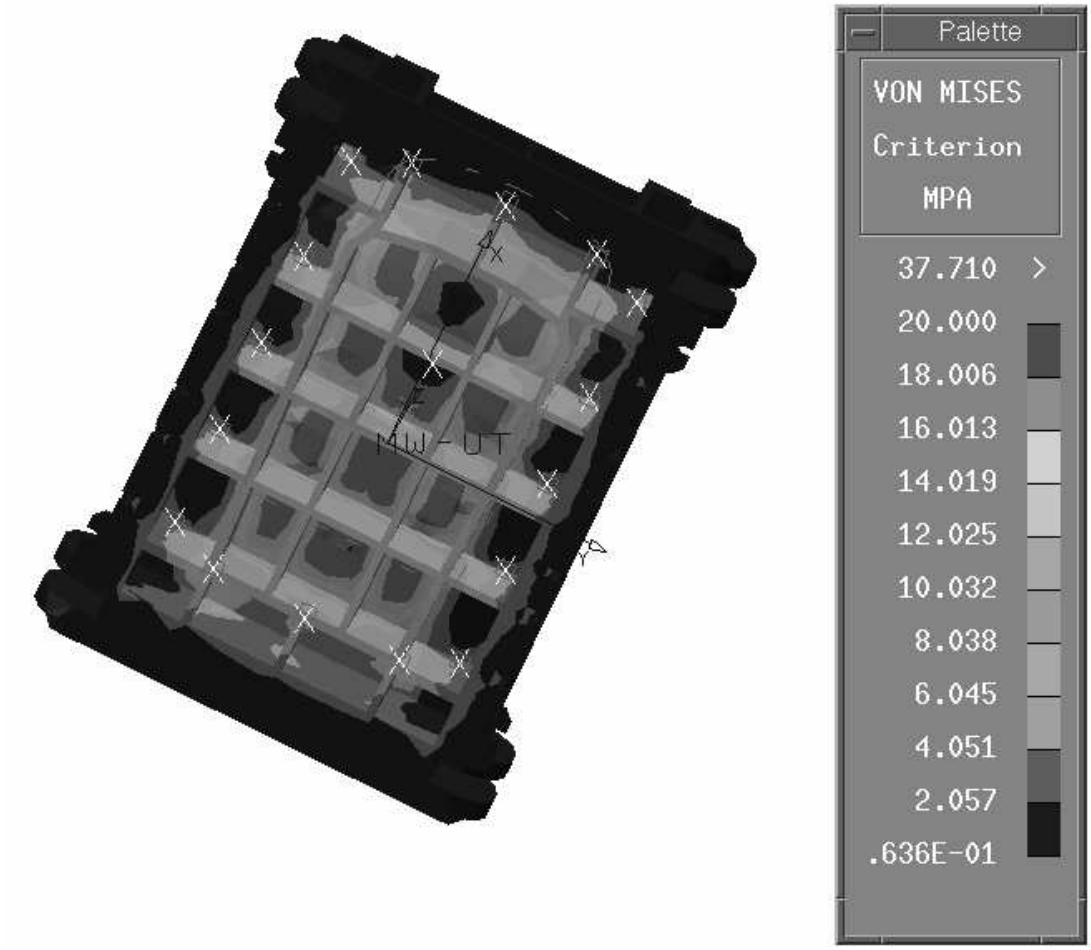

Fig. 9.3.1.6. Stress distribution in the lower die when the die is closed

Load case XIV, Area 3

(7.3.1.41) can be used to calculate the deflections in flat lower dies as well, but firstly the load q is calculated

$$q = \frac{F_P}{S} = \frac{6 \cdot 10^6}{2241360}\,\text{MPa} = 2.68\,\text{MPa} \tag{9.3.1.17}$$

Insertion in (7.3.1.41) yields

$$u = \frac{15q\left(1-\nu^2\right)}{32Et^3}\frac{A^4B^4}{7A^2B^2 - 2A^2B^2\nu + 10A^4 + 10B^4} =$$
$$\frac{15 \cdot 2.68\left(1 - 0.28^2\right)}{32 \cdot 165 \cdot 10^3 \cdot 90^3}\frac{440^4 \cdot 360^4}{7 \cdot 440^2 \cdot 360^2 - 2 \cdot 440^2 \cdot 360^2 \cdot 0.28 + 10 \cdot 440^4 + 10 \cdot 360^4}\,\text{mm} = 0.009\,\text{mm}$$

(9.3.1.18)

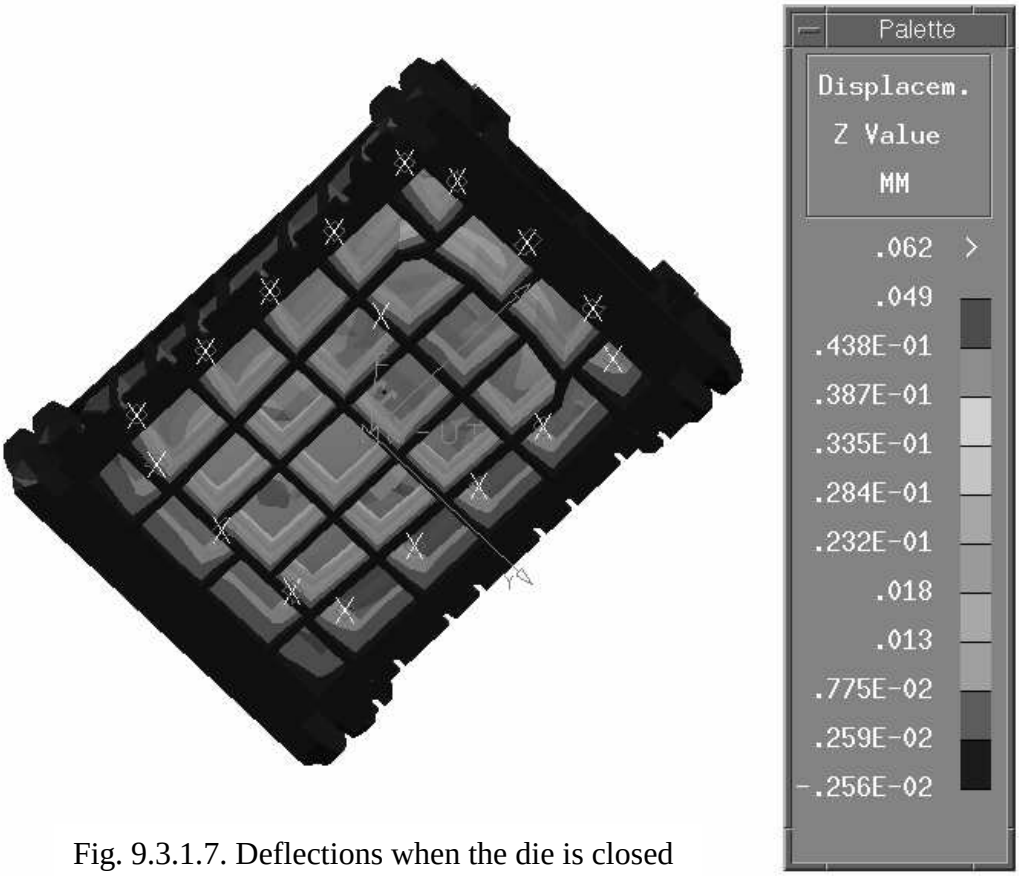

Fig. 9.3.1.7. Deflections when the die is closed

Comments load case XIV, Area 3

The calculation above was performed regarding the area with the largest deflection in Figure 9.3.1.7. The deflection in the surroundings shall be subtracted from the deflection at the center to obtain a value which can be compared to value from the analytical expression. This means that 0.044-0.033=0.01 mm shall be compared to 0.009 mm, an unexpected small difference, since the thickness of 90 mm implies that the range of validity is exceeded according to what has been mentioned in section 7.3.1. It was concluded in appendix A, that the derived expression predicts too large deflections, when the thickness exceeds about one tenth of the length of the shortest sides. The explanation to the result is probably found in how the load is applied. In the FE-calculation the load is applied along the depression, i.e. more concentrated compared to the equally distributed load in the analytical expression, and this yields a larger deflection which in this case happens to contribute to make the results agree.

9.3.2. Punch – evaluation (Load case XV, XVI, XVII and XVIII)

The load is, just as in the case of the lower die (see section 9.3.1), applied in two different ways depending on the type of cross section. Regarding flat punches, a solid body corresponding to the lower die is merged with the punch in those areas where the force transmission is said to take place. At the top of the merged body, i.e. the bottom of the lower die, a contact load is applied corresponding to the reactive forces from the bolster. Of the same reasons as mentioned regarding the lower die (see section 9.3.1) the load over the punch is applied as a pressure in dies with a V-shaped cross section.

Load case XV, Area 4

Figure 9.3.2.1 shows where the load is applied in a V-shaped punch.

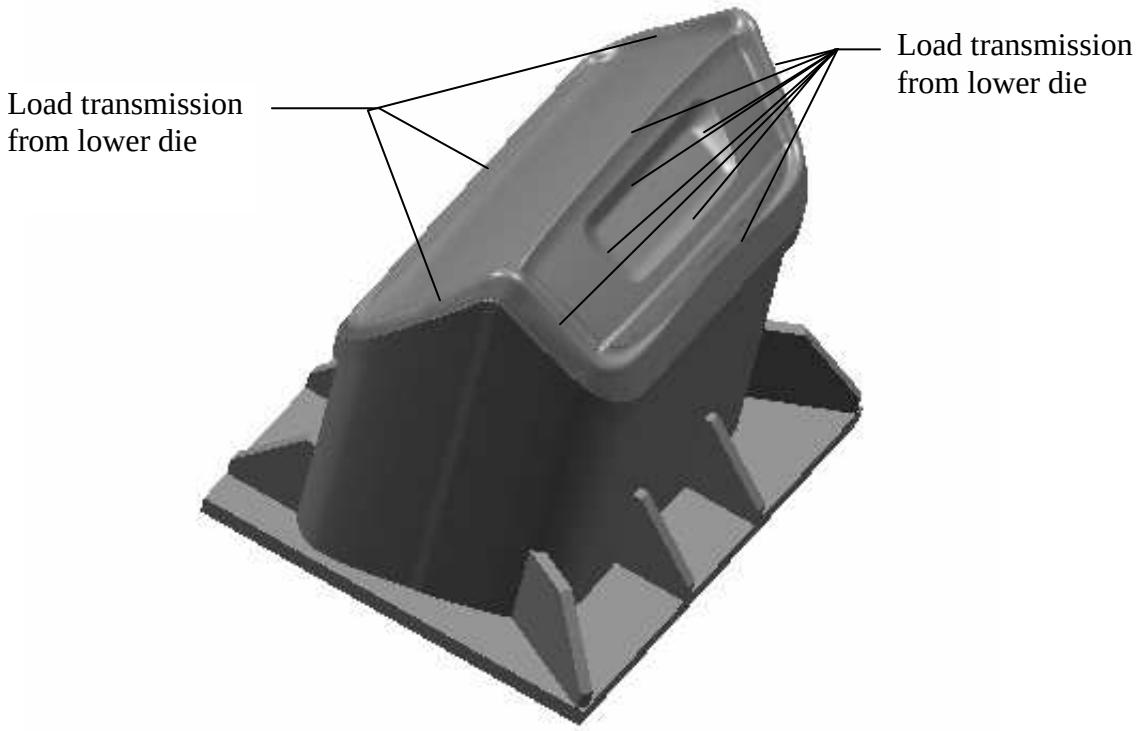

Fig. 9.3.2.1. Load acting at V-shaped punch when the die is closed.

The situation is the same as in section 9.3.1, regarding the lower die, and (7.3.1.34) and (7.3.1.35) are used once more in order to calculate the stress in the walls due to the load from the lower die.

$$\begin{aligned}\sigma_{WA} &= F_p \tan\alpha / \left(\left(\tan\alpha + \tan\beta\right)\left(-n\left(IJ + B_a^2 - B_a\left(I + J\right)\right) + A_{PA}\right)\right) = \\ &6 \cdot 10^6 \tan 45° / \left(\left(\tan 45° + \tan 52°\right)\left(-4\left(330 \cdot 305 + 40^2 - 40\left(330 + 305\right)\right) + 546375\right)\right) = \\ &11\,\text{MPa}\end{aligned} \tag{9.3.2.1}$$

$$\begin{aligned}\sigma_{WB} &= F_p \tan\beta / \left(\left(\tan\alpha + \tan\beta\right)\left(-n\left(EF + B_b^2 - B_b\left(E + F\right)\right) + A_{PB}\right)\right) = \\ &6 \cdot 10^6 \tan 52° / \left(\left(\tan 45° + \tan 52°\right)\left(-4\left(315 \cdot 245 + 40^2 - 40\left(315 + 245\right)\right) + 370570\right)\right) = \\ &23\,\text{MPa}\end{aligned} \tag{9.3.2.2}$$

Comments load case XV, Area 4

Considering Figure 9.3.2.2, σ_{WA} = 11 MPa corresponds to the half where the stress in the outer wall equals 25-30 MPa and σ_{WB} = 23 MPa corresponds to the other half where the stress in the outer wall equals 10-15 MPa. Therefore it is tempting to assume that the load mainly affects the wall at the opposite side to the side where the load is applied. In order to

investigate the assumption closer the structure shown in Figure 9.3.2.3 is considered. In this case all sections have the same lengths, but the calculations can equally well be performed using different lengths. Force and moment equilibrium yields

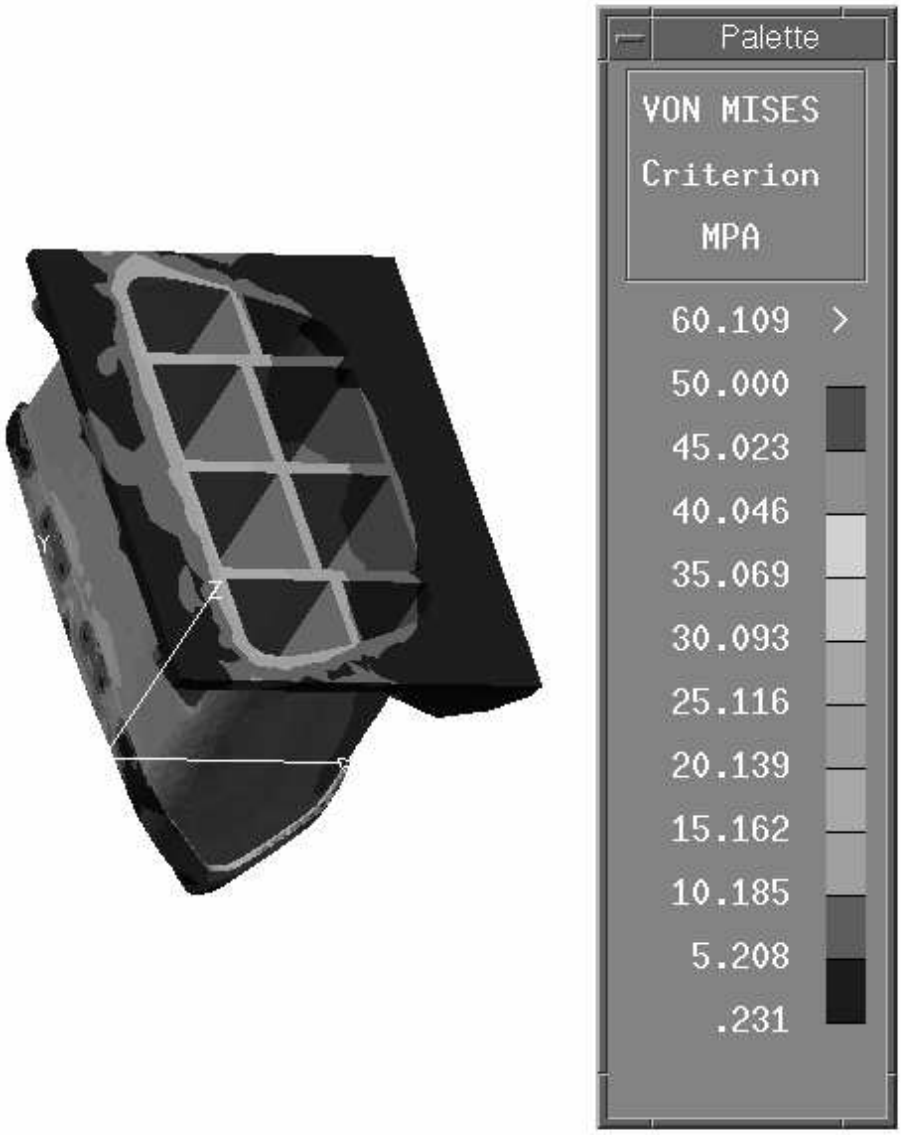

Fig. 9.3.2.2. Stresses in V-shaped punch when the die is closed

$$(\uparrow)\quad \frac{F_A}{\sqrt{2}} - V_1 + V_5 = 0 \tag{9.3.2.3}$$

$$(\rightarrow)\quad \frac{F_A}{\sqrt{2}} + H_1 - H_5 = 0 \tag{9.3.2.4}$$

$$(M_O)\quad M_1 - M_5 + (H_1 - H_5)L\left(1+\frac{1}{2\sqrt{2}}\right) - V_1\frac{L}{2\sqrt{2}} - V_5 L\left(\sqrt{2}-\frac{1}{2\sqrt{2}}\right) = 0 \qquad (9.3.2.5)$$

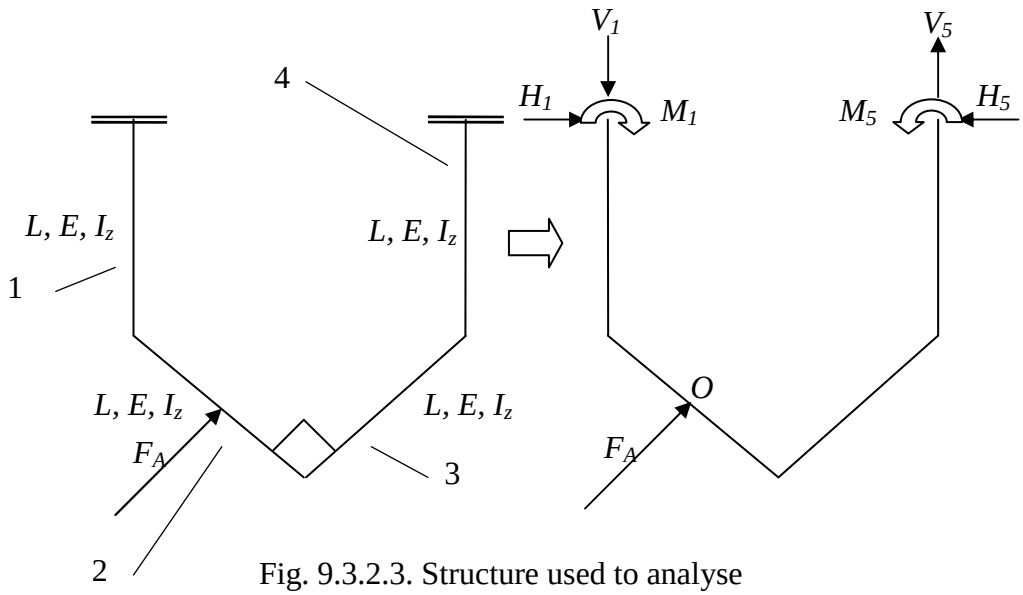

Fig. 9.3.2.3. Structure used to analyse the force distribution in a punch.

Since there are six unknowns another three equations are required. Several approaches exist to solve this kind of problem and in this case an energy method will be used. The structure is divided into smaller parts according to Figure 9.3.2.6 and for each part the elastic energy is calculated. The energy for the whole structure is calculated by summing up the contributions from each part. Considering a beam according to Figure 9.3.2.4 and assuming the cross section to be thin, i.e. only one stress component exists, and the material linear elastic, the expression for the internal energy contribution due to bending reads

$$U_{bend} = \int_V \frac{\sigma_x \varepsilon_x}{2} dV = \int_V \frac{\sigma_x^2}{2E} dV = \int_0^L \int_A \frac{M_b^2(x)}{2EI_z^2} y^2 dS dx = \left[I_z = \int_A y^2 dS \right] = \int_0^L \frac{M_b^2(x)}{2EI_z} dx \quad (9.3.2.6)$$

The internal energy due to uniaxial tension is

$$U_{tens} = \int_V \frac{\sigma_x^2}{2E} dV = \int_V \frac{1}{2E}\left(\frac{P}{S}\right)^2 dV = \int_0^L \frac{1}{2E}\frac{P^2}{S} dx \qquad (9.3.2.7)$$

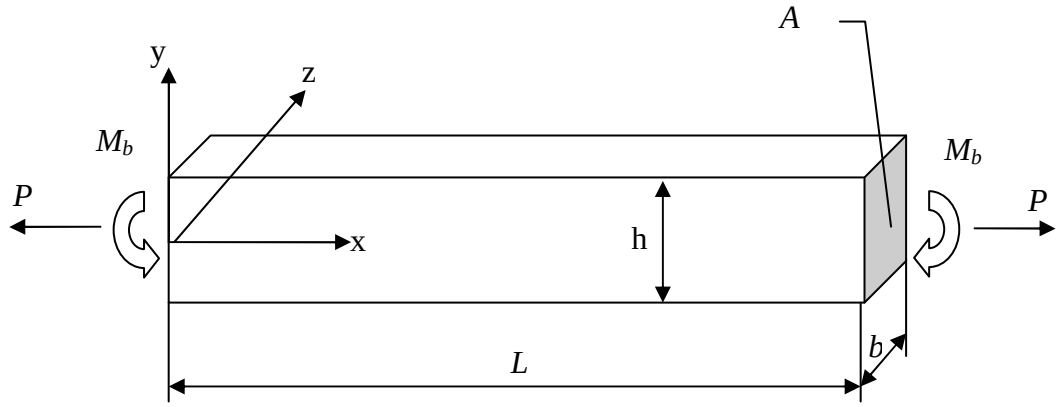

Fig. 9.3.2.4. Beam used to derive the expressions for the internal energy.

As can be seen from Figure 9.3.2.6 all segments are subjected to bending and tension. In order to make a comparison between the magnitudes of the energies, U_{bend} is divided by U_{tens}

$$\frac{U_{bend}}{U_{tens}} = \frac{\dfrac{M_b^2(x)}{2EI_z}}{\dfrac{1}{2E}\dfrac{P^2}{S}} = \frac{M_b^2(x)S}{IP^2} = \left[M_b = PL,\ I_z = \frac{bh^3}{12},\ \mathrm{S} = bh\right] = \frac{12(PL)^2 bh}{bh^3P^2} = \tag{9.3.2.8}$$

$$= \frac{12L^2}{h^2} >> 1$$

The conclusion is that if a beam is subjected to both bending and tension only the contribution from bending has to be considered, provided that the force which gives rise to moment is of the same order as the tensile force. All segments are loaded in the same way and therefore an expression is derived for the bending energy, which can be used for all parts. Considering Figure 9.3.2.5 the expression for the reaction forces reads

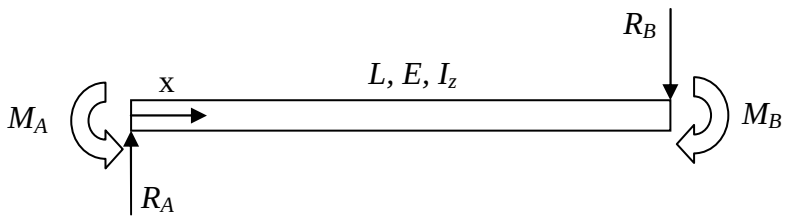

Fig. 9.3.2.5. Typical segment in the structure analyzed

$$M_5 = M_1 + H_1 L + \frac{H_1 - V_1}{\sqrt{2}}\frac{L}{2} + \left(F_A - \frac{V_1 - H_1}{\sqrt{2}}\right)\frac{L}{2} - \frac{H_1 + V_1}{\sqrt{2}} L - \left(\frac{H_1 + V_1}{2} + \frac{F_A - \frac{V_1 - H_1}{\sqrt{2}}}{\sqrt{2}}\right) L$$

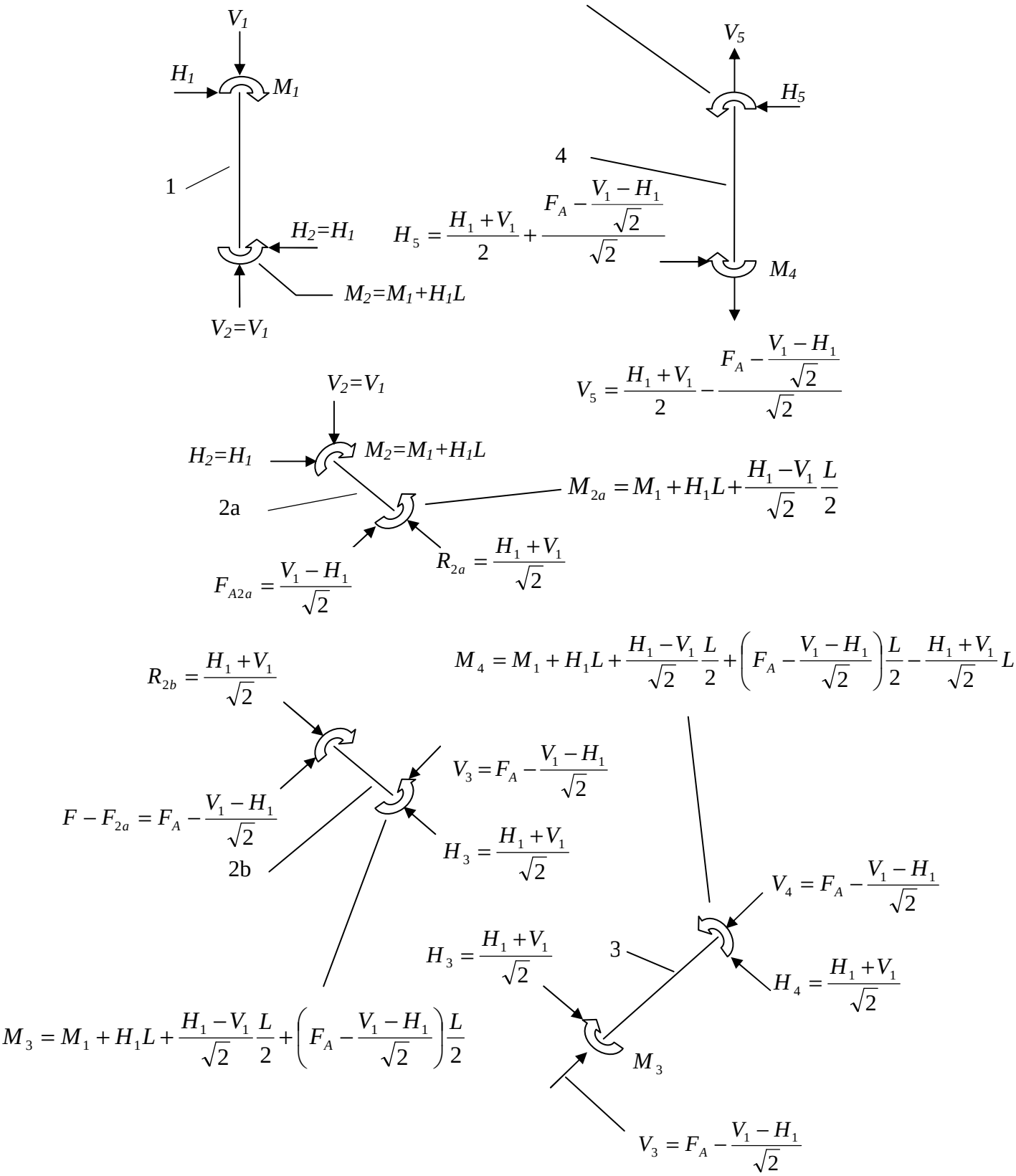

Fig. 9.3.2.6. Free body diagram of the structure shown in Figure 9.3.2.3

$$R_A = R_B = \frac{M_A - M_B}{L} \tag{9.3.2.9}$$

With use of this expression for the moment at an arbitrary position reads

$$M(x) = M_A - R_A x = M_A - \frac{M_A - M_B}{L} x \tag{9.3.2.10}$$

If (9.3.2.10) is inserted in the expression for the internal energy, (9.3.2.6), the following is obtained

$$U = \int_0^L \frac{M_b^2(x)}{2EI_z} dx = \frac{1}{2EI_z} \int_0^L \left(M_A - \frac{M_A - M_B}{L} x \right)^2 dx = \frac{L}{6EI_z} \left(M_A^2 + M_B^2 + M_A M_B \right) \tag{9.3.2.11}$$

which can be used to derive expressions for the internal energies for each part according to Figure 9.3.2.6.

$$U_1 = \frac{L}{6EI_z}\left(M_1^2 + (M_1 + H_1 L)^2 + M_1(M_1 + H_1 L)\right)$$

$$U_{2a} = \frac{L}{6EI_z}\left(\begin{array}{l} (M_1 + H_1 L)^2 + \left(M_1 + H_1 L + \frac{H_1 - V_1}{\sqrt{2}}\frac{L}{2}\right)^2 + \\ (M_1 + H_1 L)\left(M_1 + H_1 L + \frac{H_1 - V_1}{\sqrt{2}}\frac{L}{2}\right) \end{array}\right)$$

$$U_{2b} = \frac{L}{6EI_z}\left(\begin{array}{l} \left(M_1 + H_1 L + \frac{H_1 - V_1}{\sqrt{2}}\frac{L}{2}\right)^2 + \\ \left(M_1 + H_1 L + \frac{H_1 - V_1}{\sqrt{2}}\frac{L}{2} + \left(F_A - \frac{V_1 - H_1}{\sqrt{2}}\right)\frac{L}{2}\right)^2 + \\ \left(M_1 + H_1 L + \frac{H_1 - V_1}{\sqrt{2}}\frac{L}{2}\right) \\ \left(M_1 + H_1 L + \frac{H_1 - V_1}{\sqrt{2}}\frac{L}{2} + \left(F_A - \frac{V_1 - H_1}{\sqrt{2}}\right)\frac{L}{2}\right) \end{array}\right)$$

$$U_3 = \frac{L}{6EI_z}\left(\begin{array}{l} \left(M_1 + H_1 L + \frac{H_1 - V_1}{\sqrt{2}}\frac{L}{2} + \left(F_A - \frac{V_1 - H_1}{\sqrt{2}}\right)\frac{L}{2}\right)^2 + \\ \left(M_1 + H_1 L + \frac{H_1 - V_1}{\sqrt{2}}\frac{L}{2} + \left(F_A - \frac{V_1 - H_1}{\sqrt{2}}\right)\frac{L}{2} - \frac{H_1 + V_1}{\sqrt{2}}L\right)^2 + \\ \left(M_1 + H_1 L + \frac{H_1 - V_1}{\sqrt{2}}\frac{L}{2} + \left(F_A - \frac{V_1 - H_1}{\sqrt{2}}\right)\frac{L}{2}\right) \\ \left(M_1 + H_1 L + \frac{H_1 - V_1}{\sqrt{2}}\frac{L}{2} + \left(F_A - \frac{V_1 - H_1}{\sqrt{2}}\right)\frac{L}{2} - \frac{H_1 + V_1}{\sqrt{2}}L\right) \end{array}\right) \qquad (9.3.2.12)$$

$$U_4 = \frac{L}{6EI}\left(\begin{array}{l}\left(M_1 + H_1 L + \frac{H_1 - V_1}{\sqrt{2}}\frac{L}{2} + \left(F_A - \frac{V_1 - H_1}{\sqrt{2}}\right)\frac{L}{2} - \frac{H_1 + V_1}{\sqrt{2}}L\right)^2 + \\ \left(M_1 + H_1 L + \frac{H_1 - V_1}{\sqrt{2}}\frac{L}{2} + \left(F_A - \frac{V_1 - H_1}{\sqrt{2}}\right)\frac{L}{2} - \frac{H_1 + V_1}{\sqrt{2}}L - \left(\frac{H_1 + V_1}{2} + \frac{F_A - \frac{V_1 - H_1}{\sqrt{2}}}{\sqrt{2}}\right)L\right)^2 + \\ \left(M_1 + H_1 L + \frac{H_1 - V_1}{\sqrt{2}}\frac{L}{2} + \left(F_A - \frac{V_1 - H_1}{\sqrt{2}}\right)\frac{L}{2} - \frac{H_1 + V_1}{\sqrt{2}}L\right) \\ \left(M_1 + H_1 L + \frac{H_1 - V_1}{\sqrt{2}}\frac{L}{2} + \left(F_A - \frac{V_1 - H_1}{\sqrt{2}}\right)\frac{L}{2} - \frac{H_1 + V_1}{\sqrt{2}}L - \left(\frac{H_1 + V_1}{2} + \frac{F_A - \frac{V_1 - H_1}{\sqrt{2}}}{\sqrt{2}}\right)L\right)\end{array}\right) \qquad (9.3.2.13)$$

Except from (9.3.2.3), (9.3.2.4) and (9.3.2.5) another three equations are required to solve the six unknowns. The remaining relations are obtained by using Castigliano's hypothesis. Considering the left hand end in Figure (9.3.2.3), the ends are clamped which yields following boundary conditions:

$$\begin{aligned}&\frac{\partial U}{\partial H_1} = 0 \;\Rightarrow\; \text{No displacement horisontally}\\ &\frac{\partial U}{\partial V_1} = 0 \;\Rightarrow\; \text{No displacement vertically}\\ &\frac{\partial U}{\partial M_1} = 0 \;\Rightarrow\; \text{No slope at the end point}\end{aligned} \qquad (9.3.2.14)$$

In the third boundary condition use of the differential equation of the deflection curve has been made.

$$\frac{d^2 v}{dx^2} = \frac{M}{EI_z} \;\Rightarrow\; \theta = \frac{dv}{dx} = \int \frac{M}{EI_z}dx \qquad (9.3.2.15)$$

v denotes the deflection and θ the slope. A comparison with (9.3.2.6) reveals that

$$\theta = \frac{dv}{dx} = \frac{\partial U}{\partial M} = \int \frac{M_b}{EI_z}dx \qquad (9.3.2.16)$$

$$0=\frac{\partial U}{\partial H_1}=\frac{\partial\left(U_1+U_{2a}+U_{2b}+U_3+U_4\right)}{\partial H_1}=$$

$$\frac{L^2}{6EI}\left(\begin{array}{l}
4\left(M_1+H_1L\right)+M_1+4\left(M_1+H_1L+\frac{H_1-V_1}{\sqrt{2}}\frac{L}{2}\right)\left(1+\frac{1}{2\sqrt{2}}\right)+\\
\left(M_1+H_1L\right)\left(1+\frac{1}{2\sqrt{2}}\right)+\left(M_1+H_1L+\frac{H_1-V_1}{\sqrt{2}}\frac{L}{2}\right)+\\
4\left(M_1+H_1L+\frac{H_1-V_1}{\sqrt{2}}\frac{L}{2}+\left(F_A-\frac{V_1-H_1}{\sqrt{2}}\right)\frac{L}{2}\right)\left(1+\frac{1}{\sqrt{2}}\right)+\\
\left(M_1+H_1L+\frac{H_1-V_1}{\sqrt{2}}\frac{L}{2}\right)\left(1+\frac{1}{\sqrt{2}}\right)+\\
\left(M_1+H_1L+\frac{H_1-V_1}{\sqrt{2}}\frac{L}{2}+\left(F_A-\frac{V_1-H_1}{\sqrt{2}}\right)\frac{L}{2}\right)\left(1+\frac{1}{2\sqrt{2}}\right)+\\
4\left(M_1+H_1L+\frac{H_1-V_1}{\sqrt{2}}\frac{L}{2}+\left(F_A-\frac{V_1-H_1}{\sqrt{2}}\right)\frac{L}{2}-\frac{H_1+V_1}{\sqrt{2}}L\right)+\\
\left(M_1+H_1L+\frac{H_1-V_1}{\sqrt{2}}\frac{L}{2}+\left(F_A-\frac{V_1-H_1}{\sqrt{2}}\right)\frac{L}{2}\right)+\\
\left(M_1+H_1L+\frac{H_1-V_1}{\sqrt{2}}\frac{L}{2}+\left(F_A-\frac{V_1-H_1}{\sqrt{2}}\right)\frac{L}{2}-\frac{H_1+V_1}{\sqrt{2}}L\right)\left(1+\frac{1}{\sqrt{2}}\right)+\\
\left(\begin{array}{l}M_1+H_1L+\frac{H_1-V_1}{\sqrt{2}}\frac{L}{2}+\left(F_A-\frac{V_1-H_1}{\sqrt{2}}\right)\frac{L}{2}-\frac{H_1+V_1}{\sqrt{2}}L-\\
\left(\frac{H_1+V_1}{2}+\frac{F_A-\frac{V_1-H_1}{\sqrt{2}}}{\sqrt{2}}\right)L\end{array}\right)
\end{array}\right) \qquad (9.3.2.17)$$

$$0=\frac{\partial U}{\partial V_1}=\frac{\partial\left(U_1+U_{2a}+U_{2b}+U_3+U_4\right)}{\partial V_1}=$$

$$\frac{L^2}{6EI}\left(\begin{array}{l}
-4\left(M_1+H_1L+\frac{H_1-V_1}{\sqrt{2}}\frac{L}{2}\right)\left(\frac{1}{2\sqrt{2}}\right)-\left(M_1+H_1L\right)\left(\frac{1}{2\sqrt{2}}\right)- \\
2\sqrt{2}\left(M_1+H_1L+\frac{H_1-V_1}{\sqrt{2}}\frac{L}{2}+\left(F_A-\frac{V_1-H_1}{\sqrt{2}}\right)\frac{L}{2}\right)- \\
\left(M_1+H_1L+\frac{H_1-V_1}{\sqrt{2}}\frac{L}{2}\right)\frac{1}{\sqrt{2}}- \\
\left(M_1+H_1L+\frac{H_1-V_1}{\sqrt{2}}\frac{L}{2}+\left(F_A-\frac{V_1-H_1}{\sqrt{2}}\right)\frac{L}{2}\right)\left(\frac{1}{2\sqrt{2}}\right)- \\
4\sqrt{2}\left(M_1+H_1L+\frac{H_1-V_1}{\sqrt{2}}\frac{L}{2}+\left(F_A-\frac{V_1-H_1}{\sqrt{2}}\right)\frac{L}{2}-\frac{H_1+V_1}{\sqrt{2}}L\right)- \\
\sqrt{2}\left(M_1+H_1L+\frac{H_1-V_1}{\sqrt{2}}\frac{L}{2}+\left(F_A-\frac{V_1-H_1}{\sqrt{2}}\right)\frac{L}{2}\right)- \\
\left(M_1+H_1L+\frac{H_1-V_1}{\sqrt{2}}\frac{L}{2}+\left(F_A-\frac{V_1-H_1}{\sqrt{2}}\right)\frac{L}{2}-\frac{H_1+V_1}{\sqrt{2}}L\right)\left(\frac{1}{\sqrt{2}}\right)- \\
\left(\begin{array}{l}M_1+H_1L+\frac{H_1-V_1}{\sqrt{2}}\frac{L}{2}+\left(F_A-\frac{V_1-H_1}{\sqrt{2}}\right)\frac{L}{2}-\frac{H_1+V_1}{\sqrt{2}}L- \\ \left(\frac{H_1+V_1}{2}+\frac{F_A-\frac{V_1-H_1}{\sqrt{2}}}{\sqrt{2}}\right)L\end{array}\right)2\sqrt{2}- \\
\left(M_1+H_1L+\frac{H_1-V_1}{\sqrt{2}}\frac{L}{2}+\left(F_A-\frac{V_1-H_1}{\sqrt{2}}\right)\frac{L}{2}-\frac{H_1+V_1}{\sqrt{2}}L\right)\sqrt{2}- \\
\left(\begin{array}{l}M_1+H_1L+\frac{H_1-V_1}{\sqrt{2}}\frac{L}{2}+\left(F_A-\frac{V_1-H_1}{\sqrt{2}}\right)\frac{L}{2}-\frac{H_1+V_1}{\sqrt{2}}L- \\ \left(\frac{H_1+V_1}{2}+\frac{F_A-\frac{V_1-H_1}{\sqrt{2}}}{\sqrt{2}}\right)L\end{array}\right)\sqrt{2}
\end{array}\right) \qquad (9.3.2.18)$$

$$0=\frac{\partial U}{M_1}=\frac{\partial\left(U_1+U_{2a}+U_{2b}+U_3+U_4\right)}{\partial M_1}=$$

$$\frac{L}{6EI}\left(\begin{array}{l}4M_1+4\left(M_1+H_1L\right)+H_1L+6\left(M_1+H_1L+\frac{H_1-V_1}{\sqrt{2}}\frac{L}{2}\right)+\\ \left(M_1+H_1L\right)+6\left(M_1+H_1L+\frac{H_1-V_1}{\sqrt{2}}\frac{L}{2}+\left(F_A-\frac{V_1-H_1}{\sqrt{2}}\right)\frac{L}{2}\right)+\\ 6\left(M_1+H_1L+\frac{H_1-V_1}{\sqrt{2}}\frac{L}{2}+\left(F_A-\frac{V_1-H_1}{\sqrt{2}}\right)\frac{L}{2}-\frac{H_1+V_1}{\sqrt{2}}L\right)+\\ 3\left(\begin{array}{l}M_1+H_1L+\frac{H_1-V_1}{\sqrt{2}}\frac{L}{2}+\left(F_A-\frac{V_1-H_1}{\sqrt{2}}\right)\frac{L}{2}-\frac{H_1+V_1}{\sqrt{2}}L-\\ \left(\frac{H_1+V_1}{2}+\frac{F_A-\frac{V_1-H_1}{\sqrt{2}}}{\sqrt{2}}\right)L\end{array}\right)\end{array}\right) \qquad (9.3.2.19)$$

Solving the system of equations consisting of (9.3.2.3), (9.3.2.4), (9.3.2.5), (9.3.2.17), (9.3.2.18) and (9.3.2.19) yields

$$\begin{aligned}
H_1&=-\frac{1}{4}\frac{F_A\left(58+81\sqrt{2}\right)}{110+47\sqrt{2}}\\
H_5&=\frac{1}{4}\frac{F_A\left(130+139\sqrt{2}\right)}{110+47\sqrt{2}}\\
M_1&=\frac{31}{2}\frac{LF_A\left(1+\sqrt{2}\right)}{110+47\sqrt{2}}\\
M_5&=-\frac{1}{6}\frac{LF_A\left(134+141\sqrt{2}\right)}{110+47\sqrt{2}}\\
V_1&=\frac{5}{12}\frac{F_A\left(55+9\sqrt{2}\right)\sqrt{2}}{110+47\sqrt{2}}\\
V_5&=-\frac{1}{12}\frac{F_A\left(385+237\sqrt{2}\right)\sqrt{2}}{110+47\sqrt{2}}
\end{aligned} \qquad (9.3.2.20)$$

and

$$\boxed{\frac{V_1}{V_5}=-0{,}47} \qquad (9.3.2.21)$$

(9.3.2.21) states that, if the conditions are like in Figure 9.3.2.3, then the vertically directed reaction force at the side opposite to the side where the load is applied is approximately two times larger than the force at the same side. Under assumption that (9.3.2.21) reflects the force distribution between the two sides in Figure 9.3.2.1 it is possible to determine the distribution of F_{VA} and F_{VB} given by (7.3.1.29) and (7.3.1.30).

$$F_{VA} = F_{VA}^{A} + F_{VA}^{B} = 0{,}47F_{VA}^{B} + F_{VA}^{B} = 1{,}47F_{VA}^{B}$$
$$F_{VB} = F_{VB}^{A} + F_{VB}^{B} = F_{VB}^{A} + 0{,}47F_{VB}^{A} = 1{,}47F_{VB}^{A} \qquad (9.3.2.22)$$

The superscripts refer to the position where the actual portion of the load acts. For example F_{VA}^{B} refers to that portion of F_{VA} which acts at the same side as F_{VB}. The corrected loads are then calculated as

$$\boxed{\begin{aligned} F_{VA}^{*} &= \frac{F_{VB}}{1{,}47} + F_{VA} - \frac{F_{VA}}{1{,}47} = \frac{F_{VB}}{1{,}47} + \frac{0{,}47F_{VA}}{1{,}47} \\ F_{VB}^{*} &= \frac{F_{VA}}{1{,}47} + F_{VB} - \frac{F_{VB}}{1{,}47} = \frac{F_{VA}}{1{,}47} + \frac{0{,}47F_{VB}}{1{,}47} \end{aligned}} \qquad (9.3.2.23)$$

If the expressions for F_{VA} and F_{VB}, (7.3.1.29) and (7.3.1.30) respectively, are inserted in (9.3.2.23) and F_{VA}^{*} and F_{VB}^{*} are inserted in (7.3.1.34) and (7.3.1.35) and solved for the stress following expressions are obtained

$$\sigma_{WA} = \frac{0{,}64 \cdot 10^{-8} F_p \left(0.106292517 \cdot 10^{9} \cos\alpha \sin\beta + 0.49957483 \cdot 10^{8} \cos\beta \sin\alpha\right)}{\left(\cos\alpha \sin\beta + \cos\beta \sin\alpha\right)\left(A_{PA} + n\left(-IJ + IB_a + JB_a - B_a^2\right)\right)} =$$
$$\frac{0{,}64 \cdot 10^{-8} \cdot 6 \cdot 10^{6} \left(0.106292517 \cdot 10^{9} \cos 45° \sin 52° + 0.49957483 \cdot 10^{8} \cos 52° \sin 45°\right)}{\left(\cos 45° \sin 52° + \cos 52° \sin 45°\right)\left(546375 + 4\left(-330 \cdot 305 + 330 \cdot 40 + 305 \cdot 40 - 40^2\right)\right)} \text{MPa} = 13 \text{ MPa}$$
(9.3.2.24)

$$\sigma_{WB} = \frac{0{,}64 \cdot 10^{-8} F_p \left(0.106292517 \cdot 10^{9} \cos\alpha \sin\beta + 0.49957483 \cdot 10^{8} \cos\beta \sin\alpha\right)}{\left(\cos\alpha \sin\beta + \cos\beta \sin\alpha\right)\left(A_{PB} + n\left(-EF + EB_b + FB_b - B_b^2\right)\right)} =$$
$$\frac{0{,}64 \cdot 10^{-8} \cdot 6 \cdot 10^{6} \left(0.106292517 \cdot 10^{9} \cos 45° \sin 52° + 0.49957483 \cdot 10^{8} \cos 52° \sin 45°\right)}{\left(\cos 45° \sin 52° + \cos 52° \sin 45°\right)\left(370570 + 4\left(-315 \cdot 245 + 315 \cdot 40 + 245 \cdot 40 - 40^2\right)\right)} \text{MPa} = 22 \text{ MPa}$$
(9.3.2.25)

It is concluded that almost no changes occurred compared to (9.3.2.1) and (9.3.2.2), since F_A and F_B in this case are of the same order. In the analytical expression, it has been assumed that the load is equally distributed over the whole forming area, whilst the load in the FE-calculation only has been applied at the forming radii. This may explain the difference in stress at the wall at the side corresponding to the up-side of the trunk lid, since the forming radii are located at the boundary (see Figure 9.3.2.2). It is more difficult to give an explanation to why stress is lower in FE-calculation compared to the analytical result at the opposite wall. Therefore a closer analysis of the principal stresses is recommended, in order to determine if a description considering more than one stress component has to be adopted.

Load case XVI, Area 3

(7.3.1.41) is used to calculate the deflection in the area between the walls in V-shaped punches. Firstly, it is necessary to calculate the force, which is done using (7.3.1.9)

$$F_B = F_P \cos\alpha / (\cos\alpha \sin\beta + \cos\beta \sin\alpha) =$$
$$6 \cdot 10^6 \cos 45° / (\cos 45° \sin 52° + \cos 52° \sin 45°) \text{ N} = 4{,}27 \cdot 10^6 \text{ N} \tag{9.3.2.26}$$

Secondly the load per unit area is determined

$$q = \frac{F_B}{S} = \frac{4.27 \cdot 10^6}{624000} \text{ MPa} = 6.84 \text{ MPa} \tag{9.3.2.27}$$

Finally, the deflection is calculated using (7.3.1.41)

$$u = \frac{15q(1-\nu^2)}{32Et^3} \frac{A^4 B^4}{7A^2B^2 - 2A^2B^2\nu + 10A^4 + 10B^4} =$$
$$\frac{15 \cdot 6.84(1-0.28^2)}{32 \cdot 165 \cdot 10^3 \cdot 60^3} \frac{360^4 \cdot 395^4}{7 \cdot 360^2 \cdot 395^2 - 2 \cdot 360^2 \cdot 395^2 \cdot 0.28 + 10 \cdot 360^4 + 10 \cdot 395^4} \text{ mm} =$$
$$0.063 \text{ mm} \tag{9.3.2.28}$$

Comments load case XVI, Area 3

From Figure 9.3.2.7 it is seen that the deflection normal to the surface is 0.202-0.225 mm. The deflection in the surroundings has to be subtracted in order to make a comparison with the calculated value, which yields 0.068-0.067 mm. The analytical result and the FE-calculation are in good agreement, which is unexpected since it was concluded in appendix A, that the analytical expression over estimates the deflection when the thickness exceeds approximately one tenth. In this case the average thickness is 60 mm. The explanation lies probably in how the load is applied. In the analytical expression the load is assumed to be equally distributed whilst it is concentrated to the forming radii in the FE-model.

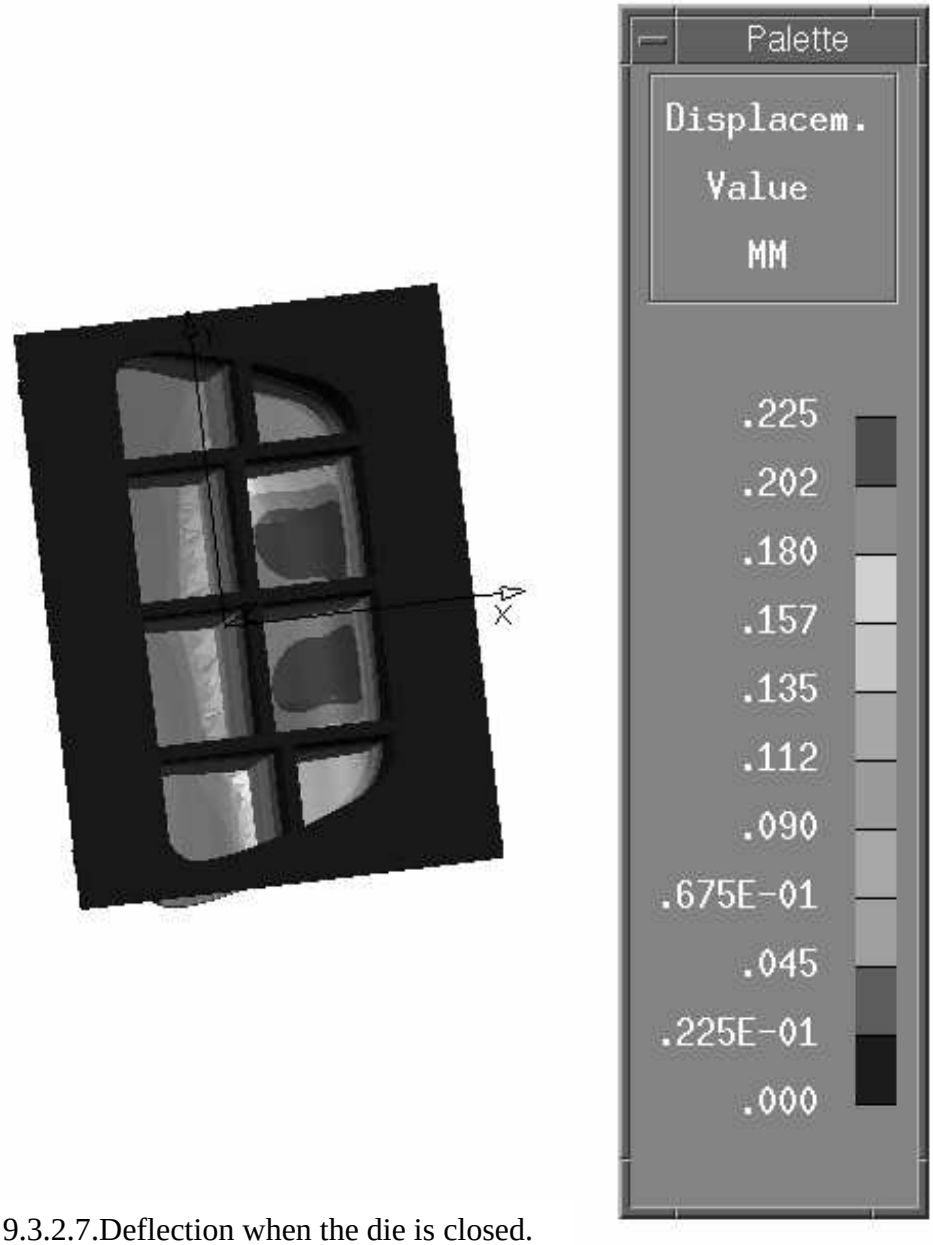

Fig. 9.3.2.7.Deflection when the die is closed.

Load case XVII, Area 4

Regarding flat punches, Figure 9.3.2.8 shows the areas where the load transmission is assumed to occur. The load is applied via a solid body, corresponding to the lower die, merged with the punch at the contact areas. At the bottom of the merged body, corresponding to the interface between the lower die and bolster is a contact load applied. This arrangement is assumed to reflect the effect of the reaction forces from the bolster.

Just as in the case regarding flat lower dies, (7.3.1.42) is valid for calculation of the stress in the walls in flat punches due to the load from the lower die, which if solved for the stress reads

$$\sigma_W = \frac{F_P}{A + n\left(G\left(B - H\right) + B\left(H - B\right)\right)} = \frac{6 \cdot 10^6}{2180800 + 16\left(390\left(40 - 350\right) + 40\left(350 - 40\right)\right)} \text{ MPa} = 13 \text{ MPa} \tag{9.3.2.29}$$

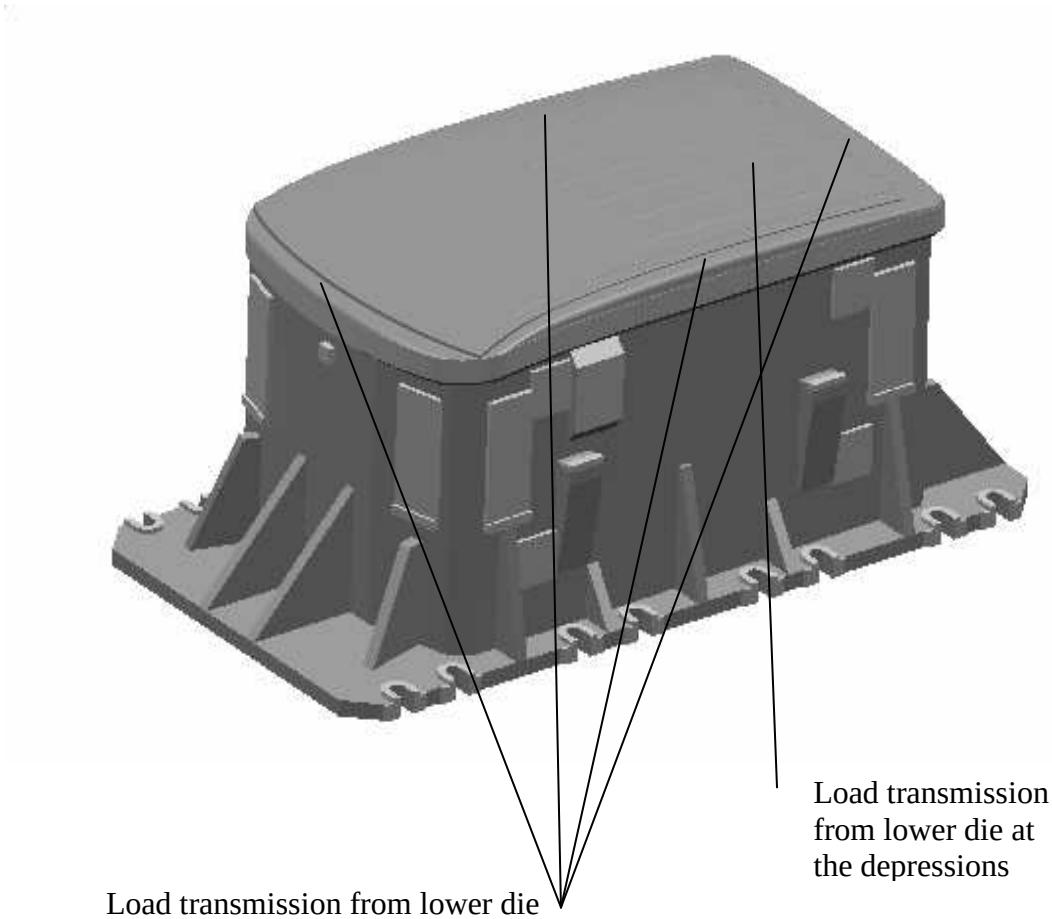

Fig. 9.3.2.8. Load acting at punch with flat shape when the die is closed.

Comments load case XVII, Area 4

The result, shown in Figure 9.3.2.9, is in fair agreement with the analytical result.
Load case XVIII, Area 3

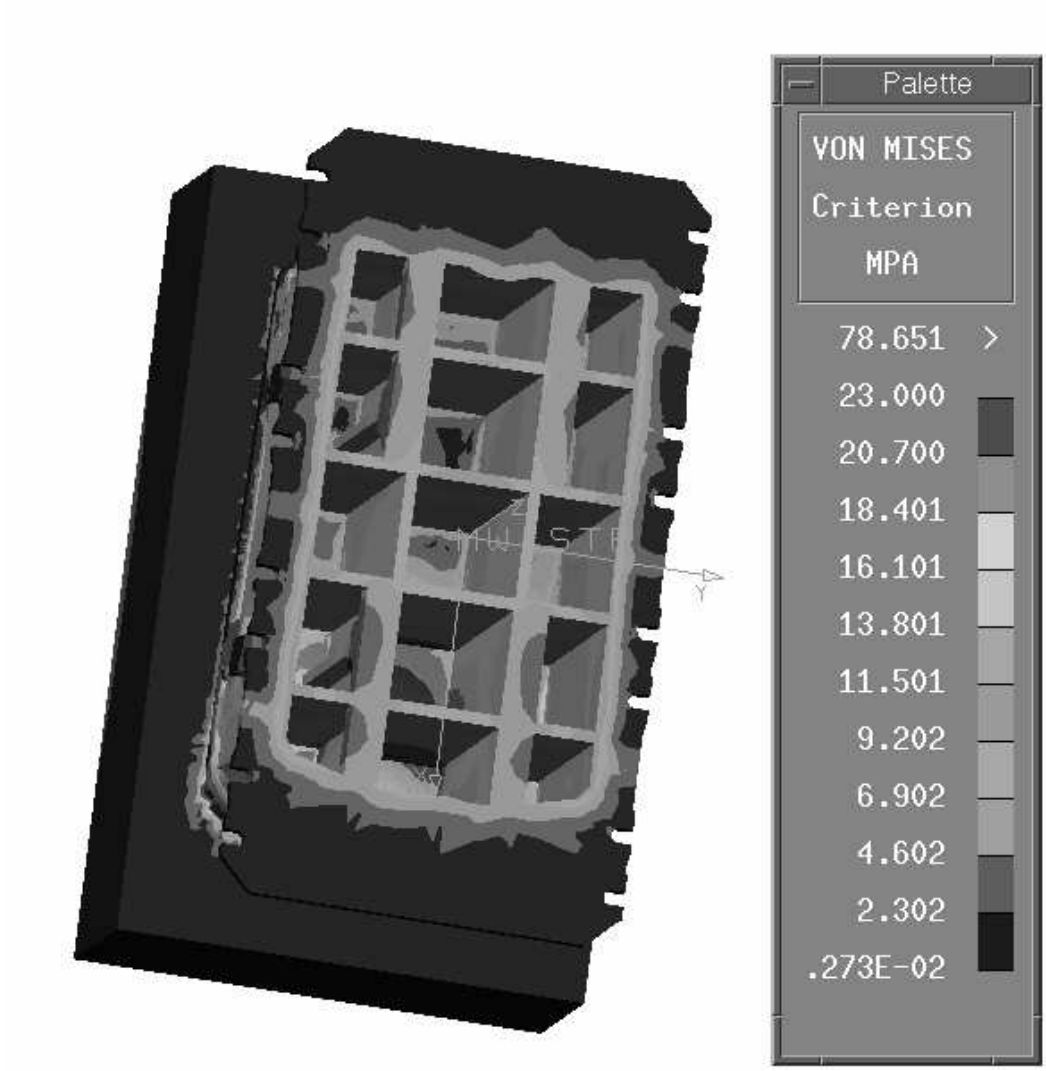

Fig. 9.3.2.9. Stresses in punch due to load from the lower die

Knowing the punch force and the area over which it is distributed, the force per unit area is calculated

$$q = \frac{F_p}{S} = \frac{6 \cdot 10^6}{2180800}\,\text{MPa} = 2{,}75\,\text{MPa} \qquad (9.3.2.30)$$

(7.3.1.41) is now used to calculate the deflection in the frame at the centre in fig. 9.3.2.10

$$u = \frac{15q\left(1-\nu^2\right)}{32Et^3}\frac{A^4B^4}{7A^2B^2 - 2A^2B^2\nu + 10A^4 + 10B^4} =$$
$$\frac{15\cdot 2.75\left(1-0.28^2\right)}{32\cdot 165\cdot 10^3\cdot 93^3}\frac{360^4\cdot 395^4}{7\cdot 360^2\cdot 380^2 - 2\cdot 360^2\cdot 380^2\cdot 0.28 + 10\cdot 360^4 + 10\cdot 380^4}\text{ mm} =$$
$$0.007\text{ mm}$$

(9.3.2.31)

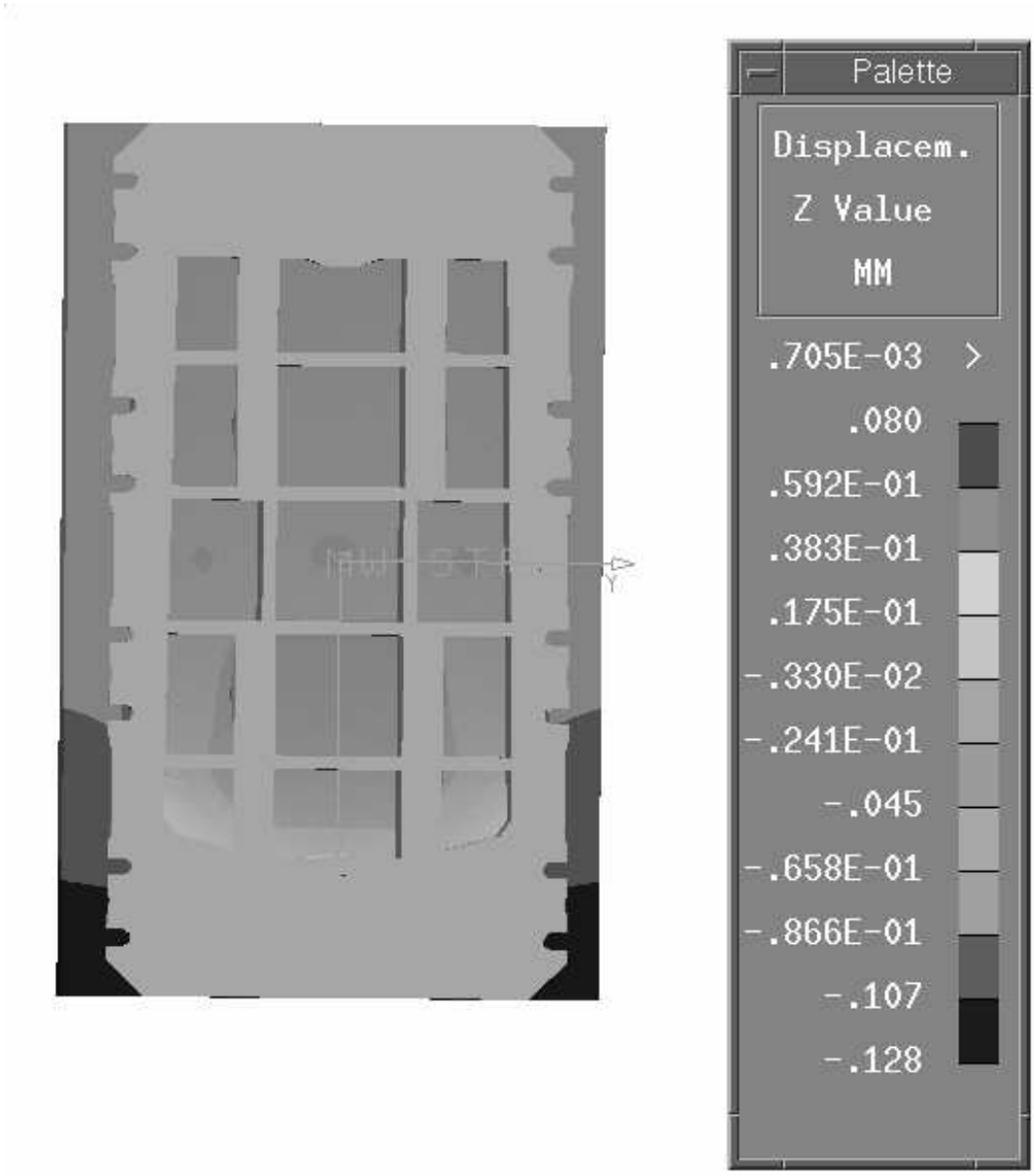

Fig. 9.3.2.10. Deflection due to the load from the lower die.

Comments load case XVIII, Area 3

In order to make a comparison with the results from the FE-calculation, the deflection in the surroundings has to be subtracted. This means that 0,056-0,046 shall be subtracted from 0,0866-0,0568 which yields 0,03-0,01 mm. Once again it is concluded that the thickness of

the casting, ≈90 mm, compared to the dimensions of the frame is too thick to allow the shear stresses to be neglected, which means that (7.3.1.41) is not applicable. The absence of the expected overestimation is explained from how the load is applied. In the analytical expression the load from the lower die is assumed to be equally distributed, whilst it in the FE-model is distributed over those areas with forming radii, which means that the load locally is higher in the FE-model.

9.3.3. Blank holder – evaluation (Load case XIX and XX)

When the die is closed the load from the lower die is assumed to take place only at the distance plates. In the FE-calculations the load transmitted from the lower die, is distributed equally over the distance plates. Over each distance plate the load is applied as a contact pressure.

Load case XIX, Area 1 and 5

Using (7.3.1.37) on the part of the die indicated in Figure 9.3.3.1, yields the following stress in the walls

$$\sigma_W = \frac{F_{BH}}{nB(A+C)} = \frac{1{,}2 \cdot 10^6}{14 \cdot 40(365+365)} \text{MPa} = 3\,\text{MPa} \tag{9.3.3.1}$$

where alternative c from section 7.3.1 has been used. The deflection is calculated using (7.3.1.38)

$$u_z = \frac{\sigma_W}{E} H = \frac{3}{165 \cdot 10^3} 317\text{ mm} = 6 \cdot 10^{-3}\text{ mm} \tag{9.3.3.2}$$

Comments load case XIX, Area 1 and 5

Regarding the stress 3 MPa from the analytical expression, it shall be compared to 2,4-9,6 MPa from the FE-calculation. It is seen in from Figure 9.3.3.1 that the stress is in fair agreement with the analytical expression in the lower half of the wall. If the stress distribution shown in the figure turns out to be representative for this load case, it is possible to adopt a description where the stress varies with the height. Figure 9.3.3.2 shows the deflection, which varies between 0.0051-0.0074 mm. This is in fair agreement with 0.006 mm from the analytical expression flat though the stress distribution is not uniform. If a non-uniform stress distribution is used in the analytical model the deflection is calculated using

$$\varepsilon_z = \frac{du_z}{dz} \Rightarrow u_z = \int_0^H \varepsilon_z dz = \int_0^H \frac{F_{BH}}{S(z)E} dz \tag{9.3.3.3}$$

where *S(z)* indicates that the area over which the stress is distributed is a function of the position in the z-direction. It is also concluded, by comparing the distance plates located close to the sides with the others, that the position of the distance plates has a clear influence on the stresses and deflections.

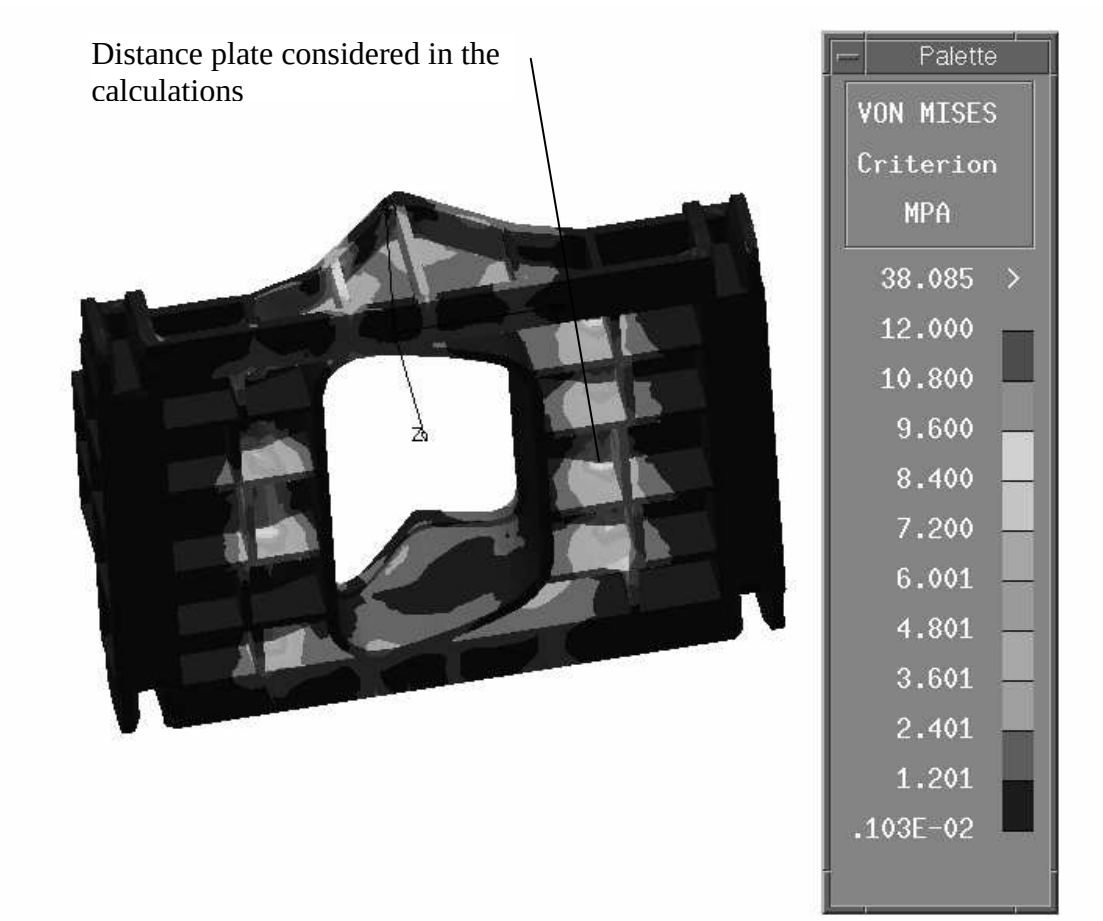

Fig. 9.3.3.1. Stress in V-shaped blank holder due to the load from the lower die

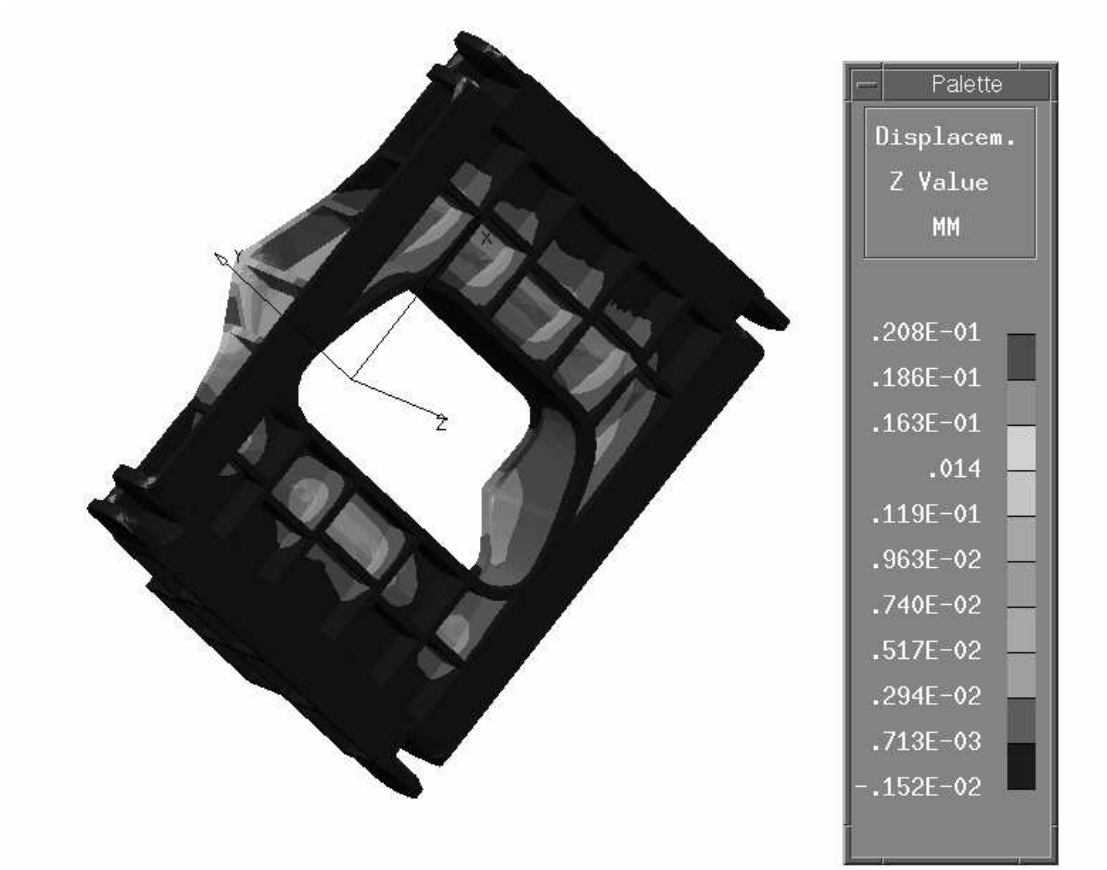

Fig. 9.3.3.2. Deflection in V-shaped blank holder due to the load from the lower die

Load case XX, Area 1 and 5

Following the procedure concerning V-shaped blank holders, (7.3.1.37) is used to calculate the stress in the walls in flat blank holders due to the load from the lower die,

$$\sigma_W = \frac{F_{BH}}{nB(A+C)} = \frac{1{,}2 \cdot 10^6}{16 \cdot 40(245+490)} \text{MPa} = 3\,\text{MPa} \qquad (9.3.3.4)$$

where alternative b from section 7.3.1 has been used. The deflection is calculated using (7.3.1.38)

$$u_z = \frac{\sigma_W}{E} H = \frac{3}{165 \cdot 10^3} 480\,\text{mm} = 9 \cdot 10^{-3}\ \text{mm} \qquad (9.3.3.5)$$

Comments load case XX, Area 1 and 5

Just as in the results regarding V-shaped blank holders, it is concluded that in the lower half of the wall, the FE-calculation is in fair agreement with the analytical expression. This means that 2,4-3,6 MPa from fig. 9.3.3.3 shall be compared with 3 MPa. In the upper half of the wall the stress locally takes values about 6 MPa. With regards to the deflection 0,009 mm from the analytical expression it shall be compared to 0.012-0.014 mm in Figure 9.3.3.4.

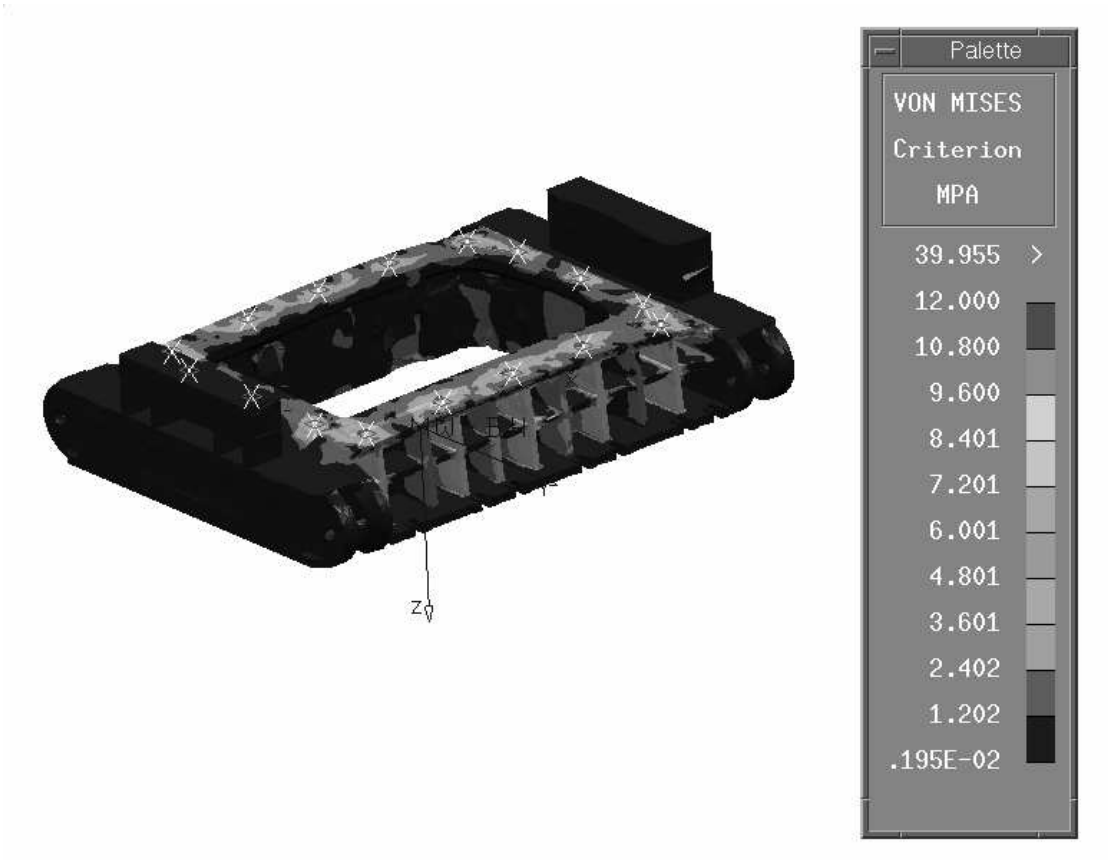

Figure 9.3.3.3. Stress in flat blank holder when the die is closed

A even better agreement will probably be achieved if a non-uniform stress distribution is used. As indicated in (9.3.3.3) the deflection in such cases is calculated by integrating the strain.

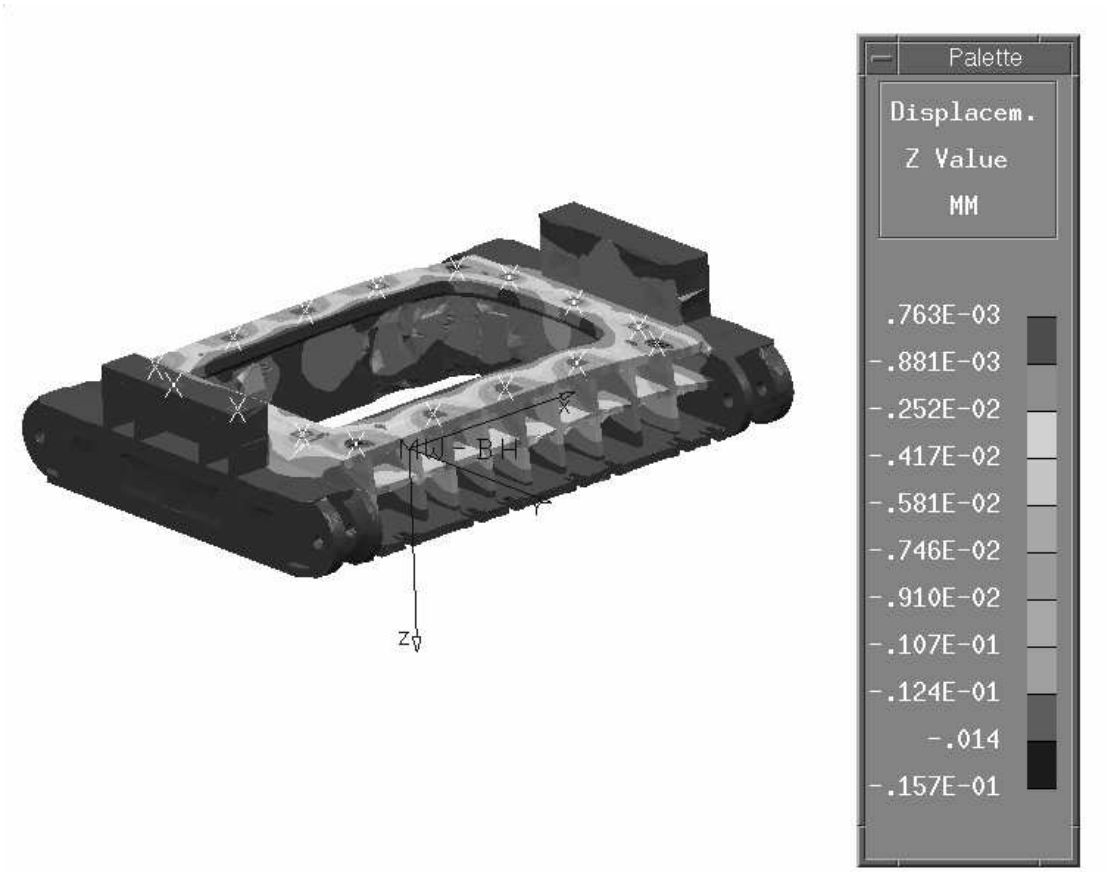

Figure 9.3.3.4. Deflection in flat blank holder when the die is closed

9.4. Die on trestles – evaluation (Load case XXI and XXII)

Load case XXI

Starting with a flat lower die, following values applies

$$
\begin{aligned}
&h = 600\ \text{mm}\\
&l = 3160\ \text{mm}\\
&n = 4\\
&A = 155\ \text{mm}\\
&B = 50\ \text{mm}\\
&C = 155\ \text{mm}\\
&D = 300\ \text{mm}\\
&J = 90\ \text{mm}\\
&F = 40\ \text{mm}\\
&H = 600\ \text{mm}\\
&W = 106929\ \text{N}
\end{aligned}
\tag{9.4.1}
$$

which inserted in (8.2.4) yields

$$\delta = 0{,}027 \text{ mm} \tag{9.4.2}$$

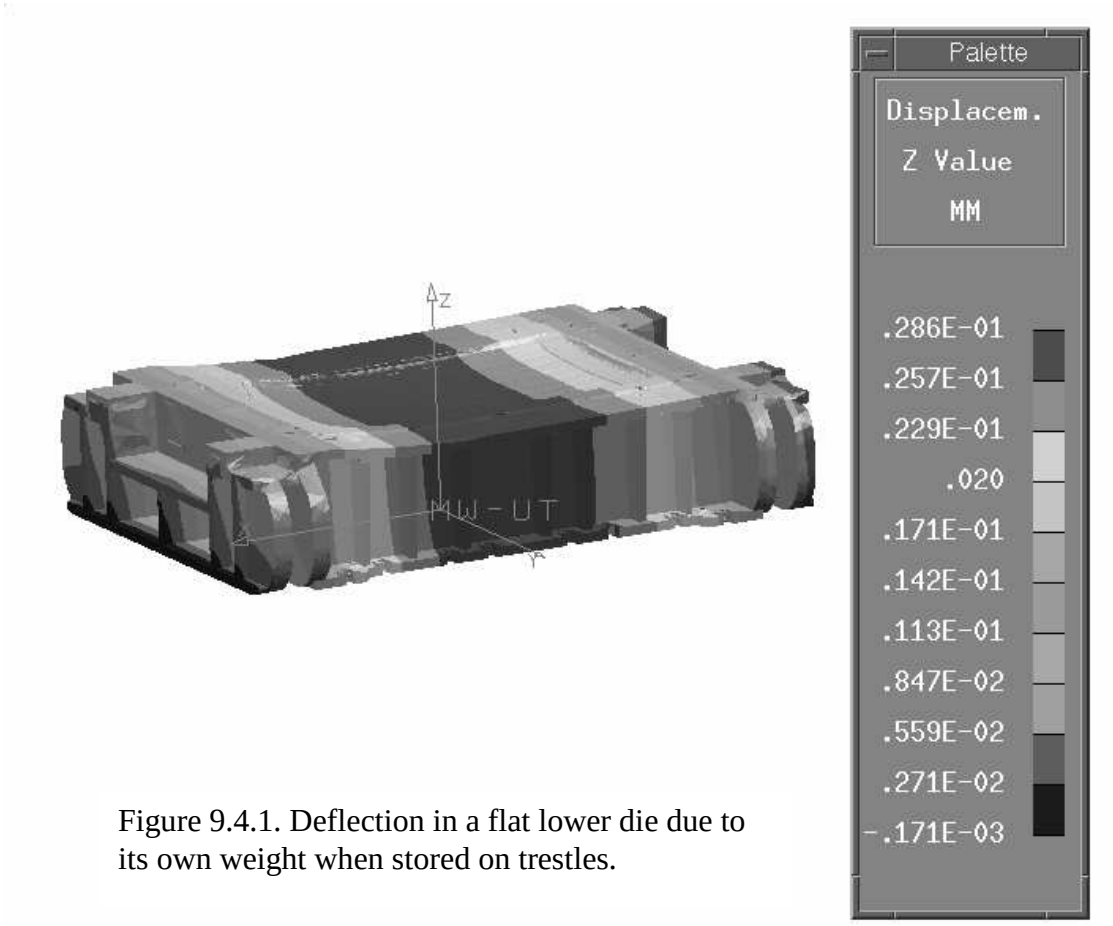

Figure 9.4.1. Deflection in a flat lower die due to its own weight when stored on trestles.

Comments load case XXI

As expected, the result is in agreement with the finite element calculation, since the shape of the lower die is similar to the shape used in the derivation, see Figure 9.4.1.

Load case XXII

The same calculations carried out for a V-shaped lower die using (8.2.7) with

$$
\begin{aligned}
&h = 235\ \text{mm}\\
&l = 2905\ \text{mm}\\
&n = 6\\
&A = 190\ \text{mm}\\
&B = 50\ \text{mm}\\
&C = 190\ \text{mm}\\
&D = 225\ \text{mm}\\
&J = 60\ \text{mm}\\
&F = 40\ \text{mm}\\
&H = 235\ \text{mm}\\
&W = 90252\ \text{N}
\end{aligned}
\tag{9.4.3}
$$

yields

$$\delta = 0.24\ \text{mm} \tag{9.4.4}$$

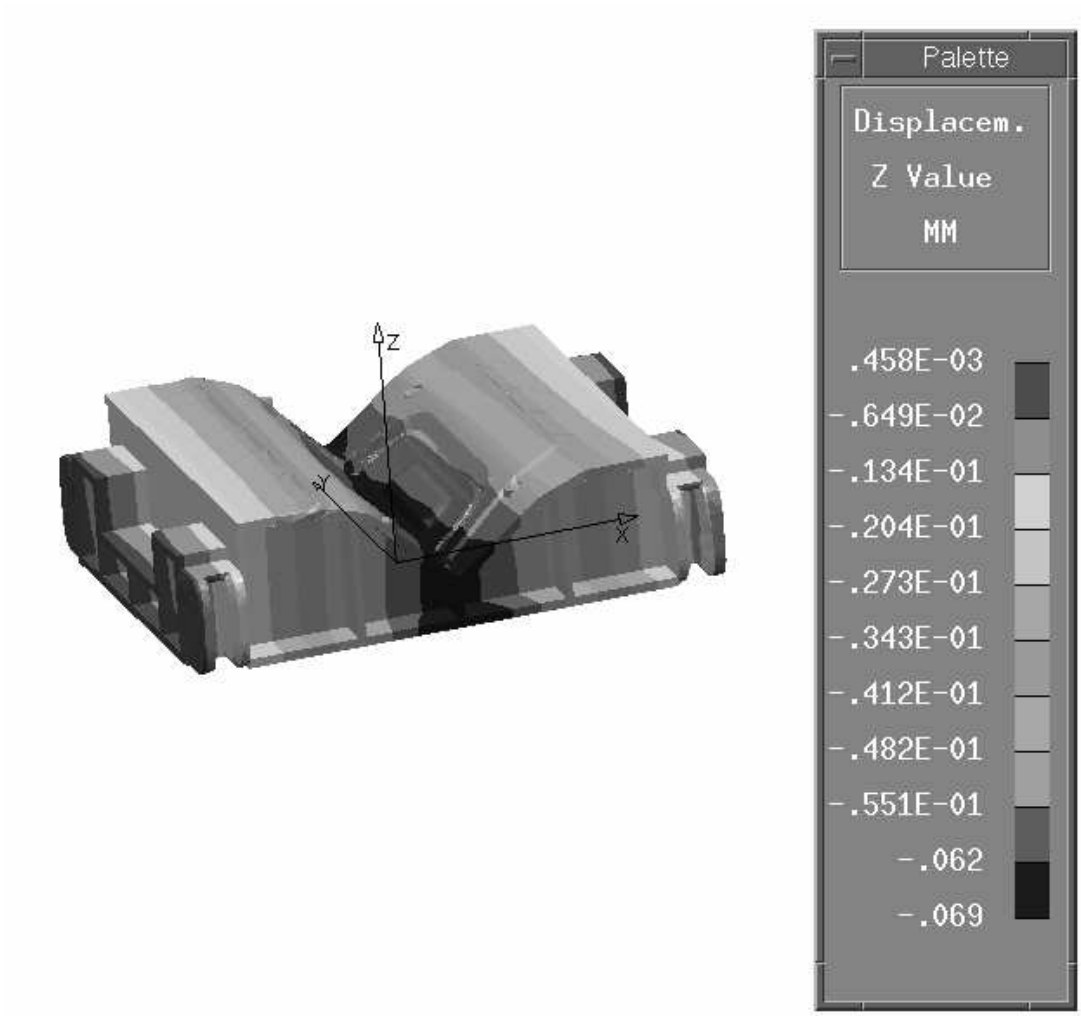

Figure 9.4.2. Deflection in a V-shaped lower die due to its own weight when stored on trestles.

Comments load case XXII

The inserted values applies to the lowest section, i.e. at x=0. As can be seen when the analytical result is compared with the finite element calculation (see Figure 9.4.2), (8.2.7) over estimates the deflection by a bit more than a factor three. The explanation probably lies in geometrical differences. Due to the V-shape the load as well as the moment of inertia varies with the position along the x-axis, whilst it in (8.2.7) is assumed that the load is equally distributed and the moment of inertia constant. By taking the variation of moment (load) and moment of inertia into account when integrating the differential equation of the deflection (see (9.3.2.15)), an expression for the deflection is obtained, which probably would yield a better agreement.

10. Results

The outcome from the comparisons between analytical calculations and FE-calculations, made in Section 9, are summarised in Table 10.1. A summing-up of the load cases is shown in Table 6.2.

Load case	Analytical expressions	Analytical result	FE result	Figure
I	(7.1.1.9),(7.1.1.10)	10 MPa, 17 MPa	4-12 MPa, 10-14 MPa	9.1.1.3
II	(7.1.1.11)	4 MPa	2 MPa	9.1.1.5
III	(7.1.1.9),(7.1.1.10)	10 MPa, 17 MPa	6-19 MPa, 6-40 MPa	9.1.2.2
IV	(7.1.1.11)	4 MPa	2-4 MPa	9.1.2.4
V	(7.1.2.8)	0.005 mm	0.06 mm	9.1.2.6
VI	(7.2.3), (7.2.5)	0.2 mm	0.045 mm	9.2.1
VII	(7.2.3), (7.2.5)	0.02 mm	0.055 mm	9.2.2
VIII	(7.3.1.10), (7.3.1.11), (7.3.1.12), (7.3.1.20), (7.3.1.26)	44 MPa	15-50 MPa	9.3.1.2
IX	(7.3.1.29), (7.3.1.30), (7.3.1.34), (7.3.1.35)	7 MPa, 10 MPa	0-28 MPa, 8-32 MPa	9.3.1.3
X	(7.3.1.37), (7.3.1.38)	4 MPa, 5 MPa 0.02 mm, 0,02 mm	0-20 MPa, 0-16 MPa 0.03-0.045 mm	9.3.1.3
XI	(7.3.1.9), (7.3.1.41)	0.02 mm	0.059 mm	9.3.1.4
XII	(7.3.1.42)	15 MPa	12 MPa	9.3.1.6
XIII	(7.3.1.37), (7.3.1.38)	3 MPa, 0.01 mm	2-8 MPa, 0.01 mm	9.3.1.6, 9.3.1.7
XIV	(7.3.1.41)	0.009 mm	0.01 mm	9.3.1.7
XV	(7.3.1.29), (7.3.1.30), (7.3.1.34), (7.3.1.35), (9.3.2.21), (9.3.2.23)	13 MPa, 22 MPa	25-30 MPa, 10-15 MPa	9.3.2.2
XVI	(7.3.1.9), (7.3.1.41)	0.063 mm	0.068 mm	9.3.2.7
XVII	(7.3.1.42)	13 MPa	5–13 MPa	9.3.2.9
XVIII	(7.3.1.41)	0.007 mm	0.01-0.03 mm	9.3.2.10
XIX	(7.3.1.37), (7.3.1.38)	3 MPa, 0.006 mm	2.4-9.6 MPa, 0.0051-0.0074 mm	9.3.3.1 9.3.3.2
XX	(7.3.1.37), (7.3.1.38)	3 MPa, 0.009 mm	2.4-6.0 MPa, 0.012-0.014 mm	9.3.3.3 9.3.3.4
XXI	(8.2.4)	0.027 mm	0.029 mm	9.4.1
XXII	(8.2.4)	0.24 mm	0.069	9.4.2

Table 10.1.

11. Discussion

In this work analytical expressions have been derived. Based on knowledge of punch force, blank holder force, thickness and yield stress of the blank and geometrical quantities, the casting structure can be dimensioned with respect to certain load cases. These load cases are assumed to reflect the significant sequences during a press stroke. Dies with a flat profile and a V-shaped profile were studied.

A concentrated summing-up of the comments made in connection to the results in section 9 is made in Table 10.1.

Load case	Comments
I	The results from analytical calculations are in fair agreement with the results from the FE-calculation.
II	The analytical expression seems to be usable, but since no draw bead exists in the CAD model, the load in the FE-calculation was applied on the radius surrounding the forming area. This means that the blank holder load not only was transmitted in the vertical direction, which yielded a lower stress in the considered walls (see Figure 9.1.1.6) compared to the result from the analytical expression.
III	In the lower half of the walls the results from the analytical expressions are in fair agreement with the results from the FE-calculations. However, in the area close to the position of the draw bead, the stress level is considerable higher. This is explained from a high surface pressure and is more related to the positioning of the draw beads, than the dimension of the walls themselves. The used model can be refined considering a horizontal force contribution as well and a stress distribution that vary with position.
IV	The results from analytical calculations are in fair agreement with the results from the FE-calculation.
V	The deflection due to torsion is 10 times larger in the result from the FE-calculation compared to the result from the analytical calculation. The explanation probably lies in the boundary conditions. In the analytical expression the ends are clamped, whilst the result from the FE-calculation shows upon torsion of the ends as well. A suggestion is to add a parameter in the analytical expression, which takes this effect into account.
VI	It seems to be a too coarse approximation, only considering that parts of the cross section indicated in Figure 7.2.1. The analytical expressions predict a 5 times larger deflection than the FE-calculation. The result from the FE-calculation indicates that other parts than the considered contributes to make the cross section stiffer. However, the deflection may be larger in reality than the result from the FE-calculation, since the blank holder and lower die, to some extent, are able to move independently. More dies have to be analysed before a definite statement regarding the analytical expression can be made.
VII	The same expression, (7.2.3), as in load case VI has been used, but in

	contradiction the deflection according to the analytical expression is approximately three times smaller compared the deflection according to the FE-calculation. This indicates the need for more simulations or measurements before reliable expressions can be derived.
VIII	The analytical expression assumes the stress only to be distributed over the upper half of the wall, i.e. the area L x B/2 (see Figure 7.3.1.1). According to the result from the analytical expression, the stress in the lower half at most regions does not exceed 15 MPa. In the upper half the stress level mainly varies between 15-50 MPa. The analytical expression seems to be useable, but can be refined considering the stress no to be equally distributed over the cross section.
IX	Regarding area 4, it seems to be a too coarse approximation assuming the load to be equally distributed over the whole forming area. It is suggested to distribute the load equally over the forming areas instead. The expression can probably be refined by adopting a bi-axial stress state.
X	The predicted stresses from the analytical expressions are too low compared to the FE-calculation. This is due to the influence of the punch load in area 1 and 5, which is neglected in the analytical expression. The influence can be taken into account by introducing a parameter dependent on the punch load and the distance between forming area and distance plate.
XI	Some uncertainties regarding the result exist. The thickness of the casting exceeds 1/10 of the length and width. This means, according to what has been mentioned in Appendix A, that the range of validity of the analytical expression is exceeded. On the other hand, in the FE-calculation the load is not distributed over the whole area, as has been assumed in the derivation of the analytical expression, but in those areas containing forming radii. Such load distribution may contribute making the result become less erroneous.
XII	The analytical model seems to be applicable, since forming radii is spread over the major forming area. In the area without forming radii, the FE-calculation predict a lower stress and the conclusion is the same as in the case of V-shaped dies, load case IX.
XIII	See load case X.
XIV	See load case XI.
XV	See comments to load case IX. Besides, a closer analysis of the principal stresses is recommended in order to determine an analytical expression that takes more than one stress component into account.
XVI	See load case XI
XVII	See load XII
XVIII	See load case XI
XIX	The results from the analytical calculations are in fair agreement with the results from the FE-calculation, with respect to stresses as well as to deflections. I probably possible to refine the expression by letting the area, over which the stress is distributed over, depend on the position.
XX	See load case XIX
XXI	The results agree
XXII	Due to the V-shape the load as well as the moment of inertia varies with the position along the x-axis, whilst it in (8.2.7) is assumed that the load

	is equally distributed and the moment of inertia constant. By taking the variation of moment (load) and moment of inertia into account when integrating the differential equation of the deflection (see (9.3.2.15)), an expression for the deflection is obtained, which probably would yield a better agreement.

Table 11.1

It must be kept in mind that the die items, lower die, punch and blank holder, were considered one by one. This implies that the load distributions were user defined. No consideration was taken to the complicated force transmission between the die items. Before any effort is made to refine the analytical expressions, it is therefore suggested to perform FE-calculations on the studied dies as well as other dies that take contact problems into account.

It is also worth mentioning that, since the applied blank holder and punch loads are representative for deep drawing operations and the stresses and deflections in common are low, there seems to be a potential to reduce weight and cost by reducing the die casting dimensions.

A yield criterion that takes the hydrostatic dependence in cast iron into account was suggested. In this, which was proposed by Drucker and Prager, the deviatoric stress state varies linearly with the hydrostatic. However, in the software used in the FE-calculations in this work, only von Mises yield criterion was implemented.

The comparisons between the results from the analytical expressions and the results from the FE-calculations show upon some indications. Regarding dimensioning of the walls located directly under the draw beads, area 1, with respect to the load case when the blank holder hit the lower die, the uni-axial stress state used in the analytical expression seems to be applicable. This applies to blank holders and lower dies irrespective of die type. The stress level close to the draw bead is higher than the analytically calculated value. This is explained from a high surface pressure and is more related to the position of the draw bead relative the boundary than the dimension of the wall.

For that case when the die is run in a single acting press, the blank holder is placed on nitrogen springs or air cushion pins. Since the blank holder is subjected to torsion, expressions for derivation of the position of the shear center were derived. However, the FE-calculation indicated that the moment axis not were located in the shear center. Instead the torsion occurred about the contact point at the springs / pins. In the analytical expression the ends of the section subjected to torsion were assumed to be clamped, which was not the case in the FE-calculation. This yielded an approximately 10 times higher deflection in FE-calculation. Anyway, the derived expression is judged to be usable if a parameter dependent on geometry can be incorporated.

When it comes to dimensioning of area 2 when the punch hits the blank, it is hard to make a statement regarding the reliability of the analytical expressions. It seems to be a too coarse approximation, only considering the blank holder surfaces to contribute to the stiffness (see Figure 7.2.1). There are numerous of variants of casting structures, which makes it hard to derive analytical expressions. Besides, to some extent the blank holder probably will move independently of the lower die. In the FE-calculations performed in this work the blank holder and the lower die were prevented to move independently. Data from simulations incorporating

contact problems or measurements are required before reliable analytical expressions can be derived.

Concerning dimensioning of the walls under the forming area, area 4, the load throughout this work has been assumed to be equally distributed over the whole forming area as far as the analytical expressions concerns. In the FE-calculations the load has been applied only on the forming radii, which probably reflect the reality better. From the results it is concluded that the load only influence a limited area close to where it acts. In the analytical expressions shall therefore not the load be distributed over the whole forming area, but the area containing forming radii. A uni-axial stress state seems to be applicable for lower die and punch in flat dies. For V-shaped dies there is a need for being able to determine the distribution over the vertical walls given an applied load. Such expression was derived for the structure shown in Figure 9.3.2.3 with the result stated in (9.3.2.21). Neither this expression nor the differences between how the load is applied in the analytical expression and the FE-calculation, fully explains the lack of agreement. Regarding area 4 in V-shaped lower dies and punches, it is therefore suggested to investigate the possibilities to incorporate a model that take a bi-axial stress state into account.

The calculation of deflection in the forming area, area 3, was done using an expression based on Kirchoff plate theory. This theory is valid for thin plates i.e. plane stress. In Appendix A it was concluded that the theory works well for plates where the shortest side exceeds one tenth of the thickness. The analytical calculations showed upon fair agreement with the FE-calculation for all studied dies, despite that the thickness in the studied dies exceed one tenth of the thickness. The explanation probably lies in the load distribution. In the analytical expression the load was assumed to be equally distributed, whilst the load only was distributed over the areas with forming radii in the FE-calculations. The fact that the loads in the FE-calculations only were located to areas with forming radii seems to compensate for the expected under estimation using the analytical expression.

A load case when the die is closed, which applies for V-shaped lower dies only, is that which covers the forces trying to split the die in area 6. The suggested tri-axial stress state seems to work well. The stress was assumed to be distributed equally over the upper half of the cross section and the expression can be refined if position dependent distribution is adopted.

The force transmission between blank holder and lower die when the die is closed takes place at the bottom plates. This affects the walls in area 1 and 5. The adopted analytical model, only taking a uni-axial stress state into account, seems to be usable regardless of die type. The analytical expression can be refined by introducing a position dependence on the area in which the stress acts. This would allow the stress to increase with a decreasing distance to the distance plate. In addition, in the lower dies the influence from the load in the forming area has to be considered to make the analytical expression agree with the FE-calculation. This can be done by introducing a parameter that is dependent on the punch load and the distance between the boundary of the forming area and the distance plate.

The derived analytical expressions for calculation of deflection of the die when stored on trestles worked well for the flat die, but not for the V-shaped die. By incorporating the variation with the position regarding the load as well as the moment of inertia when integrating the differential equation of the deflection curve, (9.3.2.15) the expression will be usable.

The aim was to derive expressions to be used during the die design and this work ends with an example on a suggested program structure for dimensioning of a V-shaped lower die. Required input is punch load, blank holder load, yield stress and thickness of the blank, geometrical quantities of the casting structure and allowed maximum stresses and deflections of the casting structure.

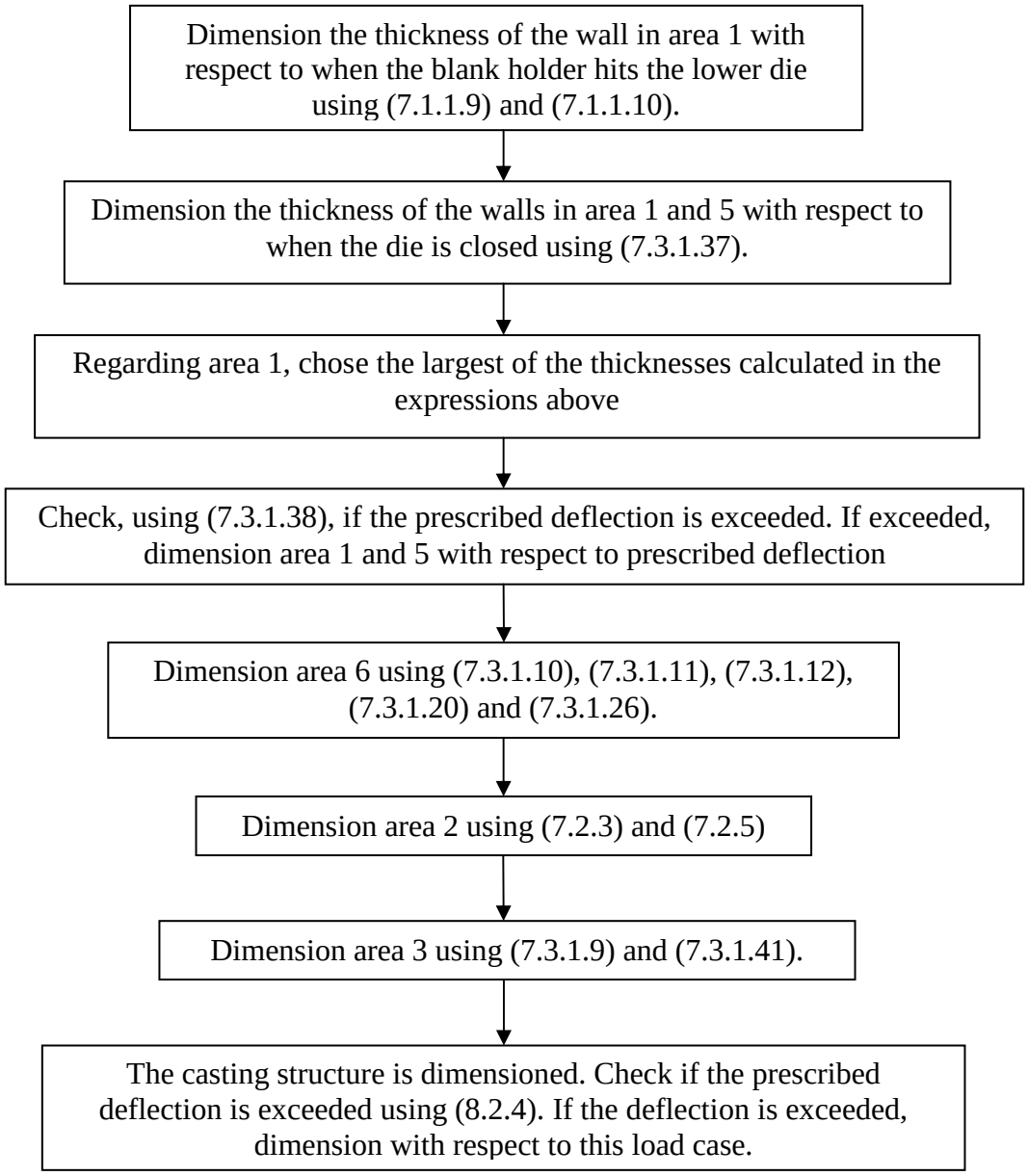

12. References

[1] Niels Saabye Ottosen, *The coincidence of shear center and center of twist*, Department of Solid Mechanics, Lund University, Box 118, 22100 Lund, Sweden, September 17, 1997.

[2] Kungliga Tekniska Högskolan, *Formelsamling i hållfasthetslära*, 9th issue, Civiltryck AB, Stockholm, 1996.

[3] Benham, Crawford & Armstrong, *Mechanics of engineering materials*, 2nd edition, Prentice Hall, Essex, 1996.

[4] Ottosen & Ristinmaa, *The mechanics of constitutive modelling*, Division of Solid Mechanics, Lund University, 221 00 Lund, 1999.

[5] Ottosen & Petersson, *Introduction to the finite element method*, 1st edition, Prentice Hall, Essex, 1992.

[6] Austrell et al, *CALFEM*, version 3.3, Division of Structural Mechanics and the Department of Solid Mechanics at Lund University, Lund, 1999.

[7] Thelandersson, *Analysis of thin-walled beams*, Lund University, Lund, 1987.

13. Mathematical appendix

13.1. Part A-Plate with equally distributed load

The task is to determine the deflections of a plate with an equally distributed load. The problem is originally three dimensional but here the Kirchoff plate theory is adopted, which means that the problem is transformed in to two dimensions at the expense of the range of validity of the solution. The resulting differential equation to be solved according to this theory reads [5]

$$\frac{\partial^2 M_{xx}}{\partial x^2} + 2\frac{\partial^2 M_{xy}}{\partial x \partial y} + \frac{\partial^2 M_{yy}}{\partial y^2} + q = 0 \qquad \text{(A.1)}$$

where M_{xx} and M_{yy} are the bending moments per unit length, M_{xy} the twisting moment per unit length and q is a transverse load (force per unit area) measured positive in the positive z-direction, c.f. the Figure A.1. The moments are defined as

$$M_{xx} = \int_{-t/2}^{t/2} z\sigma_{xx} dz$$

$$M_{yy} = \int_{-t/2}^{t/2} z\sigma_{yy} dz \qquad \text{(A.2)}$$

$$M_{xy} = M_{yx} = \int_{-t/2}^{t/2} z\sigma_{xy} dz$$

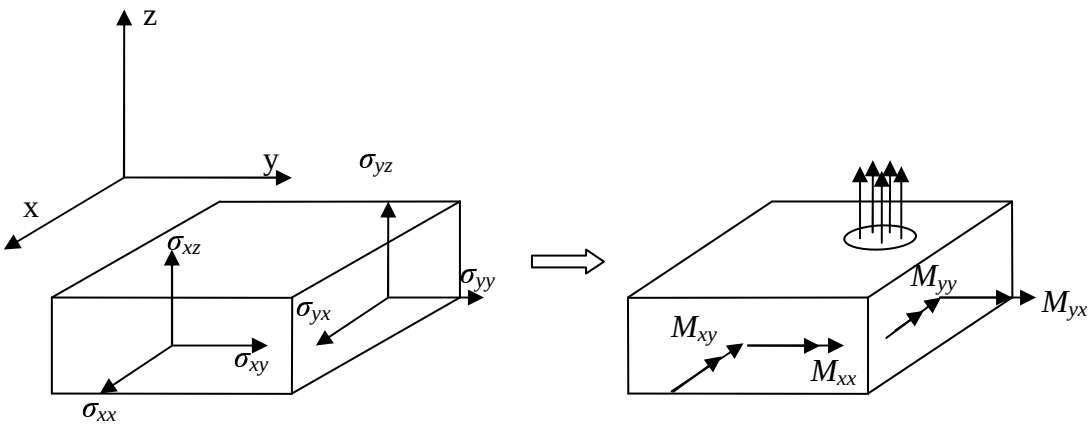

Figure A.1. Definitions of stresses and moments

When deriving (A.1) the shear strains γ_{xz} and γ_{yz} were set to zero but σ_{xz} and σ_{yz} were used to maintain equilibrium. To get rid of this contradiction σ_{xz} and σ_{yz} were assumed to be small and plane stress was adopted. The consequence is that this theory is only valid for thin plates.

To solve (A.1) an approximate solution strategy was chosen, i.e. the finite element method. Before this method can be used, some manipulations of (A.1) have to be performed: firstly establish the weak form of the differential equation, secondly make an element wise approximation over the plate of the unknown variable and finally choose the weight function according to the Galerkin method. When this is applied to (A.1) under the assumption of linear elastic isotropic material behaviour and with the plate thickness set to constant, the resulting finite element formulation is given by [5]

$$\left(\int_S \mathbf{B}^{\mathbf{T}}\tilde{\mathbf{D}}\mathbf{B}dS\right)\mathbf{a} = \oint_l \mathbf{N}^{\mathbf{T}}\left(V_{nz} + \frac{dM_{nm}}{dm}\right)dl - \oint_l (\nabla\mathbf{N})^{\mathbf{T}}\mathbf{n}M_{nn}dl + \int_A \mathbf{N}^{\mathbf{T}}qdS \qquad \text{(A.3)}$$

which can be written in a compact format as

$$\mathbf{Ka} = \mathbf{f_b} + \mathbf{f_l} \quad \text{(A.4)}$$

using **K**, i.e. the stiffness lower die, as

$$\mathbf{K} = \int_S \mathbf{B}^{\mathbf{T}}\tilde{\mathbf{D}}\mathbf{B}dS \qquad \text{(A.5)}$$

the boundary vector $\mathbf{f}_b$

$$\mathbf{f}_b = \oint_l \mathbf{N}^{\mathbf{T}}\left(V_{nz} + \frac{dM_{nm}}{dm}\right)dl - \oint_l (\nabla\mathbf{N})^{\mathbf{T}}\mathbf{n}M_{nn}dl \qquad \text{(A.6)}$$

and $\mathbf{f}_l$ the load vector, as

$$\mathbf{f}_l = \int_S \mathbf{N}^{\mathbf{T}}qdS \qquad \text{(A.7)}$$

In the derivation of (A.3) the unknown deflection w was approximated as

$$w = \mathbf{Na} \qquad \text{(A.8)}$$

N denotes the global shape functions and **a** the nodal values given by

$$\mathbf{N} = \begin{bmatrix} N_1 & N_2 & \cdots & N_{ndof} \end{bmatrix}, \ \mathbf{a} = \begin{bmatrix} u_1 \\ u_2 \\ \vdots \\ u_{ndof} \end{bmatrix} \qquad \text{(A.9)}$$

and *ndof* is the number of degrees of freedom. **B** is defined as

$$\mathbf{B} = \overset{*}{\nabla}\,\mathbf{N}, \quad \overset{*}{\nabla} = \begin{bmatrix} \dfrac{\partial^2}{\partial x^2} \\ \dfrac{\partial^2}{\partial y^2} \\ 2\dfrac{\partial^2}{\partial x \partial y} \end{bmatrix} \qquad \text{(A.10)}$$

and $\tilde{\mathbf{D}}$ as

$$\tilde{\mathbf{D}} = \frac{t^3 E}{12\left(1-\nu^2\right)} \begin{bmatrix} 1 & \nu & 0 \\ \nu & 1 & 0 \\ 0 & 0 & \frac{1}{2}(1-\nu) \end{bmatrix} \qquad \text{(A.11)}$$

where E denotes the modulus of elasticity, t the plate thickness, l the boundary and ν Poisson's ratio. The interpretation of V_{nz}, **m**, **n**, M_{nn} and M_{nm} is clarified from Figure A.2 in analogy with Figure A.1 and equation (A.2).

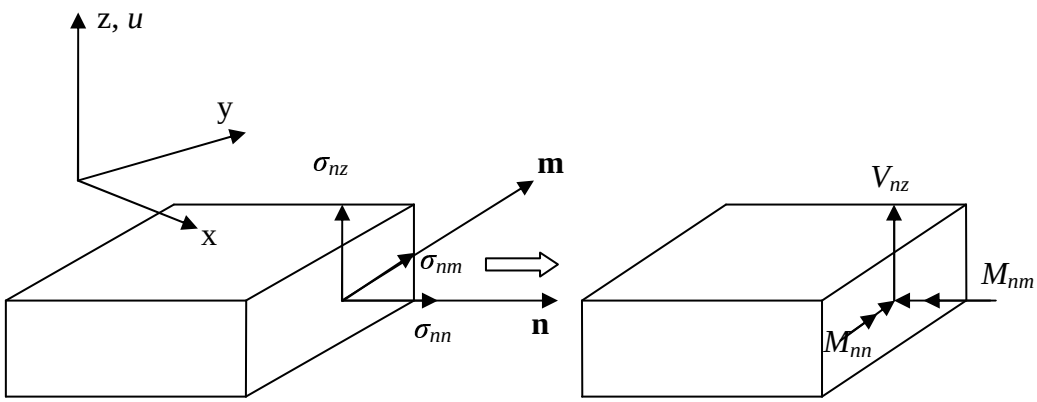

Fig. A.2. Definitions of stresses and moments in an arbitrary section

The plate is represented with rectangular elements according to Figure A.3 [6]. Each element has 12 degrees of freedom where u_1, u_4, u_7 and u_{10} denote deflections and u_2, u_3, u_5, u_6, u_8, u_9, $u_{11}$and u_{12} rotations. The deflections are measured as positive in the positive z-direction. The rotations are defined by dw/dn and if the coordinate system shown in Figure A.3 is chosen the rotations can be calculated as

$$\begin{aligned} \frac{dw}{dx} &\Leftrightarrow u_3, u_6, u_9, u_{12} \\ \frac{dw}{dy} &\Leftrightarrow u_2, u_5, u_8, u_{11} \end{aligned} \qquad \text{(A.12)}$$

The rotations defined as positive are shown in Figure A.4.

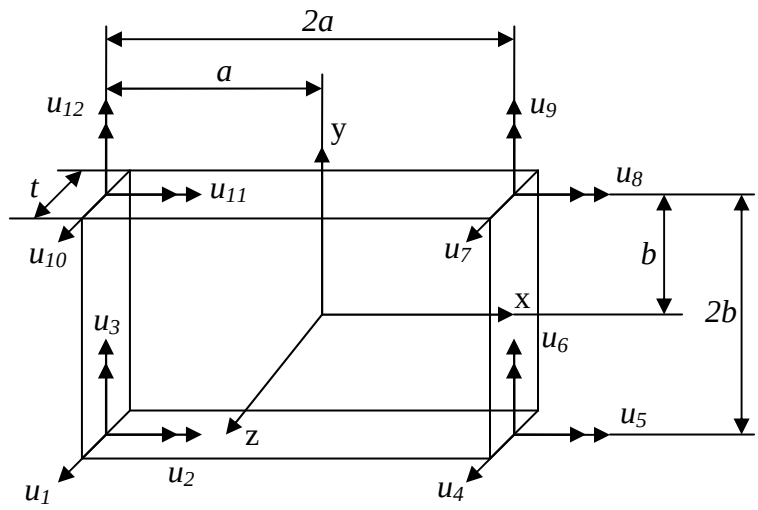

Fig. A.3. Rectangular 12 degrees of freedom plate element.

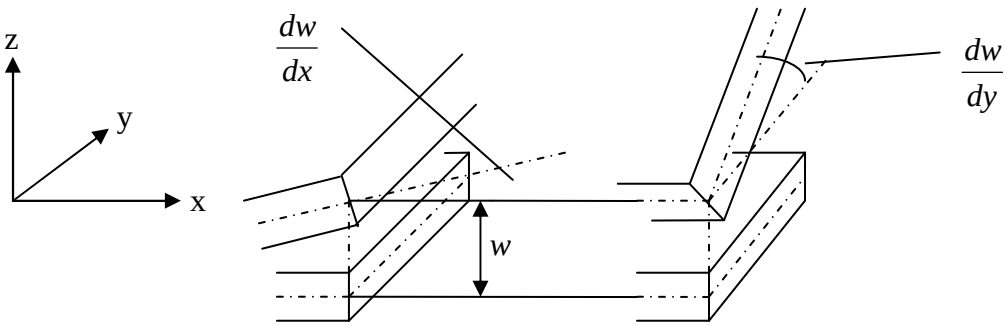

Fig. A.4. Definition of rotations

Now, when the type of element to build up the plate has been chosen the next step is to derive an expression for the element stiffness lower die, $\mathbf{K}^e$, and the element load vector, $\mathbf{f}_l^e$. When these are known, they are assembled using topology data to the global stiffness lower die, **K**, and the global load vector, $\mathbf{f}_l$. After this has been done, (A.4) is used together with specified boundary conditions to obtain a linear system of equations. The final step is to solve this system of equations for the unknown degrees of freedom, **a**, which specifies the deflections and rotations in each node.

Following the procedure outlined above, it is necessary to firstly approximate the deflection over one element corresponding to the global approximation (A.8). Since the element has 12 degrees of freedom a polynomial containing 12 terms has to be used which yields the approximation

$$w = \alpha_1 + \alpha_2 x + \alpha_3 y + \alpha_4 x^2 + \alpha_5 xy + \alpha_6 y^2 + \alpha_7 x^3 + \alpha_8 x^2 y + \alpha_9 xy^2 + \alpha_{10} y^3 + \alpha_{11} x^3 y + \alpha_{12} xy^3 \tag{A.13}$$

which rewritten in lower die form reads

$$w = \overline{\mathbf{N}}\boldsymbol{\alpha},\ \overline{\mathbf{N}} = \begin{bmatrix} 1 & x & y & x^2 & xy & y^2 & x^3 & x^2 y & xy^2 & y^3 & x^3 y & xy^3 \end{bmatrix}$$

$$\boldsymbol{\alpha} = \begin{bmatrix} \alpha_1 \\ \alpha_2 \\ \vdots \\ \alpha_{12} \end{bmatrix} \tag{A.14}$$

The unknown constant coefficients $\boldsymbol{\alpha}$ are undesirable, but by expressing these coefficients in terms of the deflection in the nodal points, they do not enter the calculations. This is done in the **C**-lower die method as follows [5]. With (A.12) and A.4 in mind the nodal values are expressed with help from (A.14) as

$$\mathbf{a}^e = \mathbf{C}\boldsymbol{\alpha} \tag{A.15}$$

where

$$\mathbf{a}^e = \begin{bmatrix} u_1 \\ u_2 \\ \vdots \\ u_{12} \end{bmatrix} \tag{A.16}$$

and

$$\mathbf{C} = \begin{bmatrix} 1 & -a & -b & a^2 & ab & b^2 & -a^3 & -a^2 b & -ab^2 & -b^3 & a^3 b & ab^3 \\ 0 & 0 & 1 & 0 & -a & -2b & 0 & a^2 & 2ab & 3b^2 & -a^3 & -3ab^2 \\ 0 & -1 & 0 & 2a & b & 0 & -3a^2 & -2ab & -b^2 & 0 & 3a^2 b & b^3 \\ 1 & a & -b & a^2 & -ab & b^2 & a^3 & -a^2 b & ab^2 & -b^3 & -a^3 b & -ab^3 \\ 0 & 0 & 1 & 0 & a & -2b & 0 & a^2 & -2ab & 3b^2 & a^3 & 3ab^2 \\ 0 & -1 & 0 & -2a & b & 0 & -3a^2 & 2ab & -b^2 & 0 & 3a^2 b & b^3 \\ 1 & a & b & a^2 & ab & b^2 & a^3 & a^2 b & ab^2 & b^3 & a^3 b & ab^3 \\ 0 & 0 & 1 & 0 & a & 2b & 0 & a^2 & 2ab & 3b^2 & a^3 & 3ab^2 \\ 0 & -1 & 0 & -2a & -b & 0 & -3a^2 & -2ab & -b^2 & 0 & -3a^2 b & -b^3 \\ 1 & -a & b & a^2 & -ab & b^2 & -a^3 & a^2 b & -ab^2 & b^3 & -a^3 b & -ab^3 \\ 0 & 0 & 1 & 0 & -a & 2b & 0 & a^2 & -2ab & 3b^2 & -a^3 & -3ab^2 \\ 0 & -1 & 0 & 2a & -b & 0 & -3a^2 & 2ab & -b^2 & 0 & -3a^2 b & -b^3 \end{bmatrix} \tag{A.17}$$

where the coordinates according to Figure A.3 have been inserted. Solving (A.15) for $\boldsymbol{\alpha}$ yields

$$\boldsymbol{\alpha} = \mathbf{C}^{-1}\mathbf{a}^{e} \qquad \text{(A.18)}$$

which inserted in (A.14) gives an expression without $\boldsymbol{\alpha}$ for the deflections in one element as

$$w = \overline{\mathbf{N}}\mathbf{C}^{-1}\mathbf{a}^{e} = \mathbf{N}^{e}\mathbf{a}^{e} \qquad \text{(A.19)}$$

where $\mathbf{N}^{e}$ denotes the element shape functions. There is no need for calculating the element shape functions explicit. Instead (A.5), (A.10), (A.11), (A.17) and (A.19) are used to calculate the element stiffness lower die $\mathbf{K}^{e}$.

$$\begin{aligned}
\mathbf{K}^{e} &= \int_{S} \mathbf{B}^{e\mathbf{T}}\tilde{\mathbf{D}}\mathbf{B}^{e}\,dA = \int_{S}\left(\overset{*}{\nabla}\mathbf{N}^{e}\right)^{\mathbf{T}}\tilde{\mathbf{D}}\overset{*}{\nabla}\mathbf{N}^{e}\,dS = \int_{S}\left(\overset{*}{\nabla}\left(\overline{\mathbf{N}}\mathbf{C}^{-1}\right)\right)^{\mathbf{T}}\tilde{\mathbf{D}}\overset{*}{\nabla}\left(\overline{\mathbf{N}}\mathbf{C}^{-1}\right)dS = \\
&\int_{S}\left(\left(\overset{*}{\nabla}\overline{\mathbf{N}}\right)\mathbf{C}^{-1}\right)^{\mathbf{T}}\tilde{\mathbf{D}}\left(\overset{*}{\nabla}\overline{\mathbf{N}}\right)\mathbf{C}^{-1}dS = \mathbf{C}^{-1\mathbf{T}}\int_{S}\left(\overset{*}{\nabla}\overline{\mathbf{N}}\right)^{\mathbf{T}}\tilde{\mathbf{D}}\overset{*}{\nabla}\overline{\mathbf{N}}\,dS\,\mathbf{C}^{-1} = \\
&\mathbf{C}^{-1\mathbf{T}}\int_{-a}^{a}\int_{-b}^{b}\left(\overset{*}{\nabla}\overline{\mathbf{N}}\right)^{\mathbf{T}}\tilde{\mathbf{D}}\overset{*}{\nabla}\overline{\mathbf{N}}\,dx\,dy\,\mathbf{C}^{-1}
\end{aligned} \qquad \text{(A.20)}$$

Carrying out the integral $\int_{-a}^{a}\int_{-b}^{b}\left(\overset{*}{\nabla}\overline{\mathbf{N}}\right)^{\mathbf{T}}\tilde{\mathbf{D}}\overset{*}{\nabla}\overline{\mathbf{N}}\,dx\,dy$ following lower die is obtained

$$Et^{3}\begin{bmatrix}
0 & 0 & 0 & 0 & 0 & 0 & 0 & 0 & 0 & 0 & 0 & 0 \\
0 & 0 & 0 & 0 & 0 & 0 & 0 & 0 & 0 & 0 & 0 & 0 \\
0 & 0 & 0 & 0 & 0 & 0 & 0 & 0 & 0 & 0 & 0 & 0 \\
0 & 0 & 0 & -\frac{4ab}{3(\nu^{2}-1)} & 0 & -\frac{4ab\nu}{3(\nu^{2}-1)} & 0 & 0 & 0 & 0 & 0 & 0 \\
0 & 0 & 0 & 0 & \frac{2ab}{3(\nu+1)} & 0 & 0 & 0 & 0 & 0 & \frac{2a^{3}b}{3(\nu+1)} & \frac{2ab^{3}}{3(\nu+1)} \\
0 & 0 & 0 & -\frac{4ab\nu}{3(\nu^{2}-1)} & 0 & -\frac{4ab}{3(\nu^{2}-1)} & 0 & 0 & 0 & 0 & 0 & 0 \\
0 & 0 & 0 & 0 & 0 & 0 & \frac{4a^{3}b}{(\nu^{2}-1)} & 0 & -\frac{4a^{3}b\nu}{3(\nu^{2}-1)} & 0 & 0 & 0 \\
0 & 0 & 0 & 0 & 0 & 0 & 0 & -\frac{4\left(\frac{ab^{3}}{3}+\frac{2a^{3}b}{3}-\frac{2a^{3}b\nu}{3}\right)}{3(\nu^{2}-1)} & 0 & -\frac{4ab^{3}\nu}{3(\nu^{2}-1)} & 0 & 0 \\
0 & 0 & 0 & 0 & 0 & 0 & -\frac{4a^{3}b\nu}{3(\nu^{2}-1)} & 0 & -\frac{4\left(-\frac{ab^{3}}{3}-\frac{2ab^{3}}{3}+\frac{2ab^{3}\nu}{3}\right)}{3(\nu^{2}-1)} & 0 & 0 & 0 \\
0 & 0 & 0 & 0 & 0 & 0 & 0 & -\frac{4ab^{3}\nu}{3(\nu^{2}-1)} & 0 & -\frac{4ab^{3}}{(\nu^{2}-1)} & 0 & 0 \\
0 & 0 & 0 & 0 & \frac{2a^{3}b}{3(\nu+1)} & 0 & 0 & 0 & 0 & 0 & -\frac{6\left(\frac{2a^{3}b^{3}}{9}+\frac{a^{5}b}{5}-\frac{a^{5}b\nu}{5}\right)}{(\nu^{2}-1)} & -\frac{2a^{3}b^{3}}{3(\nu-1)} \\
0 & 0 & 0 & 0 & \frac{2ab^{3}}{3(\nu+1)} & 0 & 0 & 0 & 0 & 0 & -\frac{2a^{3}b^{3}}{3(\nu-1)} & \frac{6\left(-\frac{2a^{3}b^{3}}{9}-\frac{ab^{5}}{5}+\frac{ab^{5}\nu}{5}\right)}{(\nu^{2}-1)}
\end{bmatrix}$$

(A.21)

where

$$\overset{*}{\nabla}\overline{\mathbf{N}} = \begin{bmatrix} \dfrac{\partial^2}{\partial x^2} \\ \dfrac{\partial^2}{\partial y^2} \\ 2\dfrac{\partial^2}{\partial x \partial y} \end{bmatrix} \begin{bmatrix} 1 & x & y & x^2 & xy & y^2 & x^3 & x^2y & xy^2 & y^3 & x^3y & xy^3 \end{bmatrix} = \tag{A.22}$$

$$\begin{bmatrix} 0 & 0 & 0 & 2 & 0 & 0 & 6x & 2y & 0 & 0 & 6xy & 0 \\ 0 & 0 & 0 & 0 & 0 & 2 & 0 & 0 & 2x & 6y & 0 & 6xy \\ 0 & 0 & 0 & 0 & 2 & 0 & 0 & 4x & 4y & 0 & 6x^2 & 6y^2 \end{bmatrix}$$

was used. Thus to obtain $\mathbf{K}^e$, the lower die in (A.21) has to be pre-multiplied with $\mathbf{C}^{-1\mathbf{T}}$ and post-multiplied with $\mathbf{C}^{-1}$. The final expression will not be shown because it would occupy too much space.

The next task is to determine the element load vector $\mathbf{f}_l^e$, which is calculated in the same manner as global load vector given by (A.7) i.e.

$$\mathbf{f}_l^e = \int_S \mathbf{N}^{e\mathbf{T}} q dS = \int_S \left(\overline{\mathbf{N}}\mathbf{C}^{-1}\right)^{\mathbf{T}} q dS = q\mathbf{C}^{-1\mathbf{T}} \int_S \overline{\mathbf{N}}^{\mathbf{T}} dS = q\mathbf{C}^{-1\mathbf{T}} \int_{-a}^{a}\int_{-b}^{b} \overline{\mathbf{N}}^{\mathbf{T}} dxdy \tag{A.23}$$

where it was assumed that the load q is constant over the whole area. After the integrations and lower die operations have been carried out the result is

$$\mathbf{f}_l^e = q \begin{bmatrix} ab \\ \dfrac{ab^2}{3} \\ -\dfrac{a^2b}{3} \\ ab \\ \dfrac{ab^2}{3} \\ \dfrac{a^2b}{3} \\ ab \\ -\dfrac{ab^2}{3} \\ \dfrac{a^2b}{3} \\ ab \\ -\dfrac{ab^2}{3} \\ -\dfrac{a^2b}{3} \end{bmatrix} \tag{A.24}$$

Now when the element stiffness lower die, calculated with help of (A.21) and (A.17), and the element load vector, (A.24) are known, these are used for each element in the structure, to be assembled in a systematic manner by using topology data, to obtain the global stiffness lower

die, **K**, given by (A.5) and the global load vector, $\mathbf{f}_l$, given by (A.7). But before this can be done the plate has to be divided into elements. This is shown in Figure A.5 where also the global node numbering is shown.

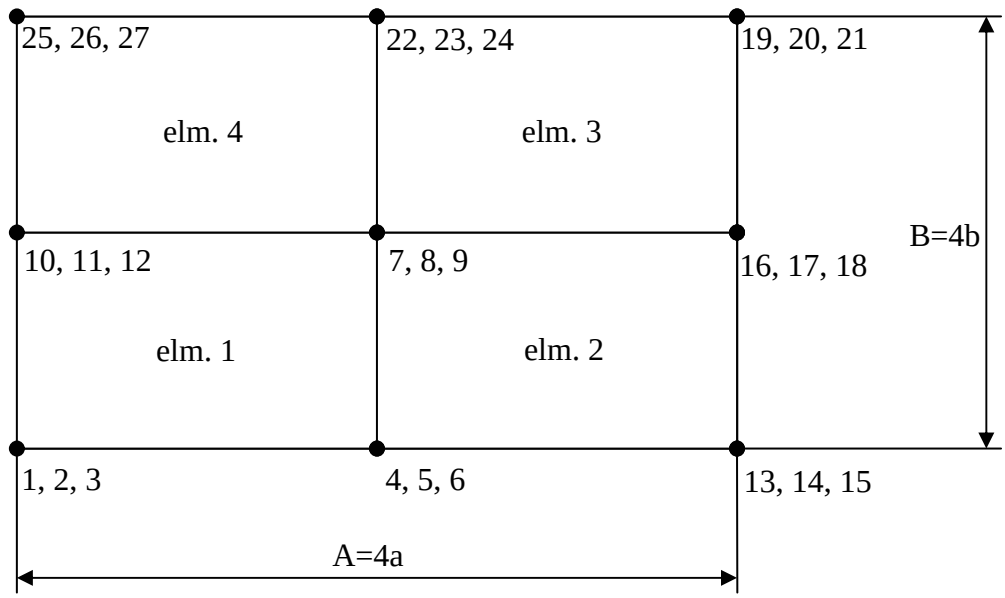

Fig. A.5. Two dimensional mesh.

The connection between global and local numbering is determined by the topology data. This means for example, considering element 2, that the local nodes 10, 11 and 12 (ref. Figure A.3) corresponds to the global nodes 7, 8 and 9. Only considering the element (7,7) in the global stiffness lower die the local lower die element (10,10) shall be added. Continuing with element 3 it is observed that the global nodes 7, 8 and 9 corresponds to the local nodes 1, 2 and 3. Consequently the local lower die element (1,1) shall be added to the global lower die element (7,7). Proceeding with element 1 and 4 it is realized that the global lower die element (7,7) will contain four terms. When this assembly process has been carried out for all nodes and elements the resulting global stiffness lower die **K** will have the size 27x27. The same procedure gives the global load vector the size 27x1.

Two load cases will be treated:

- All four edges clamped.
- Three edges clamped and the fourth free.

Beginning with the case when all four edges are clamped, the boundary conditions correspond to all degrees of freedom along the edges set to zero, since a clamped condition imply neither deflection nor slopes. It can be shown that in order to obtain an unique solution, proper boundary conditions have to be applied and that these lead to a partitioning of **K** when solving for the unknown degrees of freedom [5]. This is done by extracting those rows with the same number as the degrees of freedom with prescribed boundary values and the columns with the same numbers as the extracted rows from the calculations. In this case it implies that all the rows and columns shall be extracted except from those corresponding to the degrees of freedom number 7, 8 and 9. With (i,j) referring to the elements in stiffness lower die, $\mathbf{K}^e$, and element load vector, $\mathbf{f}_l^e$, the partitioned lower dies reads

$$\underset{\sim}{\mathbf{K}} = \begin{bmatrix} (1,1)+(4,4)+(7,7)+(10,10) & (1,2)+(4,5)+(7,8)+(10,11) & (1,3)+(4,6)+(7,9)+(10,12) \\ (2,1)+(5,4)+(8,7)+(11,10) & (2,2)+(5,5)+(8,8)+(11,11) & (2,3)+(5,6)+(8,9)+(11,12) \\ (3,1)+(6,4)+(9,7)+(12,10) & (3,2)+(6,5)+(9,8)+(12,11) & (3,3)+(6,6)+(9,9)+(12,12) \end{bmatrix} =$$

$$Et^3 \begin{bmatrix} -\dfrac{\left(7a^2b^2 - 2a^2b^2\nu + 10a^4 + 10b^4\right)}{30a^3b^3\left(\nu^2 - 1\right)} & 0 & 0 \\ 0 & -\dfrac{4\left(5a^2 + b^2 - b^2\nu\right)}{45ab\left(\nu^2 - 1\right)} & 0 \\ 0 & 0 & -\dfrac{4\left(a^2 - a^2\nu + 5b^2\right)}{45ab\left(\nu^2 - 1\right)} \end{bmatrix}$$

(A.25)

$$\underset{\sim}{\mathbf{f}} = \begin{bmatrix} (1,1)+(4,1)+(7,1)+(10,1) \\ (2,1)+(5,1)+(8,1)+(11,1) \\ (3,1)+(6,1)+(9,1)+(12,1) \end{bmatrix} = \begin{bmatrix} 4abq \\ 0 \\ 0 \end{bmatrix} \qquad \text{(A.26)}$$

It is to be noted that no use has been made of (A.6) since this vector only influences the boundary where, in this case, all the degrees of freedom are prescribed. The last step is now to solve the system of equations

$$\underset{\sim}{\mathbf{K}} \begin{bmatrix} u_7 \\ u_8 \\ u_9 \end{bmatrix} = \underset{\sim}{\mathbf{f}} \qquad \text{(A.27)}$$

which yields

$$\begin{aligned} u_7 &= \frac{120q\left(1-\nu^2\right)}{Et^3} \frac{a^4b^4}{7a^2b^2 - 2a^2b^2\nu + 10a^4 + 10b^4} \\ u_8 &= 0 \\ u_9 &= 0 \end{aligned} \qquad \text{(A.28)}$$

The fact that the deflections u_8 and u_9 are equal to zero, which is interpreted as that there will be no slope at mid point, is in agreement with the expectations. Instead of expressing the deflection in terms of the length of the sides in one element, *a* and *b*, it is more convenient to express it in terms of the sides of the whole structure, *A* and *B*, according to Figure A.5.

$$\boxed{u_7 = \frac{15q\left(1-\nu^2\right)}{32Et^3} \frac{A^4B^4}{7A^2B^2 - 2A^2B^2\nu + 10A^4 + 10B^4}} \qquad \text{(A.29)}$$

Since the structure only consists of four elements, it implies that the finite element solution will differ from the true. However, there is no need for the exact solution. The main thing is

that the approximate solution predicts the deflection at mid point well. To investigate this closer, the derived solution was evaluated for typical dimensions of *A* and *B* in a die, and compared with the results when more elements were used. The results are specified in Figure A.6.

A=400 mm, *B*=300 mm, *q*=-10 MPa, *E*=210000 MPa, *ν*=0.3				
Nbr. of elements		U_7 (mm)		U_7 (mm)
4	*t*=30 mm	-0,3635	*t*=80 mm	-0,1917
16		-0,3399		-0,1792
32		-0,3228		-0,1702

Fig. A.6. Comparison of deflection between different meshes and thicknesses.

With the application of draw dies in mind, the differences between the meshes are to be considered as small. However, it may not be forgotten that plane stress was assumed to be valid and that the problem was considered as a plane problem. Therefore, finite element calculations with ten-node tetrahedral elements were performed. Using the same input as in Figure A.6, it was possible to make a comparison between a three dimensional solution and the more simple Kirchoff theory adopted here. The result of the finite element calculations are shown in Figure A.7 and A.8.

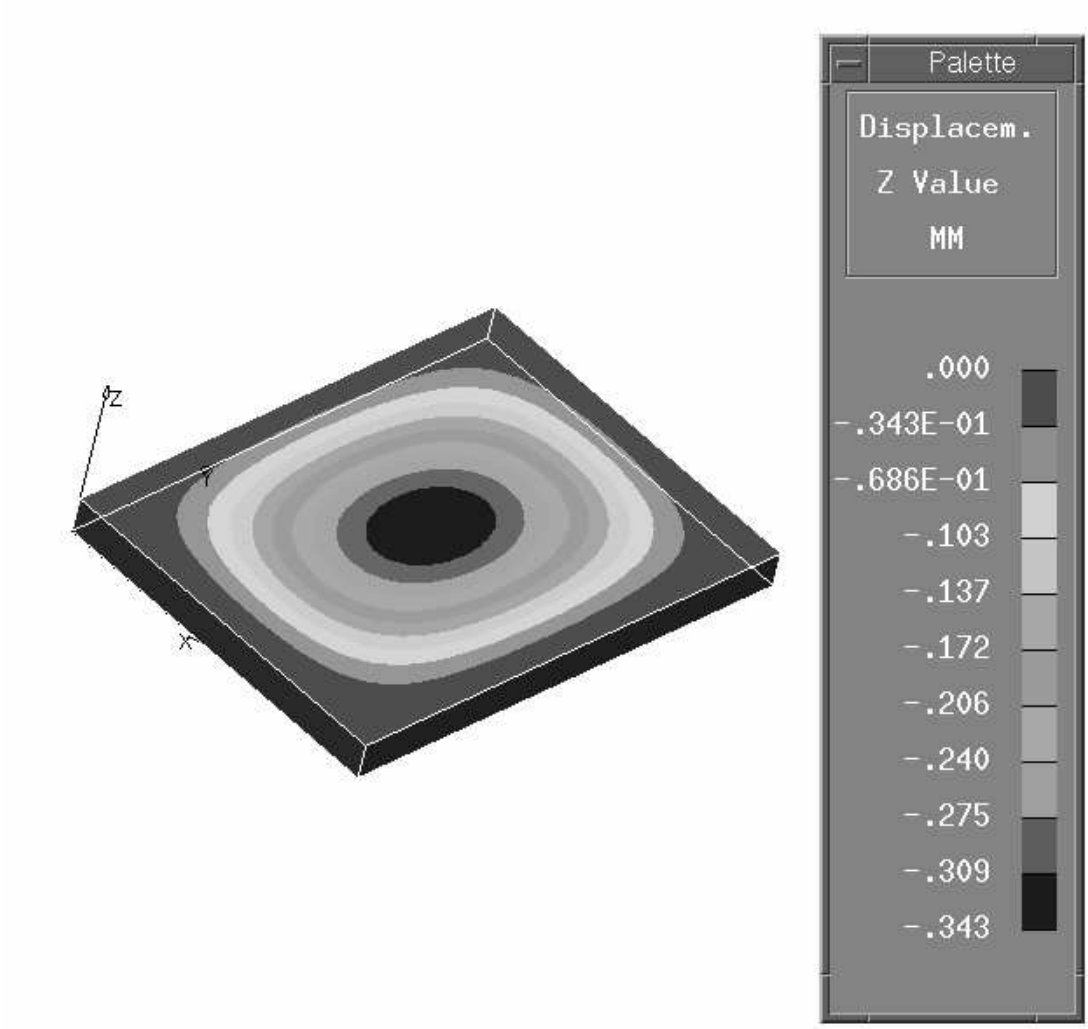

Fig. A.7. Deflections in a 30 mm plate consisting of 2288 ten-node tetrahedral elements. Input as in fig. A.6.

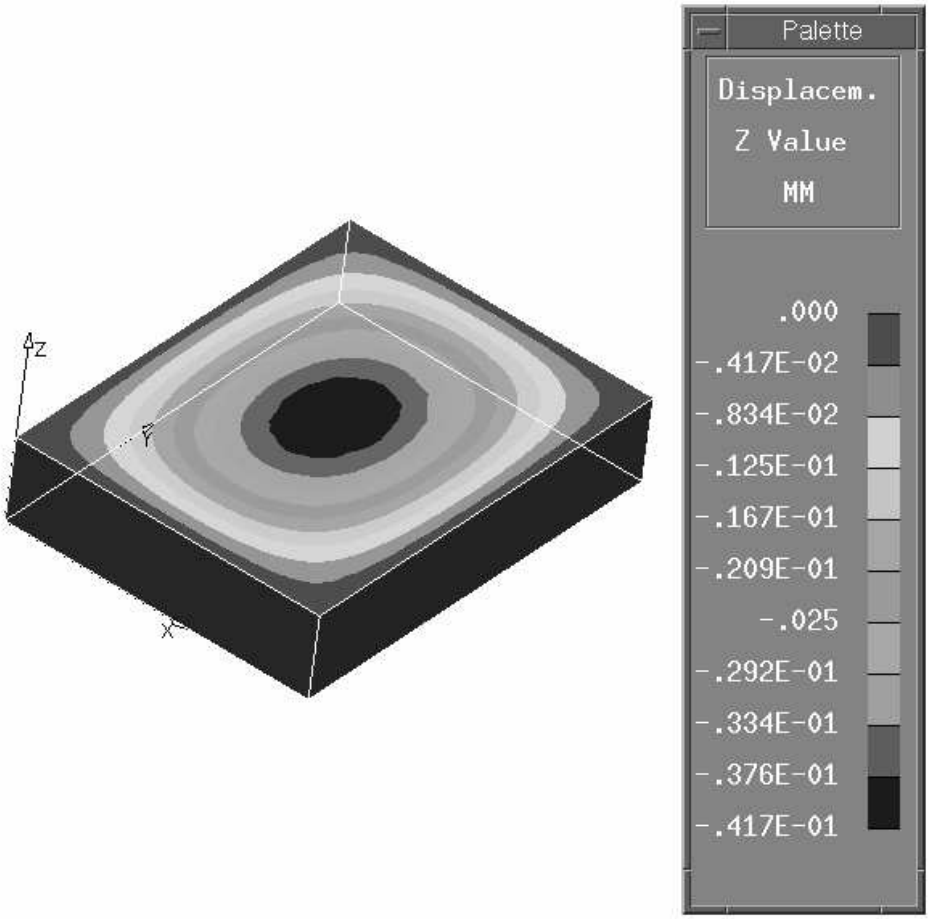

Fig. A.8. Deflections in an 80 mm plate consisting of 3669 ten-node tetrahedral elements. Input as in fig. A.6.

By comparing Figure A.6-A.8, it is concluded that the two dimensional model works well for t=30. Surprisingly is the 16-element mesh in better agreement with the three dimensional solution than that with 32 elements. When the plate with t=80 is considered it turns out that the two dimensional model fails. It seems that the two dimensional model works well at least for structures where the shortest dimension is larger or equal to one tenth of the thickness.

The last case to treat is when three edges are clamped and the fourth is free. This load case can serve as a base for analysis of the deflection of blank holder and blank holder plate, but is not treated in this work. Under assumption that the side containing the degrees of freedom 4, 5 and 6 at mid point to be free (ref. fig. A.5), the only differences in the boundary conditions are that the degrees of freedom 4 and 5 no longer are equal to zero. Of symmetrical reasons the degree of freedom 6 is still expected to be equal to zero. Since u_4 and u_5, which are located on a boundary, now are unknown, the expression for the boundary vector $\mathbf{f}_b$ from (A.6) has to be considered. The boundary is however free and this implies that no stresses act on it and consequently are $V_{nz}, \frac{dM_{nm}}{dm}$ and M_{nn} equal to zero. This means that $\mathbf{f}_b$ does not enter the calculations in this case either. The lower die corresponding to (A.25) reads

$$\underset{\sim}{\mathbf{K}} = \begin{bmatrix} (1,1)+(4,4) & (1,2)+(4,5) & (1,10)+(4,7) & (1,11)+(4,8) & (1,12)+(4,9) \\ (2,1)+(5,4) & (2,2)+(5,5) & (2,10)+(5,7) & (2,11)+(5,8) & (2,12)+(5,9) \\ (7,4)+(10,1) & (7,5)+(10,2) & (1,1)+(4,4)+(7,7)+(10,10) & (1,2)+(4,5)+(7,8)+(10,11) & (1,3)+(4,6)+(7,9)+(10,12) \\ (8,4)+(11,1) & (8,5)+(11,2) & (2,1)+(5,4)+(8,7)+(11,10) & (2,2)+(5,5)+(8,8)+(11,11) & (2,3)+(5,6)+(8,9)+(11,12) \\ (9,4)+(12,1) & (9,5)+(12,2) & (3,1)+(6,4)+(9,7)+(12,10) & (3,2)+(6,5)+(9,8)+(12,11) & (3,3)+(6,6)+(9,9)+(12,12) \end{bmatrix}$$

(A.30)

where explicit expressions have been omitted due to their size. Continuing with the load vector it reads

$$\underset{\sim}{\mathbf{f}} = \begin{bmatrix} (1,1)+(4,1) \\ (2,1)+(5,1) \\ (1,1)+(4,1)+(7,1)+(10,1) \\ (2,1)+(5,1)+(8,1)+(11,1) \\ (3,1)+(6,1)+(9,1)+(12,1) \end{bmatrix} = q \begin{bmatrix} 2ab \\ \frac{2}{3}ab^2 \\ 4ab \\ 0 \\ 0 \end{bmatrix} \qquad \text{(A.31)}$$

Solving the system of equations

$$\underset{\sim}{\mathbf{K}} \begin{bmatrix} u_4 \\ u_5 \\ u_7 \\ u_8 \\ u_9 \end{bmatrix} = \underset{\sim}{\mathbf{f}} \qquad \text{(A.32)}$$

yields

$$\begin{aligned} u4 = & -480\,(600\,b^8\,\nu^4 - 800\,b^8\,\nu^3 - 400\,b^8\,\nu^2 + 800\,b^8\,\nu - 200\,b^8 - 399\,b^6\,\nu^5\,a^2 \\ & + 1792\,b^6\,\nu^4\,a^2 - 5688\,b^6\,\nu^3\,a^2 + 902\,b^6\,a^2\,\nu^2 + 6087\,b^6\,\nu\,a^2 - 2694\,b^6\,a^2 \\ & + 5460\,b^4\,\nu^4\,a^4 - 15820\,b^4\,\nu^3\,a^4 + 6900\,a^4\,b^4\,\nu^2 + 15820\,b^4\,\nu\,a^4 - 12360\,a^4\,b^4 \\ & - 19500\,b^2\,\nu^3\,a^6 + 25000\,b^2\,a^6\,\nu^2 + 19500\,b^2\,a^6\,\nu - 25000\,b^2\,a^6 + 12000\,a^8\,\nu^2 \\ & - 12000\,a^8)\,q\,a^4\,b^4 \,/\, (t^3\,E\,(21700\,b^{12} + 11904\,b^8\,a^4\,\nu^3 - 1148320\,b^6\,a^6\,\nu \\ & + 1275640\,b^6\,a^6 - 1800\,b^4\,a^8\,\nu^2 - 302400\,b^4\,a^8\,\nu + 694200\,b^4\,a^8 + 10000\,a^{12} \\ & + 132000\,b^2\,a^{10} + 1100\,b^{10}\,\nu^3\,a^2 + 62500\,b^{10}\,a^2\,\nu^2 - 342300\,b^{10}\,a^2\,\nu \\ & + 278700\,b^{10}\,a^2 - 3311\,b^8\,\nu^4\,a^4 + 9720\,b^6\,a^6\,\nu^2 + 198454\,b^8\,a^4\,\nu^2 \\ & - 807376\,b^8\,a^4\,\nu + 970329\,b^8\,a^4 + 21700\,b^{12}\,\nu^2 - 43400\,b^{12}\,\nu - 152000\,b^2\,a^{10}\,\nu \\ & + 22960\,b^6\,\nu^3\,a^6)) \end{aligned}$$

$$u5 = 1200\,(-1600\,a^{10} + 280\,b^{10} - 1716\,b^4\,a^6\,\nu^4 + 3812\,b^4\,a^6\,\nu^3 - 3780\,b^2\,a^8\,\nu$$
$$+ 1600\,a^{10}\,\nu^2 + 280\,b^{10}\,\nu^3 - 280\,b^{10}\,\nu^2 - 280\,b^{10}\,\nu - 412\,b^8\,\nu^4\,a^2 + 984\,b^8\,\nu^3\,a^2$$
$$- 1560\,b^8\,\nu^2\,a^2 - 984\,b^8\,\nu\,a^2 + 181\,b^6\,a^4\,\nu^5 - 824\,b^6\,a^4\,\nu^4 - 3812\,b^4\,a^6\,\nu$$
$$+ 3780\,b^2\,a^8\,\nu^3 + 520\,b^2\,a^8\,\nu^2 - 520\,b^2\,a^8 + 3524\,b^6\,\nu^3\,a^4 - 3705\,b^6\,\nu\,a^4$$
$$- 3380\,a^6\,b^4\,\nu^2 + 1972\,b^8\,a^2 - 3038\,b^6\,a^4\,\nu^2 + 3862\,b^6\,a^4 + 5096\,a^6\,b^4)\,b^3\,q\,a^2 \big/ ($$
$$t^3\,E\,(-302400\,b^4\,a^8\,\nu + 62500\,b^{10}\,a^2\,\nu^2 + 198454\,b^8\,a^4\,\nu^2 - 43400\,b^{12}\,\nu$$
$$+ 11904\,b^8\,a^4\,\nu^3 - 1148320\,b^6\,a^6\,\nu + 10000\,a^{12} + 1100\,b^{10}\,\nu^3\,a^2 + 21700\,b^{12}\,\nu^2$$
$$+ 1275640\,b^6\,a^6 - 342300\,b^{10}\,a^2\,\nu + 278700\,b^{10}\,a^2 - 3311\,b^8\,a^4\,\nu^4 + 21700\,b^{12}$$
$$- 152000\,b^2\,a^{10}\,\nu - 807376\,b^8\,a^4\,\nu + 970329\,b^8\,a^4 + 9720\,b^6\,a^6\,\nu^2 - 1800\,b^4\,a^8\,\nu^2$$
$$+ 22960\,b^6\,a^6\,\nu^3 + 694200\,b^4\,a^8 + 132000\,b^2\,a^{10}))$$

$$u7 = -600\,(342\,b^8\,\nu^4 - 764\,b^8\,\nu^3 + 80\,b^8\,\nu^2 + 764\,b^8\,\nu - 422\,b^8 + 81\,b^6\,a^2\,\nu^5$$
$$+ 871\,b^6\,\nu^4\,a^2 - 5906\,b^6\,\nu^3\,a^2 + 4402\,b^6\,a^2\,\nu^2 + 5825\,b^6\,\nu\,a^2 - 5273\,b^6\,a^2$$
$$+ 2854\,b^4\,a^4\,\nu^4 - 11068\,b^4\,\nu^3\,a^4 + 13160\,a^4\,b^4\,\nu^2 + 11068\,b^4\,\nu\,a^4 - 16014\,a^4\,b^4$$
$$- 14740\,b^2\,a^6\,\nu^3 + 12940\,b^2\,a^6\,\nu^2 + 14740\,b^2\,a^6\,\nu - 12940\,b^2\,a^6 + 3400\,a^8\,\nu^2$$
$$- 3400\,a^8)\,a^4\,q\,b^4 \big/ (t^3\,E\,(-302400\,b^4\,a^8\,\nu + 62500\,b^{10}\,a^2\,\nu^2 + 198454\,b^8\,a^4\,\nu^2$$
$$- 43400\,b^{12}\,\nu + 11904\,b^8\,a^4\,\nu^3 - 1148320\,b^6\,a^6\,\nu + 10000\,a^{12} + 1100\,b^{10}\,\nu^3\,a^2$$
$$+ 21700\,b^{12}\,\nu^2 + 1275640\,b^6\,a^6 - 342300\,b^{10}\,a^2\,\nu + 278700\,b^{10}\,a^2 - 3311\,b^8\,a^4\,\nu^4$$
$$+ 21700\,b^{12} - 152000\,b^2\,a^{10}\,\nu - 807376\,b^8\,a^4\,\nu + 970329\,b^8\,a^4 + 9720\,b^6\,a^6\,\nu^2$$
$$- 1800\,b^4\,a^8\,\nu^2 + 22960\,b^6\,a^6\,\nu^3 + 694200\,b^4\,a^8 + 132000\,b^2\,a^{10}))$$

$$,\ u5 = 1200\,($$
$$-1600\,a^{10} + 280\,b^{10} - 1716\,b^4\,a^6\,\nu^4 + 3812\,b^4\,a^6\,\nu^3 - 3780\,b^2\,a^8\,\nu + 1600\,a^{10}\,\nu^2$$
$$+ 280\,b^{10}\,\nu^3 - 280\,b^{10}\,\nu^2 - 280\,b^{10}\,\nu - 412\,b^8\,\nu^4\,a^2 + 984\,b^8\,\nu^3\,a^2 - 1560\,b^8\,\nu^2\,a^2$$
$$- 984\,b^8\,\nu\,a^2 + 181\,b^6\,a^4\,\nu^5 - 824\,b^6\,a^4\,\nu^4 - 3812\,b^4\,a^6\,\nu + 3780\,b^2\,a^8\,\nu^3$$
$$+ 520\,b^2\,a^8\,\nu^2 - 520\,b^2\,a^8 + 3524\,b^6\,\nu^3\,a^4 - 3705\,b^6\,\nu\,a^4 - 3380\,a^6\,b^4\,\nu^2$$
$$+ 1972\,b^8\,a^2 - 3038\,b^6\,a^4\,\nu^2 + 3862\,b^6\,a^4 + 5096\,a^6\,b^4)\,b^3\,q\,a^2 \big/ (t^3\,E\,($$
$$-302400\,b^4\,a^8\,\nu + 62500\,b^{10}\,a^2\,\nu^2 + 198454\,b^8\,a^4\,\nu^2 - 43400\,b^{12}\,\nu$$
$$+ 11904\,b^8\,a^4\,\nu^3 - 1148320\,b^6\,a^6\,\nu + 10000\,a^{12} + 1100\,b^{10}\,\nu^3\,a^2 + 21700\,b^{12}\,\nu^2$$
$$+ 1275640\,b^6\,a^6 - 342300\,b^{10}\,a^2\,\nu + 278700\,b^{10}\,a^2 - 3311\,b^8\,a^4\,\nu^4 + 21700\,b^{12}$$
$$- 152000\,b^2\,a^{10}\,\nu - 807376\,b^8\,a^4\,\nu + 970329\,b^8\,a^4 + 9720\,b^6\,a^6\,\nu^2 - 1800\,b^4\,a^8\,\nu^2$$
$$+ 22960\,b^6\,a^6\,\nu^3 + 694200\,b^4\,a^8 + 132000\,b^2\,a^{10}))$$

$$
\begin{aligned}
u8 = {} & 120\, b^3\, q\, a^2\, (-14000\, a^{10} + 350\, b^{10} + 6840\, b^4\, a^6\, \nu^4 - 24380\, b^4\, a^6\, \nu^3 \\
& + 38100\, b^2\, a^8\, \nu + 14000\, a^{10}\, \nu^2 + 350\, b^{10}\, \nu^3 - 350\, b^{10}\, \nu^2 - 350\, b^{10}\, \nu - 65\, b^8\, \nu^4\, a^2 \\
& + 630\, b^8\, \nu^3\, a^2 + 3000\, b^8\, \nu^2\, a^2 - 630\, b^8\, \nu\, a^2 - 73\, b^6\, a^4\, \nu^5 + 314\, b^6\, a^4\, \nu^4 \\
& + 24380\, b^4\, a^6\, \nu - 38100\, b^2\, a^8\, \nu^3 + 35600\, b^2\, a^8\, \nu^2 - 35600\, b^2\, a^8 - 9836\, b^6\, \nu^3\, a^4 \\
& + 9909\, b^6\, \nu\, a^4 + 21200\, a^6\, b^4\, \nu^2 - 2935\, b^8\, a^2 + 8354\, b^6\, a^4\, \nu^2 - 8668\, b^6\, a^4 \\
& - 28040\, a^6\, b^4) \big/ (t^3\, E\, (-302400\, b^4\, a^8\, \nu + 62500\, b^{10}\, a^2\, \nu^2 + 198454\, b^8\, a^4\, \nu^2 \\
& - 43400\, b^{12}\, \nu + 11904\, b^8\, a^4\, \nu^3 - 1148320\, b^6\, a^6\, \nu + 10000\, a^{12} + 1100\, b^{10}\, \nu^3\, a^2 \\
& + 21700\, b^{12}\, \nu^2 + 1275640\, b^6\, a^6 - 342300\, b^{10}\, a^2\, \nu + 278700\, b^{10}\, a^2 - 3311\, b^8\, a^4\, \nu^4 \\
& + 21700\, b^{12} - 152000\, b^2\, a^{10}\, \nu - 807376\, b^8\, a^4\, \nu + 970329\, b^8\, a^4 + 9720\, b^6\, a^6\, \nu^2 \\
& - 1800\, b^4\, a^8\, \nu^2 + 22960\, b^6\, a^6\, \nu^3 + 694200\, b^4\, a^8 + 132000\, b^2\, a^{10}))
\end{aligned}
$$

$$u9 = 0$$

(A.33)

$u_9 = 0$ means that there is no slope in the x-direction at the mid point, which was expected of symmetrical reasons. The degree of freedom of interest is u_4, which rewritten in terms of A and B reads

$$
\begin{aligned}
u_4 = {} & -\frac{15}{2048}\Bigg(\frac{75}{8192} B^8 \nu^4 - \frac{25}{2048} B^8 \nu^3 - \frac{25}{4096} B^8 \nu^2 + \frac{25}{2048} B^8 \nu - \frac{25}{8192} B^8 - \frac{399}{65536} B^6 A^2 \nu^5 \\
& + \frac{7}{256} B^6 \nu^4 A^2 - \frac{711}{8192} B^6 \nu^3 A^2 + \frac{451}{32768} B^6 A^2 \nu^2 + \frac{6087}{65536} B^6 \nu A^2 - \frac{1347}{32768} B^6 A^2 \\
& + \frac{1365}{16384} B^4 A^4 \nu^4 - \frac{3955}{16384} B^4 \nu^3 A^4 + \frac{1725}{16384} A^4 B^4 \nu^2 + \frac{3955}{16384} B^4 \nu A^4 - \frac{1545}{8192} A^4 B^4 \\
& - \frac{4875}{16384} B^2 A^6 \nu^3 + \frac{3125}{8192} B^2 A^6 \nu^2 + \frac{4875}{16384} B^2 A^6 \nu - \frac{3125}{8192} B^2 A^6 + \frac{375}{2048} A^8 \nu^2 \\
& - \frac{375}{2048} A^8\Bigg) q A^4 B^4 \Bigg/ \Bigg(t^3 E \Bigg(-\frac{4725}{262144} B^4 A^8 \nu + \frac{15625}{4194304} B^{10} A^2 \nu^2 \\
& + \frac{99227}{8388608} B^8 A^4 \nu^2 - \frac{5425}{2097152} B^{12} \nu + \frac{93}{131072} B^8 A^4 \nu^3 - \frac{35885}{524288} B^6 A^6 \nu \\
& + \frac{625}{1048576} A^{12} + \frac{275}{4194304} B^{10} \nu^3 A^2 + \frac{5425}{4194304} B^{12} \nu^2 + \frac{159455}{2097152} B^6 A^6 \\
& - \frac{85575}{4194304} B^{10} A^2 \nu + \frac{69675}{4194304} B^{10} A^2 - \frac{3311}{16777216} B^8 A^4 \nu^4 + \frac{5425}{4194304} B^{12} \\
& - \frac{2375}{262144} B^2 A^{10} \nu - \frac{50461}{1048576} B^8 A^4 \nu + \frac{970329}{16777216} B^8 A^4 + \frac{1215}{2097152} B^6 A^6 \nu^2 \\
& - \frac{225}{2097152} B^4 A^8 \nu^2 + \frac{1435}{1048576} B^6 A^6 \nu^3 + \frac{86775}{2097152} B^4 A^8 + \frac{4125}{524288} B^2 A^{10}\Bigg)\Bigg)
\end{aligned}
$$

(A.34)

Different number of elements yields different deflections according to Figure A.9. If the calculated value in Figure A.9 is compared with the result from a three dimensional mesh, Figure A.10, it is concluded that the solution is acceptable despite of the very coarse two dimensional mesh.

A=400 mm, *B*=300 mm, *q*=-10 MPa, *E*=210000 MPa, *ν*=0.3		
Nbr. of elements		U_4 (mm)
4	*t*=30 mm	-1,2422
16		-1,3208
32		-1,3432

Fig. A.9. Comparison of deflection between different meshes.

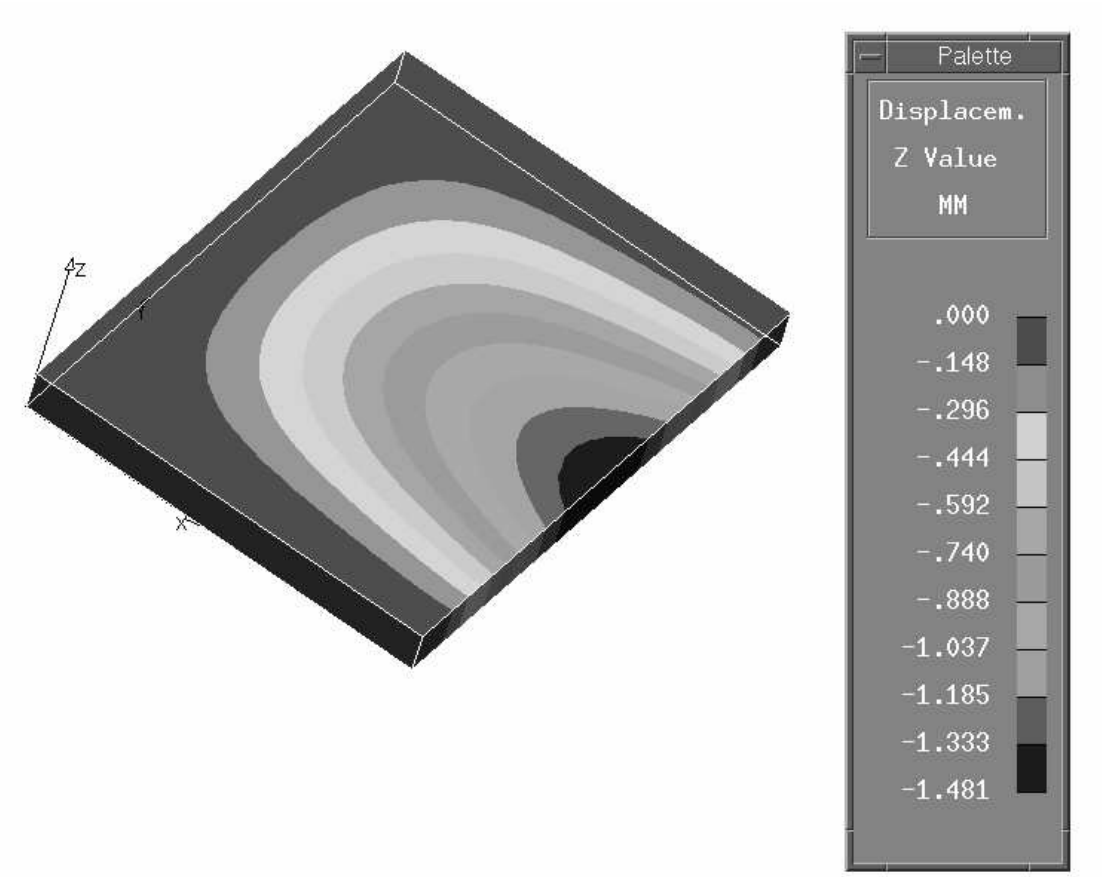

Fig. A.10. Deflections in a 30 mm plate consisting of 2449 ten-node tetrahedral elements. Input as in fig. A.9.

13.2. Part B-Determination of shear centre of U-shaped profiles with different lengths of the flanges

This section deals with determination of the shear center of U-shaped profiles with different lengths of the flanges. In order to be able to determine the shear center, knowledge about the

position of the center of mass is required. Considering Figure B.1, the position of the center of mass in the y- and the z-direction, y_{tp} and z_{tp} respectively, are determined using the principle of moments

$$y_{tp} = \frac{C\left(\frac{C}{2}+B\right)+\frac{B\,H}{2}+\mathrm{D}\left(\frac{\mathrm{D}}{2}+B\right)}{C+H+\mathrm{D}} \tag{B.1}$$

$$z_{tp} = \frac{\frac{1\,B\,C}{2}+\frac{1\,H^2}{2}+\mathrm{D}\left(H-\frac{1\,B}{2}\right)}{C+H+\mathrm{D}} \tag{B.2}$$

where O has been used as moment axis. Since the density of the body is uniform the expressions of the center of mass are pure geometrical properties.

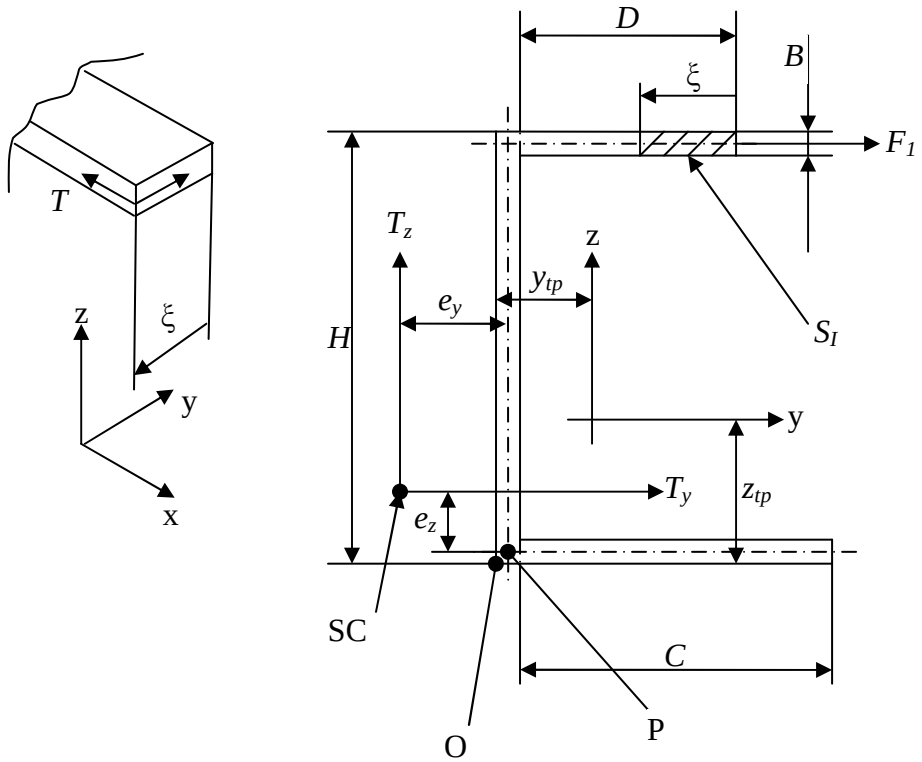

Figure B.1. The U-shaped cross section used in the derivation of the shear center.

Next the moments of inertia, I_y and I_z, about the y- and z-axis respectively, defined as

$$I_y = \int_A z^2 dS \tag{B.3}$$

$$I_z = \int_A y^2 dS \tag{B.4}$$

and the product moment of area, defined as

$$I_{yz} = \int_A yz dS \tag{B.5}$$

where S denotes the area, are determined. If (B.3), (B.4) and (B.5) are carried out for the rectangular cross section shown in Figure B.2 following results are obtained.

$$\begin{aligned} I_y &= \frac{bh^3}{12} \\ I_z &= \frac{hb^3}{12} \\ I_{yz} &= 0 \end{aligned} \tag{B.6}$$

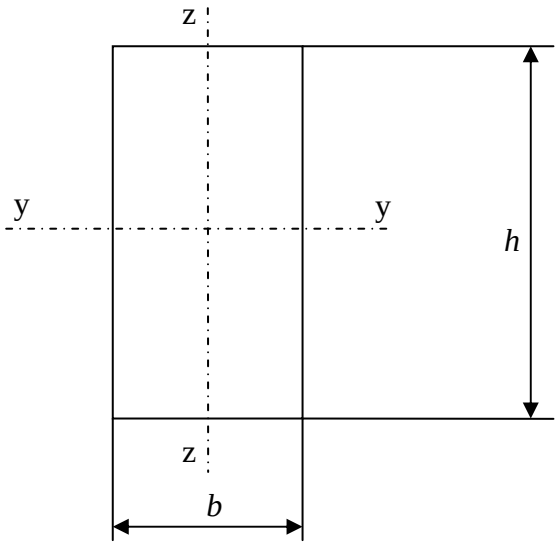

Figure B.2. Rectangular cross section with the axes y-y and z-z, passing through the center of mass, indicated.

Since the cross section of a U-shaped profile can be imagined to consist of three rectangular cross sections, the moments of inertia and product area moment for the whole structure can be determined using the parallel-axis theorem. The theorem is used when the quantities mentioned above are required with respect to other axes than those passing through the center of mass. With designations from Figure B.3, the parallel-axis theorem reads [2]

$$I_{y'} = I_y + a^2 S$$
$$I_{z'} = I_z + b^2 S \qquad \text{(B.7)}$$
$$I_{y'z'} = I_{yz} + abS$$

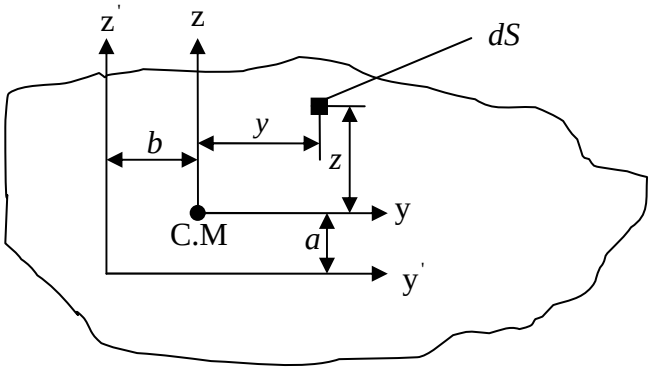

Figure B.3. Illustration *a* and *b* used in the parallel axis theorem

Employing (B.4) on the structure shown in Figure B.1 yields

$$I_y = \frac{C\,B^3}{12} + B\,C\left(z_{tp} - \frac{B}{2}\right)^2 + \frac{B\,H^3}{12} + B\,H\left(\frac{H}{2} - z_{tp}\right)^2 + \frac{\mathrm{D}\,B^3}{12} + B\,\mathrm{D}\left(H - \frac{B}{2} - z_{tp}\right)^2$$

(B.8)

$$I_z = \frac{B\,C^3}{12} + B\,C\left(\frac{C}{2} + B - y_{tp}\right)^2 + \frac{H\,B^3}{12} + B\,H\left(y_{tp} - \frac{B}{2}\right)^2 + \frac{B\,\mathrm{D}^3}{12}$$
$$+ B\,\mathrm{D}\left(B + \frac{\mathrm{D}}{2} - y_{tp}\right)^2$$

(B.9)

$$I_{yz} = -\left(z_{tp} - \frac{B}{2}\right)\left(B + \frac{C}{2} - y_{tp}\right)B\,C + \left(\frac{H}{2} - z_{tp}\right)\left(-\left(y_{tp} - \frac{B}{2}\right)\right)B\,H$$
$$+ \left(H - z_{tp} - \frac{B}{2}\right)\left(\frac{\mathrm{D}}{2} + B - y_{tp}\right)B\,\mathrm{D}$$

(B.10)

There is also need for another quantity named the first area of moment, which with designations from Figure B.1, is defined as

$$S_y = \int_A z dS$$
$$S_z = \int_A y dS \qquad \text{(B.11)}$$

The expression for the average shear stress, T, over the cross section, whose thickness in this case is uniformly equal to B, acting in the y-direction at a distance ξ from the upper flange, see Figure B.1, can be shown to read [7]

$$T = \frac{\left(S_z I_y - S_y I_{yz}\right)T_y + \left(S_y I_z - S_z I_{yz}\right)T_z}{B\left(I_y I_z - I_{yz}^2\right)} \tag{B.12}$$

Here T_y and T_z denote transversal forces indicated in Figure B.1. With reference to Figure B.1, S_y and S_z for the piece with length ξ (having an area equal to A_I) are calculated as

$$S_y = \left(H - \frac{B}{2} - z_{tp}\right)\xi B \tag{B.13}$$

,

$$S_z = \left(D + B - y_{tp} - \frac{\xi}{2}\right)\xi B \tag{B.14}$$

Since the shear center is that point the line of action of a applied load has to pass through, not to give rise to torsion, the effect of the shear stresses in the cross section can replaced with resulting transversal forces, denoted T_y and T_z in Figure B.1. In order to determine the horizontal position of the shear center, denoted e_y in Figure B.1, static equivalence about point P yields

$$T_z e_y = F_I\left(H - B\right) \tag{B.15}$$

where F_I denotes the resulting force in the upper flange due to the shear stresses. By choosing the point P there is no need for calculating the resulting forces in the lower flange and in the waist, since their lines of action are passing through this point. F_I is calculated as

$$F_I = \int_0^{D+\frac{B}{2}} T(\xi)Bd\xi = \int_0^{D+\frac{B}{2}} \frac{\left(B\xi\left(H - \frac{B}{2} - z_{tp}\right)I_z - \left(D + B - y_{tp} - \frac{\xi}{2}\right)\xi B I_{yz}\right)T_z d\xi}{I_y I_z - I_{yz}^2} \tag{B.16}$$

where use has been made of (B.12), (B.13) and (B.14). In (B.12) T_y has been set equal to zero, since no horizontal force is applied in this case. As can be seen after (B.16) has been inserted in (B.15), T_y is cancelled out, which confirms that the shear center is a quantity only dependent of the geometry. After the integral in (B.16) has been carried out and the expressions for the center of mass and the moments of inertia and product moment of inertia has been inserted, the expression for e_y is calculated

$e_y =$

$$\frac{3}{4}(-H+B)(2\mathrm{D}+B)^2(-2C^4H+2C^4B+4HBC^3-4C^3H^2+6\mathrm{D}HC^2B$$
$$-2C^2B^2\mathrm{D}-2HC^2\mathrm{D}^2-8H^2C^2B-4\mathrm{D}H^2C^2+8C^2B^2H+2BC^2\mathrm{D}^2$$
$$+4CB^2\mathrm{D}H+7CHB^3-2C\mathrm{D}^2HB-7CB^2H^2-4CH^2\mathrm{D}B+2CB^2\mathrm{D}^2$$
$$-B^2H^3+B^3\mathrm{D}H+B^3H^2-\mathrm{D}B^2H^2)\big/(-72H^2C^2B^2\mathrm{D}-36H^2C^2\mathrm{D}^2B$$
$$+36H^3C\mathrm{D}^2B-72H^2C\mathrm{D}^2B^2+48H^3C\mathrm{D}B^2-24H^2C^3\mathrm{D}B-24H^2CB\mathrm{D}^3$$
$$+36H^3\mathrm{D}C^2B-24BCH\mathrm{D}^4+42B^3C^2\mathrm{D}H+18B^2C^2\mathrm{D}^2H+42B^3CH\mathrm{D}^2$$
$$-96B^3C\mathrm{D}H^2+16B^2C^3\mathrm{D}H-24BC^4\mathrm{D}H+16B^2CH\mathrm{D}^3+7H^4CB^2$$
$$+12H^2C\mathrm{D}^4+12H^2C^4\mathrm{D}-6H^2C^4B+16H^3C\mathrm{D}^3+6H^4C^2B+6H^4\mathrm{D}^2B$$
$$+7H^4\mathrm{D}B^2+16H^3C^3\mathrm{D}+12H^3C^2\mathrm{D}^2-6B^3CH^3+6B^3C^3H+7B^2C^4H$$
$$-6BH^2\mathrm{D}^4-6B^3H^3\mathrm{D}+7H\mathrm{D}^4B^2-2C^2B^2\mathrm{D}^3+17CB^2\mathrm{D}^4+17\mathrm{D}B^2C^4$$
$$-2\mathrm{D}^2B^2C^3+4H^3C^4+4B^4H\mathrm{D}^2+4B^4\mathrm{D}H^2+B^2\mathrm{D}^5+6H\mathrm{D}^3B^3+H^5B^2$$
$$+4H^3\mathrm{D}^4+4H^4C^3+4H^4\mathrm{D}^3+56CB^4\mathrm{D}H+B^2C^5+4C^2B^4H+4CB^4H^2) \tag{B.17}$$

e_z is determined in a similar manner to e_y, but in this case it is assumed that only a horizontal load is applied. Static equivalence yields

$$T_y e_z = F_I(H-B) \tag{B.18}$$

where F_I under current conditions is calculated as

$$F_I = \int_0^{D+\frac{B}{2}} T(\xi)Bd\xi = \int_0^{D+\frac{B}{2}} \frac{\left(\xi B\left(D+B-\frac{\xi}{2}-y_{tp}\right)I_y-\xi B\left(H-\frac{B}{2}-z_{tp}\right)I_{yz}\right)T_y d\xi}{I_y I_z - I_{yz}^2} \tag{B.19}$$

Finally solving (B.18) for e_z yields

$e_z =$

$$\frac{1}{4}(-H+B)(2\mathrm{D}+B)^2(B^3\mathrm{D}^2+C^2B^3+3C^3B^2+14C\mathrm{D}B^3-4H^4\mathrm{D}-\mathrm{D}^3B^2$$
$$-C^2B^2\mathrm{D}-17CB^2\mathrm{D}^2-16CH^3\mathrm{D}+B^3\mathrm{D}H-17CHB^3-40CB^2\mathrm{D}H$$
$$+36CH^2\mathrm{D}B+24C\mathrm{D}^2HB-6H^3C^2-4H^3\mathrm{D}^2-2H^4B-9C^2B^2H$$
$$+30CB^2H^2-14CBH^3-12C\mathrm{D}^2H^2+18H^2C^2B+6\mathrm{D}^2H^2B-7H\mathrm{D}^2B^2$$
$$-6\mathrm{D}B^2H^2+4\mathrm{D}BH^3)\big/(-72H^2C^2B^2\mathrm{D}-36H^2C^2\mathrm{D}^2B+36H^3C\mathrm{D}^2B$$
$$-72H^2C\mathrm{D}^2B^2+48H^3C\mathrm{D}B^2-24H^2C^3\mathrm{D}B-24H^2CB\mathrm{D}^3+36H^3\mathrm{D}C^2B$$
$$-24BCH\mathrm{D}^4+42B^3C^2\mathrm{D}H+18B^2C^2\mathrm{D}^2H+42B^3CH\mathrm{D}^2-96B^3C\mathrm{D}H^2$$

$$
\begin{aligned}
&+ 16\, B^2\, C^3\, \mathrm{D}\, H - 24\, B\, C^4\, \mathrm{D}\, H + 16\, B^2\, C\, H\, \mathrm{D}^3 + 7\, H^4\, C\, B^2 + 12\, H^2\, C\, \mathrm{D}^4 \\
&+ 12\, H^2\, C^4\, \mathrm{D} - 6\, H^2\, C^4\, B + 16\, H^3\, C\, \mathrm{D}^3 + 6\, H^4\, C^2\, B + 6\, H^4\, \mathrm{D}^2\, B + 7\, H^4\, \mathrm{D}\, B^2 \\
&+ 16\, H^3\, C^3\, \mathrm{D} + 12\, H^3\, C^2\, \mathrm{D}^2 - 6\, B^3\, C\, H^3 + 6\, B^3\, C^3\, H + 7\, B^2\, C^4\, H - 6\, B\, H^2\, \mathrm{D}^4 \\
&- 6\, B^3\, H^3\, \mathrm{D} + 7\, H\, \mathrm{D}^4\, B^2 - 2\, C^2\, B^2\, \mathrm{D}^3 + 17\, C\, B^2\, \mathrm{D}^4 + 17\, \mathrm{D}\, B^2\, C^4 - 2\, \mathrm{D}^2\, B^2\, C^3 \\
&+ 4\, H^3\, C^4 + 4\, B^4\, H\, \mathrm{D}^2 + 4\, B^4\, \mathrm{D}\, H^2 + B^2\, \mathrm{D}^5 + 6\, H\, \mathrm{D}^3\, B^3 + H^5\, B^2 + 4\, H^3\, \mathrm{D}^4 \\
&+ 4\, H^4\, C^3 + 4\, H^4\, \mathrm{D}^3 + 56\, C\, B^4\, \mathrm{D}\, H + B^2\, C^5 + 4\, C^2\, B^4\, H + 4\, C\, B^4\, H^2)
\end{aligned}
\tag{B.20}
$$

In order to check how well the values from the derived expressions agree with data from hand books, the values for a U-bar with the dimensions 80x50x6 is compared with the values resulting from (B.17) and (B.20) [2]. The result is shown in Figure B.4.

	KTH	Calculated
e_y	18,21 mm	18.51 mm
e_z	40 mm	39,69 mm

Fig. B.4. Comparison between values from the derived expressions and hand book [2].

The U-section used in the derivation of (B.19) and (B.20) consists of purely rectangular elements, whilst the waist and flanges in the U-bar in the handbook are connected with radii. This explains the difference between the values in Figure B.4.